UNIVERSITY OF CAPE TOWN
IYUNIVESITHI YASEKAPA • UNIVERSITEIT VAN KAAPSTAD

The response of honeycomb sandwich panels to blast loads

Yunn-Chih (Yvonne) Chi 紀蘊之

Dissertation presented in partial fulfilment of the requirements for the degree of Master of Science in Mechanical Engineering

Blast Impact and Survivability Research Unit
Department of Mechanical Engineering
University of Cape Town

May 2008

DECLARATION

1. I know that plagiarism is wrong. Plagiarism is to use another's work and pretend that it is one's own.

2. I have used the scientific convention for citation and referencing. Each significant contribution to, and quotation in, this project from the work, or works, of other people has been attributed, and was cited and referenced.

3. This project is my own work.

4. I have not allowed, and will not allow, anyone to copy my work with the intention of passing it off as his or her own work.

Signature:

Yunn-Chih Chi _____

(Date) _____

ABSTRACT

Numerous studies have been performed in search of structures providing better blast protection and to understand the various effects influencing the structural performance. This thesis reports on an investigation into the behaviour of circular sandwich panels with aluminium honeycomb cores subjected to air blast loading. It focuses on the effect of varying core thickness, plate thickness and panel configuration.

In this study, aluminium honeycomb core is sandwiched between mild steel face plates. Quasi-static tensile and compression experiments are performed to characterise the face plates and the honeycombs. Four sandwich panel configurations are proposed and subjected to blast loading. The impulse is generated by detonating plastic explosives at a constant stand-off distance and measured using a ballistic pendulum. The impulse is varied by using different charge masses.

It is observed that the panels experience front plate deflection and tearing; honeycomb core crushing and densification; and back plate deflection and tearing. The deformations of the face plates and the cores increased with increasing impulse. Increasing the core thickness delayed the onset of core densification and decreased back plate deflection; and increasing the plate thickness also decreased back plate deflection. The use of an extra sandwich layer helps to provide better structural support but has the penalty of extra mass.

TABLE OF CONTENTS

LIST OF FIGURES

LIST OF TABLES

NOTATION

Notation	Definition
S	Single sandwich, consisting of a front plate and a back plate sandwiching a core.
D	Double sandwich, consisting of a front plate and a back plate, sandwiching more than one core layer.
S13 sandwich panel	1.6mm thick mild steel plates sandwiching a 13mm thick aluminium honeycomb.

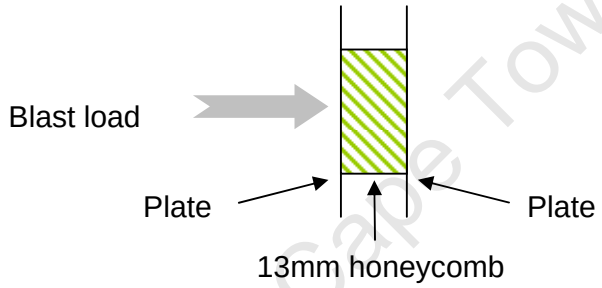

S29 sandwich panel	1.6mm thick mild steel plates sandwiching a 29mm thick aluminium honeycomb.

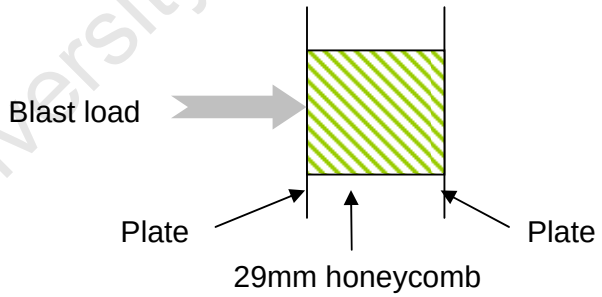

S29-1 sandwich panel	1.0mm thick mild steel plates sandwiching a 29mm thick aluminium honeycomb.

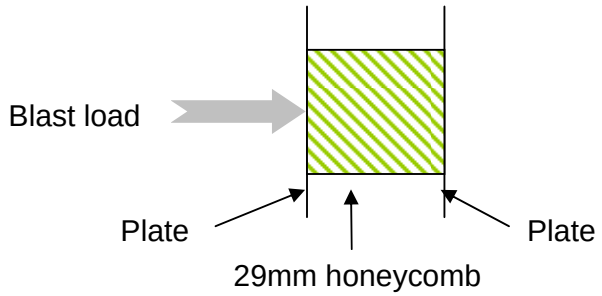

Notation	Definition
S150 sandwich panel	1.6mm thick mild steel plates sandwiching a 150mm thick aluminium honeycomb.

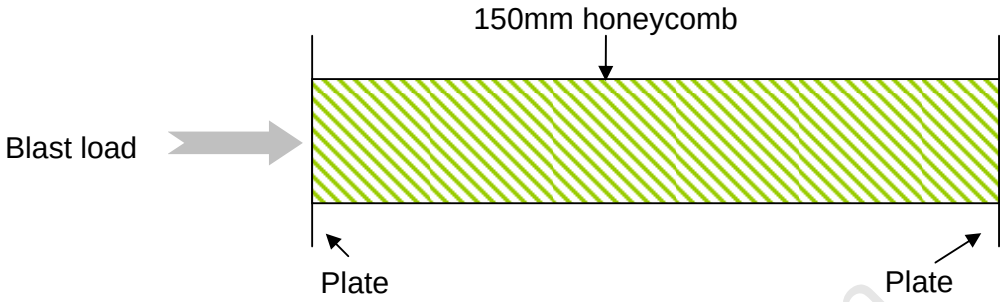

D29/13 sandwich panel	1.6mm thick mild steel plates sandwiching a 29mm and a 13mm thick aluminium honeycomb, with a middle plate

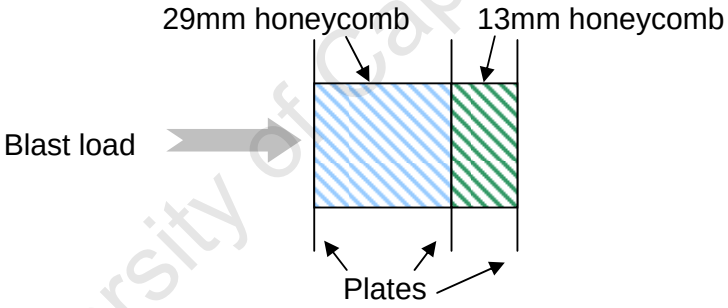

D13a/13 sandwich panel	1.6mm thick mild steel plates sandwiching a 13mm thick air gap plus a 13mm thick aluminium honeycomb, with no middle plate.

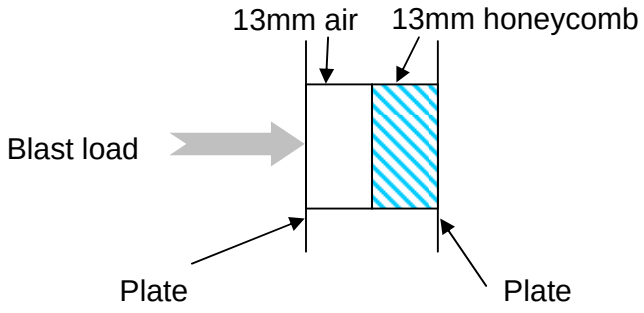

NOMENCLATURE

Symbol	Definition
a	Height of the pen
c	Length of the double cell wall in honeycomb
C	Damping coefficient
d_1	Distance
d_2	Distance
D	Material constant
h	Cell wall thickness of honeycomb
H	Plate thickness
H_m	Mean wall thickness of a square tube
I	Applied impulse
I_0	Incident impulse
I_r	Reflected impulse
I_t	Transmitted impulse
K	Scaled distance
l	Length of the single cell wall in honeycomb
m	Charge mass
M	Total mass of the pendulum
p	Pressure
P_{BLAST}	Blast load intensity
P	Applied load
q	Material constant
r	Stand-off distance
r_0	Current radius
R	Distance of the rope of the pendulum
R_0	Load radius
R_p	Plate radius
S	Cell size of honeycomb
t	Time
T	Natural period of the pendulum

Symbol	Definition
V	Velocity
W_m	Mean width of a square tube
X_0	Initial velocity of the pendulum
x_1	Horizontal displacement at t = T/4
x_2	Horizontal displacement at t = 3T/4
$\dot{x}_0$	Initial velocity of the pendulum
Z	Length of the pen
α	Branch angle of the cell of honeycomb
β	Dimensionless damping constant
δ	Deflection
δR	Forward distance of the trace
δL	Backward distance of the trace
ε	Strain
$\dot{\varepsilon}$	Strain rate
ϕ_c	Dimensionless number
η	Material constant
ρ	Material density
ρ_c	Density of the core
σ	Stress
σ'_0	Quasi-static yield stress
σ_0	Static yield stress

ACKNOWLEDGEMENTS

I would like to extend my deepest thanks to the following people:

Professor GN Nurick and Dr GS Langdon for their advice and guidance during the course of my MSc programme.

Professor D Karagiozova for her patience and advice on this research.

Mr Glen Newins, Mr Peter Jacob, and the rest of the workshop staff for their invaluable assistance.

Mrs Penny Park-Ross from the University of Cape Town (UCT), Centre for Materials Engineering, for her assistance using the Zwick machine and taking micrographs.

Blast Impact and Survivability Research Unit (BISRU) for taking me into its fold and its members, especially Steeve Chung Kim Yuen, Amit Vara and Marc Pitterman, as well as my friend Lawrence Bbosa for their assistance during the experiments.

Finally, my parents 紀雄 and 陳美瓊 for their love, support and encouragement.

1 - INTRODUCTION

1.1 BACKGROUND

Each year, thousands of casualties are caused by anti-personnel and anti-vehicle landmines. This poses an urgent need for studies on structures providing blast protection (which may be used, for example, in the bases of anti-landmine vehicles).

Early works have focused on the blast response of monolithic panels [1-6]. Recently, researchers have focused on the blasting response of sandwich panels, which consists of face plates separated by a core. Fleck and Deshpande [7] developed analytical formulae to characterize the structural response of clamped metallic sandwich beams subjected to uniform air and water blasting. The study reviewed and compared the blast performance of a monolithic plate and various core topologies. Qui et al [8] extended the analytical model [7] for clamped circular sandwich plates. In addition, Xue and Hutchinson [9, 10] performed finite element calculations to compare the blast response of a monolithic plate and a metal sandwich plate, of the same material and total mass. Xue and Hutchinson [9, 10] also investigated on a variety of core topologies. These studies have each demonstrated that the sandwich plates performed better than the monolithic plate, when subjected to underwater blast loading.

In the subsequent work, Xue and Hutchinson [11] proposed a continuum constitutive model for metallic sandwich cores for quasi-static deformations. It provides an alternative approach to full meshing of core geometry. Vaziri and Hutchinson [12]

assessed the effect of fluid-structure interaction on the response of metal sandwich plates subjected to intense air shocks. Other studies [13-18] have focused on the response of metallic sandwich structures subjected to underwater shock loading.

In addition to these studies, Zhu and Lu [19] presented a review on impact and blasting of metallic and sandwich structures, and Chung Kim Yuen et al [20] presented an overview on sandwich panels subjected to blast loading. All of these investigations have shown that metal sandwich panels perform better than monolithic plates under impact and blast situations. The core materials used included cellular materials [16, 21-35], micro-architectured structures [7, 9, 14, 17] and macro-architectured structures [36]. One of the commonly used cellular cores is aluminium honeycomb [16, 25-34, 37-40].

Despite a wealth of literature on the response of sandwich structures with various core topologies, and on the quasi-static and impact loading of honeycomb sandwich panels, very few studies investigate the air-blast response of circular aluminium honeycomb sandwich panels [28-31]. Therefore further investigation is required.

1.2 PURPOSES

This thesis investigates the air blast response of varying sandwich configurations consisting of mild steel face plates sandwiching aluminium honeycomb cores. The sandwich panels have a constant exposed circular region and a constant stand-off distance. The thesis focuses on investigating the effect of varying core thickness, core configurations and plate thickness on the response of the sandwich panel.

1.3 OBJECTIVES OF THE STUDY

The objectives of this thesis are to:

- Design and conduct blast tests on aluminium honeycomb sandwich panels.
- Investigate the blast performance of the honeycomb core in the various sandwich configurations;
- Compare the experimental observations and results amongst the test series to other relevant work;
- Draw conclusions and make recommendations based on the findings.

1.4 PLAN OF DEVELOPMENT

This thesis proceeds by presenting the literature review, the material characterisation and the experimental arrangements. Thereafter the test results are listed and the observations are described. The test results are then analysed and discussed. Finally conclusions are drawn and recommendations are included for future work.

2 - LITERATURE REVIEW

Gibson and Ashby [26] define sandwich panels as “Structural members made up of two stiff, strong skins separated by a lightweight core”. Cellular materials are often used as a core in a sandwich panel. The large space within the cells provide for a greater compressibility [27]. A cellular material is a core structure desirable for blast protection due to two characteristics. Firstly, it absorbs energy by crushing. Secondly, the stress transferred via the core to the rear is limited to the plateau stress until strain approaches densification.

An example of the many natural and man-made cellular solids is honeycomb. Honeycomb is described [26] as “a two-dimensional array of polygons which pack to fill a plane area like the hexagonal cells of the bee”, as shown in Figure 2-1.

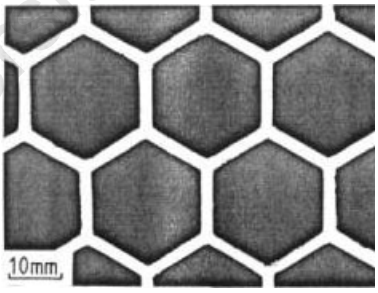

Figure 2-1: A two-dimensional cellular structure: honeycomb [26]

2.1 GEOMETRY OF A HEXAGONAL HONEYCOMB

A bare honeycomb core is defined by the geometries of its cells. Assuming the cells have regular and uniform geometries, the parameters defining a hexagonal honeycomb are shown in Figure 2-2. These are the cell wall lengths, *l* (single wall) and *c* (double wall); the branch angle α; the cell wall thickness *h*, and the cell size *S*. The length of the double wall (*c*) is sometimes shorter than that of the single wall (*l*) as noted in [40]. In particular, the value of *2h* is approximately 2.3 times that of *h*, due to the bonding between the walls.

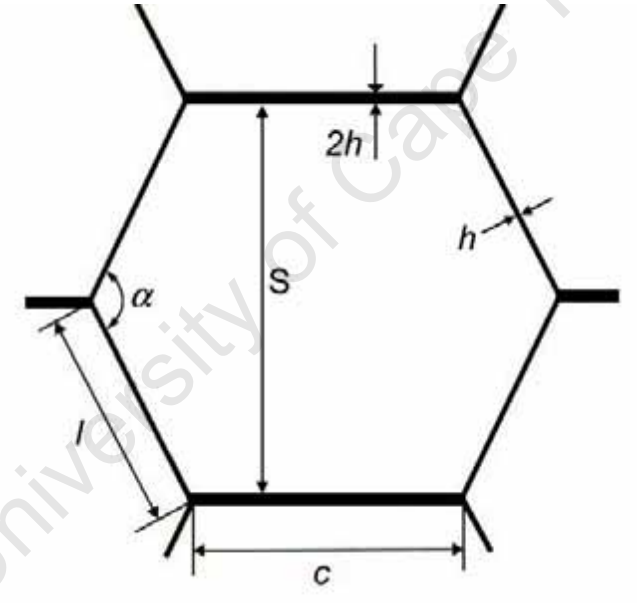

Figure 2-2: Hexagonal honeycomb cell geometry [27]

2.2 FACTORS INFLUENCING THE MATERIAL PROPERTIES OF A HONEYCOMB

This section discusses the various factors that influence the material properties and blast response of a honeycomb core. It is important to note that the aluminium honeycombs are considered strain-rate independent [31].

2.2.1 Effect of loading direction

In a honeycomb, a uniaxial loading in the direction parallel to the prismatic cell is called the out-of-plane loading (i.e. in the X_3 direction in Figure 2-3). The in-plane loading refers to the uniaxial loading applied in the X_1 and X_2 directions. The out-of-plane strength of a honeycomb is higher than the in-plane strength because the first is governed by axial deformation and the latter is pre-dominantly bending [26].

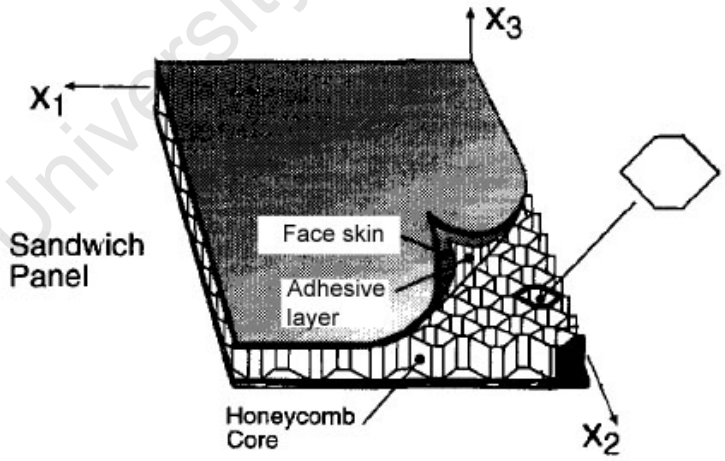

Figure 2-3: A schematic example of a honeycomb sandwich panel [41]

2.2.2 Effect of branch angle on material properties

Yamashita and Gotoh [40] investigated the effect of branch angle and foil thickness on the crush strength of bare honeycomb core with a constant cell size. Most results are numerical simulations and only a limited number of experiments were performed. The results are shown in Figure 2-4, where the open marks are computation and the solid marks are quasi-static experimental data. The numerical simulations involved branch angles from 30^o to 180^o and foil thicknesses from 0.02mm to 0.12mm. Yamashita and Gotoh [40] concluded that by changing the lateral expansion ratio of the honeycomb core, the crush strength can be manipulated. Considering the whole compressed area (as shown in Section 2.2.5), the crush strength increases with decreasing branch angle and increasing foil thickness, as shown in Figure 2-4.

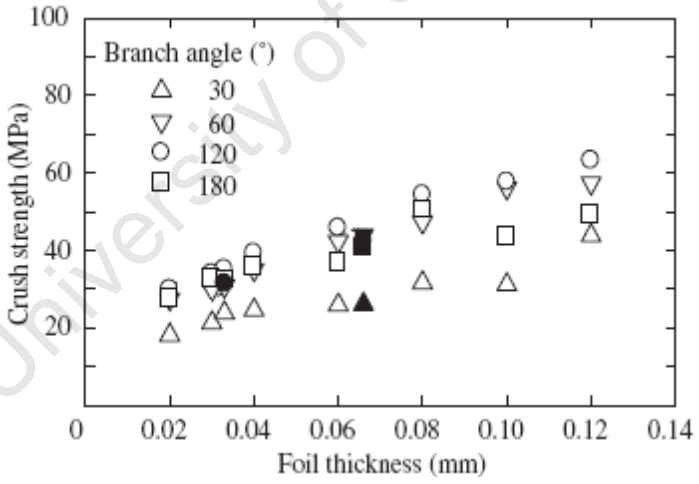

Figure 2-4: Relationship between crush strength, branch angle and foil thickness [40]

2.2.3 Effect of bonding between the cell walls

The bonding between the cell walls of the honeycomb core provides structural rigidity. In an adhesively bonded honeycomb core, the cell walls buckle by first

breaking the bond between the walls [39]. This is referred to as “peeling off”, which was also observed by Yamashita and Gotoh [40]. Yamashita and Gotoh [40] reported that the peeling process requires additional work from the applied force. In a welded honeycomb, the peeling effect can be negligible since the bonded area is intact because of the relatively high weld strength. However, in the case of a honeycomb bonded by adhesive, the peeling effect causes in-plane (i.e. in the X_1 or X_2 directions in Figure 2-3) distortion [39].

2.2.4 Effect of cell size

According to Hexcel Composites [38], a smaller cell size provides the core more area for bonding with the face skin. In addition, it provides more structural support and higher rigidity in the same area. Furthermore, the manufacturing cost will be increased with decreasing cell size.

2.2.5 Effect of relative density

Relative density is one of the most important characteristics of a cellular solid. The properties (such as the plateau stress) of a cellular solid depend on the value of the relative density. Relative density relates the honeycomb geometry to the way the honeycomb responds to load.

An increase in the relative density increases the relative cell wall thickness and reduces the pore space. This makes the cells more resistant to collapse, resulting in a higher plateau stress, and reduces the strain at which densification starts. The effect of

increasing relative density is shown in Figure 2-5. It is clear increasing the relative density increases the strength of the cellular solid.

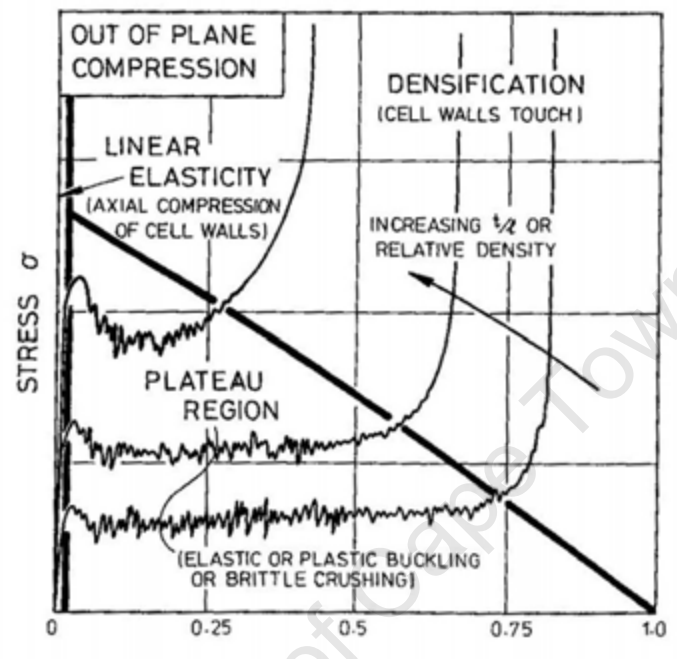

Figure 2-5: Stress-strain curves for honeycombs of different relative densities subjected to out-of-plane compression [26]

Due to the symmetry of the structure, the honeycomb can be regarded as a sequence of columns with Y cross-section, as analysed in [31, 39, 40]. The model is shown in Figure 2-6. This accounts for both the single and the double foil portions. From the model, the relative density of the honeycomb can be calculated by:

$$\textit{Relative density (\%)} = \frac{\textit{Density (H/c)}}{\textit{Density (Al)}} = \frac{\textit{Area (H/c)}}{\textit{Area (model)}} \qquad \textbf{Eq 2.1}$$

Where $\textit{Area (H/c)} = h(l + c)$

And $\textit{Area (model)} = l\sin(\alpha/2)(c + l\cos(\alpha/2))$

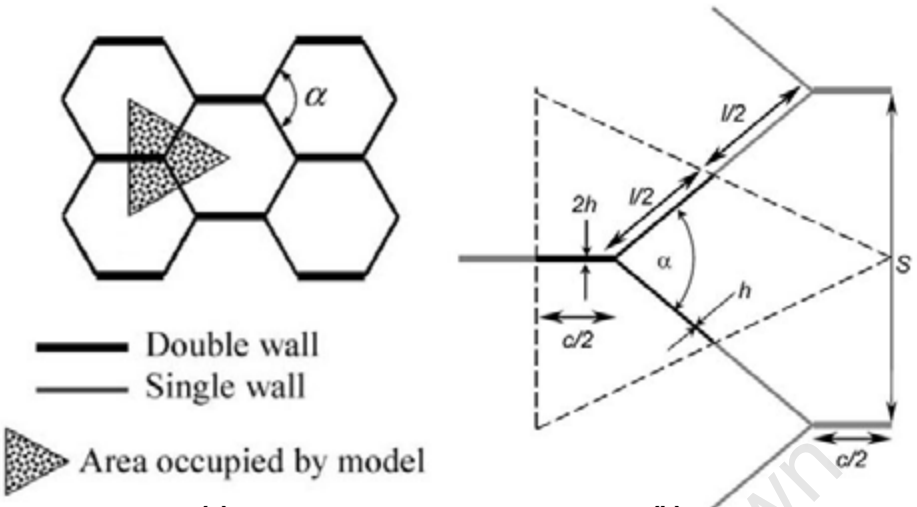

(a) (b)

Figure 2-6: A hexagonal cell structure (a) [40]; and an enlargement of the Y cross-section in the model (b) [31]

Similarly, the elastic modulus of the honeycomb can be calculated as:

Elastic modulus (H/c) = Relative density (%) x Elastic modulus (Al) **Eq 2.2**

The porosity of the honeycomb is defined as the fraction of pore space in the honeycomb [26]. This can be calculated by:

Porosity (%) = 100% - Relative density (%) **Eq 2.3**

2.3 HONEYCOMB FAILURE MODES

Nurick et al [30] investigated the behaviour of aluminium honeycomb sandwich panels subjected to intense air blasts. The face sheets were made of mild steel of thickness 1.6mm and the core was made of aluminium honeycomb of thickness 13mm. The failure modes of the honeycomb core are as follows:

- Micro-buckling of the honeycomb cells, as shown in Figure 2-7;
- Global bending of the core, as shown in Figure 2-8.

Figure 2-7: Micro-buckling is observed on the deformed cell wall [30]

Figure 2-8: Global bending exhibited on a blasted honeycomb [30]

2.3.1 Progressive buckling

Progressive buckling can be understood by examining the way a thin-walled square tube buckles under axial compression. It is found that thin-walled square tube and hexagonal honeycombs cells buckle in a similar manner when compressed axially [27].

A typical force-axial displacement curve is shown in Figure 2-9(a) for a thin-walled square tube subjected to axial compressive loading. After the initial peak load, sequential buckles are formed and each pair of peaks corresponds to the formation of a buckle. This phenomenon is called progressive buckling. This characteristic is highly desirable in an impact situation, where the structure "offers a constant deceleration throughout the entire stroke" [4]. It is most desirable when the material is crushed as much as possible, as shown in Figure 2-9(b) for a thin-walled square tube. This ensures maximum use of the tube material to provide a long stroke.

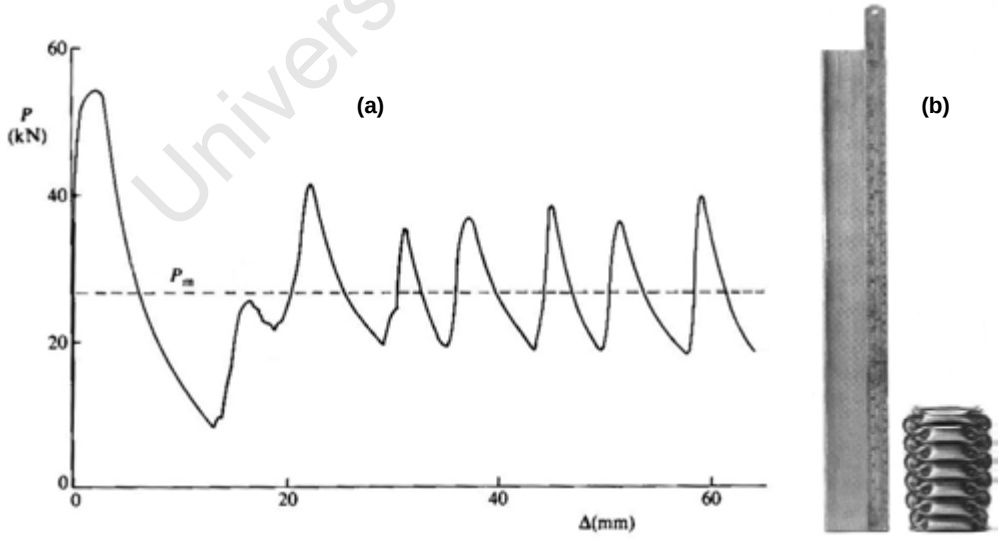

Figure 2-9: The axial compression of a thin-walled square tube.

(a) Force-displacement curve, (b) The original tube and the fully compressed tube [4]

2.3.2 Collapse modes of thin-walled square tubes

There are three collapse modes for progressive buckling of square tubes with a mean width W_m and a mean wall thickness H_m [4]. The symmetric crushing mode, as shown in Figure 2-9(b), is predicted for approximately $W_m / H_m > 40.8$ [4]. The extensional mode of crushing, as shown in Figure 2-10, is predicted for approximately $W_m / H_m < 7.5$ [4]. The asymmetric mixed crushing mode, Figure 2-11, is predicted for $7.5 \leq W_m / H_m \leq 40.8$ [4].

Figure 2-10: Extensional mode of crushing for thin-walled square tube [4]

Figure 2-11: Asymmetric mixed crushing mode exhibited on a thin-walled square tube [4]

In addition, "an overall instability can develop for thin-walled tubes which are long compared with the overall dimensions of the cross-sections" [4]. This leads to the Euler mode. Euler mode is when a plastic hinge mechanism develops in the tube,

folding the tube over itself, as seen in Figure 2-12. This is highly undesirable because it greatly reduces the energy absorption.

Figure 2-12: Aluminium tube crushed in Euler mode [42]

2.3.3 Typical stress-strain curve for honeycomb compression

As mentioned in Section 2.3.1, the axial loading behaviour of the honeycomb cells is similar to that of the thin-walled square tubes. A typical stress-strain curve of a honeycomb panel subjected to axial compression is shown in Figure 2-13.

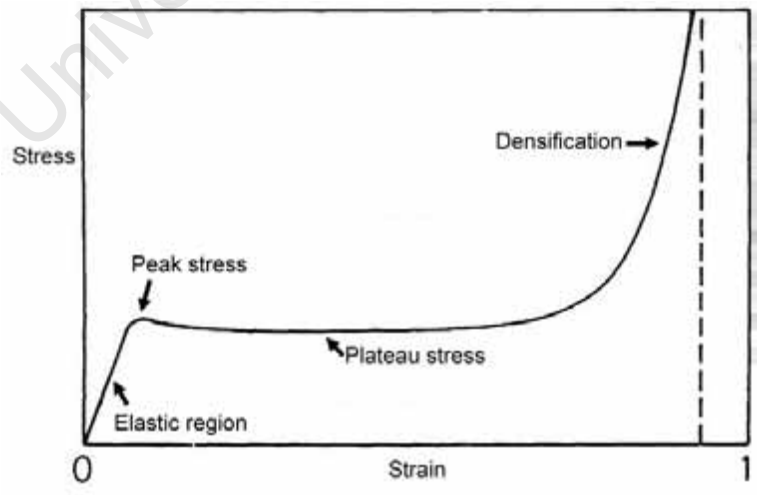

Figure 2-13: A typical engineering stress-strain graph showing compression stages [26]

When strain is applied to the honeycomb, a linear-elastic region is observed. The honeycomb is loaded and the load causes an elastic deformation, which is recoverable. The stress increases with increasing strain, until a critical stress is reached. This stress is called the peak stress or the yield stress.

With further increase in strain, the cells start to collapse. A plastic hinge is formed and the walls fold in a periodic way, as shown in Figure 2-14. Progressive buckling takes place and it results in permanent deformation. The successive lobe formation causes each subsequent peak which corresponds to the onset of a folding process [27]. The mean average of the fluctuation is called the plateau stress, as shown in Figure 2-13. The plateau stress can be described as a long, almost flat, plateau in the stress-strain curve [26].

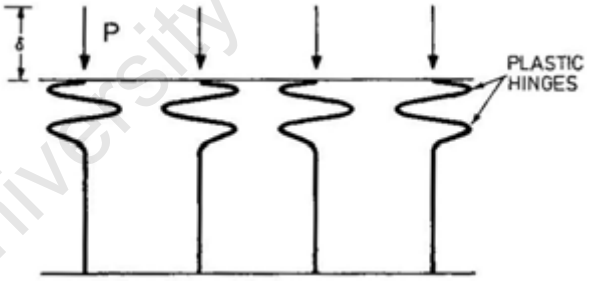

Figure 2-14: As the cell walls compress, plastic hinges are formed [26]

When the honeycomb is loaded, a large proportion of the energy is absorbed by the plastic buckling of the cells. At the same time, the stress transfer is limited to the plateau stress [26]. The combination of the two characteristics (i.e. energy absorption

and limited stress transfer) makes the honeycomb a potential core material for sandwich panels used to provide resistance against impact or blasting.

With further increase in strain, there is a steeply rising stress. This is called the densification region, as shown in Figure 2-13, which starts at approximately 70-75% strain [26, 37]. This is when the honeycomb foil starts to concertina into a “solid block” [37] and the density starts to reach the density of the solid from which the cell walls are made [26].

2.4 MANUFACTURING OF HONEYCOMB PANELS

A schematic example of a honeycomb sandwich panel is shown in Figure 2-3. It has an adhesive layer joining the face skin to the hexagonal core. A honeycomb can be manufactured in at least four ways: corrugated, expanded, moulded, and extruded [26]. Different material honeycombs are produced using different processes. A metal honeycomb core (such as the hexagonal core in Figure 2-3) is made by partially bonding thin sheets using an adhesive in a stripe pattern. The adhesive used must flow sufficiently to form a fillet and fill the gaps between the bonding surfaces [38]. The stack of sheets is then laterally expanded to create a honeycomb. The stripe pattern of the adhesive gives the cell walls single and double foils on different edges.

After the core is made, it can then be bonded to the face skin (as shown in Figure 2-3); using one of three methods: heated press, vacuum bag processing, and matched mould processing [38]. Depending on the requirements of the final sandwich product, the appropriate manufacturing method is used. A heated press is suitable for large flat sheets; the vacuum bag processing is used to provide flexible panels; and matched mould processing allows for high levels of tolerance and surface finish [38].

In this study, the purchased honeycomb panels were manufactured using the heated press method, as shown in Figure 2-15. A carrier cloth is added to the adhesive to restrict the movement of the adhesive during manufacturing.

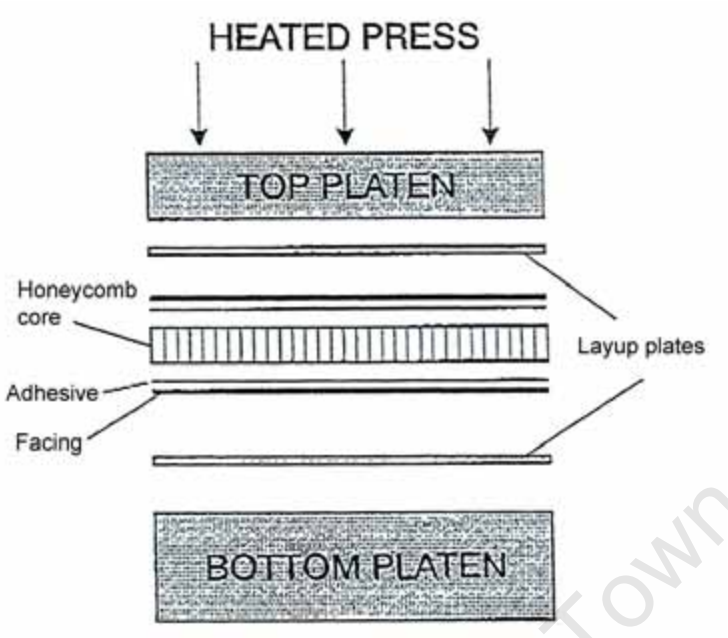

Figure 2-15: Diagram illustrating the manufacturing of a honeycomb sandwich panel using the heated press method [38]

2.5 FEATURES AND APPLICATIONS OF HONEYCOMB SANDWICH PANELS

Honeycomb sandwich panels have high specific strength, stiffness and good energy absorption. The porosity in the core provides reduction in weight but maintains some of the mechanical properties of the base material (as discussed in Section 2.2). The core increases the overall panel stiffness by increasing the second moment of area. In addition, the cellular structure offers better energy absorption than a solid structure of the same density [27]. Furthermore, the honeycomb core has good durability; is maintenance free; and is cost effective to produce.

The impact behaviour of the panel is influenced by the core properties (relative density, strength and ductility); the core geometry; the face plate material properties (yield strength and stiffness) and the panel configuration [43]. In particular, the ability of the honeycomb to develop high strains before densification. Prior to densification, the stress transfer through the honeycomb core is limited by the plateau stress of the core (as described in Section 2.3.3). This property of honeycomb sandwich panels can be manipulated to manage the impulse transfer to the rear of the panel in a crash or blast loading scenario.

The combination of the above features attracts designers to use honeycomb sandwich panels at the bottom of lift shafts; in aircrafts and space shuttles; in high speed trains; and in transport packaging [37].

2.6 GENERATING AIR BLAST LOADING

The blast loading applied to the sandwich panel is generated using plastic explosive. The blast wave from the explosion imposes impulsive or dynamic blast loads on objects in its path causing deformation or tearing. In laboratory scale experiments (such as those performed in the Blast Impact and Survivability Research Unit (BISRU) blast chamber), the plastic explosive is mounted onto a polystyrene pad, which is attached to the test specimen clamped on a ballistic pendulum. The impulse is calculated from the oscillation of the pendulum, as shown in Appendix A.

2.6.1 Localised blast loading

To generate a localised blast loading, explosive is laid out in a disc shape and attached to a polystyrene pad ranging between the thicknesses of 12mm to 16mm [44], as shown in Figure 2-16. Explosive height and diameter are arranged according to the desired loads [44]. Nurick and Radford [45] used this experimental technique to study the failure modes of mild steel circular plates subjected to localised blast loading.

2.6.2 Uniformly distributed blast loading

Conversely, to generate a uniform blast loading, the sheet explosives are positioned in concentric annuli of the shape of the plate and connected by a cross-leader of explosive, as shown in Figure 2-16. The arrangement is assumed to provide a uniform distribution of the loading over the surface area of the plate. Teeling-Smith and Nurick [2] used this experimental technique to investigate the failure modes of mild steel circular plates subjected to uniformly distributed blast loading.

A second way of generating uniformly distributed blast loading is to stand off the explosive and direct the blast wave down a tube towards the test specimen, as shown in Figure 2-17. Jacob et al [46] used this experimental technique to investigate the failure modes of mild steel circular plates at varying stand-off distances.

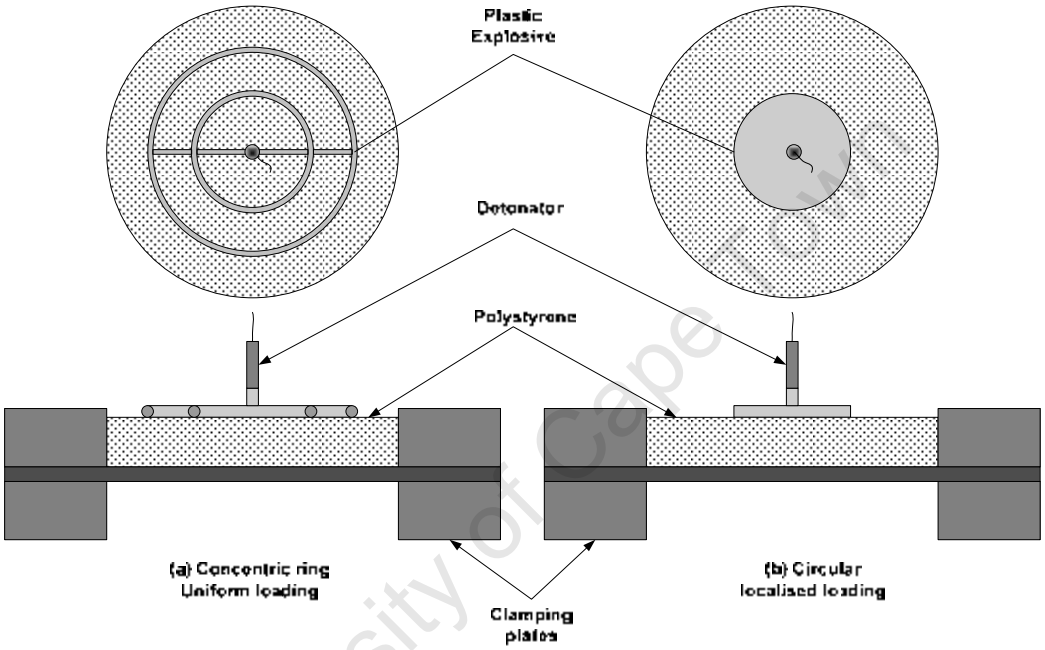

Figure 2-16: Schematic diagram of the two explosive geometries [44]

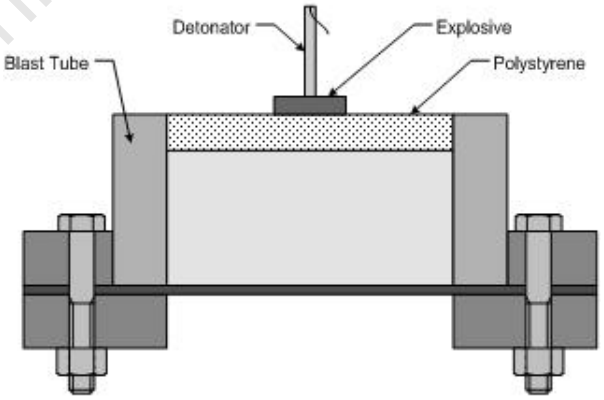

Figure 2-17: Schematic diagram of generating uniformly distributed blast loading using a blast tube [44]

2.6.3 Effect of stand-off distance

The stand-off distance between the explosives and the object governs the intensity of the blast load the object will experience. The relationship is described by Hopkinson-Cranz or "cube root" scaling as given in Eq 2.4 [44, 47, 48]:

$$\frac{r}{m^{1/3}} = K \qquad \textbf{Eq 2.4}$$

Where r is the stand-off distance; m is th charge mass and K is the scaled distance.

If the charges are of the same explosive material it follows that:

$$\frac{r_1}{r_2} = \left(\frac{m_1}{m_2}\right)^{1/3} \Rightarrow \frac{r_1}{m_1^{1/3}} = \frac{r_2}{m_2^{1/3}} = K \qquad \textbf{Eq 2.5}$$

Eq 2.5 shows that identical blast load intensity is produced by two explosions of the same explosive material at distances which are proportional to the cube root of the respective charge mass [47]. In other words, to produce a given blast intensity at twice a given distance requires eight times the charge mass. Therefore, for the same charge mass, increasing the stand-off distance, decreases the blast load intensity.

Jacob et al [46] studied the effect of stand-off distance on the response of fully clamped circular plates subjected to blast loading. Varying the tube length varied stand-off distances, as shown in Figure 2-18. Jacob et al [46] observed large global dome plate deformation profiles for stand-off distances (ranging from 100mm to 300mm) greater than the plate radius (53mm). This deformation profile concurred with experimental results reported by Teeling-Smith and Nurick [2] for uniformly loaded circular plates. Jacob et al [46] concluded that for stand-off distances greater

than the plate radius, the loading is considered uniformly distributed over the entire plate area.

Figure 2-18: Mild steel tubes used in the experiments to investigate the stand-off effect [44]

2.7 FACE PLATE FAILURE MODES

Menkes and Opat [1] performed experiments on fully clamped aluminium beams subjected to impulsive loading. The investigation was the first to define the different failure modes for structures subjected to impulsive loading, as shown in Figure 2-19.

Mode I – large inelastic deformation

Mode II – tearing (tensile failure) in outer fibres, at or over the support

Mode III – transverse shear failure at the support

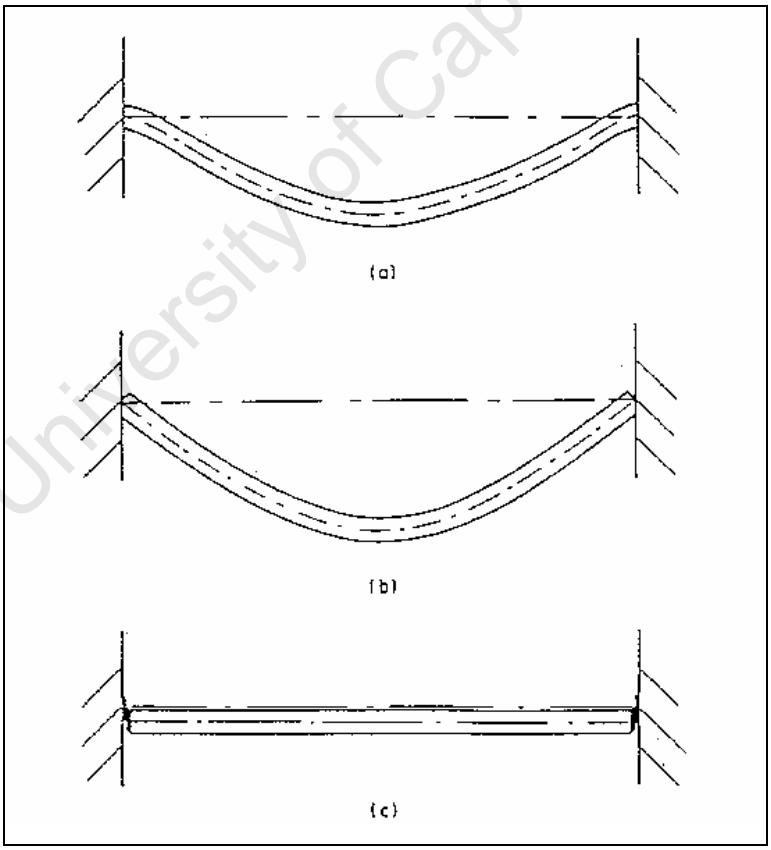

Figure 2-19: Deformation profiles for impulsively loaded plates – (a) Mode I, (b) Mode II, (c) Mode III [2]

Teeling-Smith and Nurick [2] then investigated the response of circular plates subjected to uniformly distributed impulsive loading. Teeling-Smith and Nurick [2] observed similar plate deflections to Menkes and Opat [1]. The change of deformation profile is shown in Figure 2-20. It shows that the plate deflection increased with increasing impulse and thinning occurred (Mode I failure in Figure 2-20). As the impulse increased further, partial tearing at the boundary occurred, followed by complete tearing. Further increase in impulse resulted decreasing mid-point plate deflection, and the plate response changed from complete tearing to complete shearing.

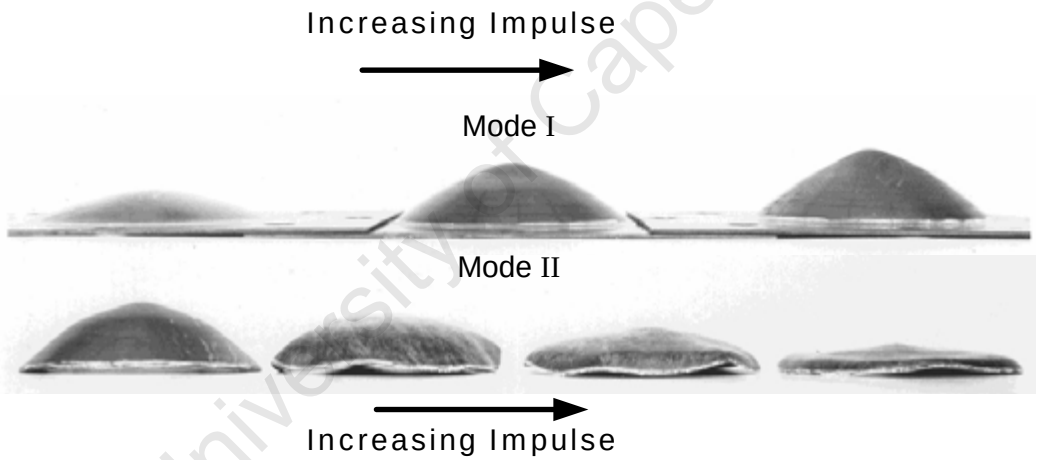

Figure 2-20: Change of deformation profile with increasing impulse (for circular plates subjected to uniformly distributed impulsive loading) [2]

Thereafter, Nurick et al [49] investigated the necking response of clamped circular plates subjected to uniformly loaded air blasts. Nurick et al [49] refined Mode I failure:

Mode I – large inelastic deformation with no necking at the boundary

Mode Ia – large inelastic deformation with necking around part of the boundary

Mode Ib – large inelastic deformation with necking around the entire boundary

In addition, Nurick and Shave [3] performed experiments on square plates subjected to uniformly distributed impulsive loading. The study refined Mode II for the various tearing conditions, as shown in Figure 2-21 and Figure 2-22.

Mode II* – large inelastic deformation with partial tearing around part of the boundary

Mode IIa – increasing mid-point deflection with increasing impulse with complete tearing at the boundary

Mode IIb – decreasing mid-point deflection with increasing impulse with complete tearing at the boundary

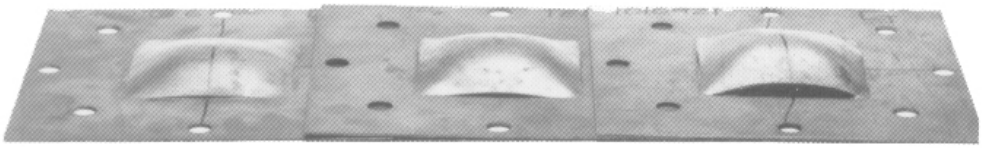

Figure 2-21: Increasing mid-point deflection for increasing impulse with partial tearing along plate boundary (uniformly loaded square plates) [3]

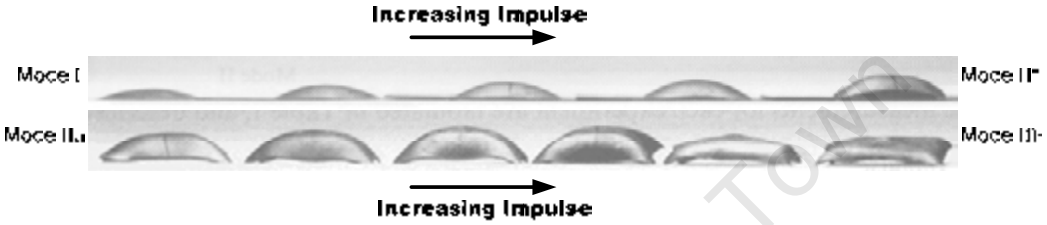

Figure 2-22: Changing mid-point deflection for increasing impulse (uniformly loaded square plates) [3]

2.8 AIR BLAST TESTING OF METAL HONEYCOMB SANDWICH PANELS

In recent years, attention has focused on the blasting response of sandwich panels [7-40]. Experiments have been performed for aluminium honeycomb sandwich panels under quasi-static and impact loading [16, 25-34, 37-40]. However, there are limited studies on the response of circular aluminium honeycomb sandwich panels under blast loading [28-31].

2.8.1 Mechanical response of metallic honeycomb sandwich panel structures to high-intensity dynamic loading

Dharmasena et al [32] investigated the response of stainless steel square honeycomb sandwich panels subjected to air-blasting. The core was brazed onto the face plates. The exposed area of the panels was 410x410mm. Three experiments were performed at a constant stand-off distance of 100mm. The same experiments were performed on solid plates with equal areal density. Dharmasena et al [32] identified three stages of the response of the sandwich components to blast loading, as shown in Figure 2-23.

- **Stage I** – The explosive is detonated near the front plate. A high pressure impulse I_0 propagated towards the front plate. Part of the impulse loading is reflected off the front plate (shown as I_r) and the rest of the impulse loading is transmitted via the front plate to the core (shown as I_t). By the end of Stage I, the front plate moves at a velocity V_1, and the back plate is not moved.

- **Stage II** – The front plate deforms most at the centre. The crush of the core follows the front plate deformation profile. The front plate velocity and deformation are slowed by the core crushing. During this stage, there is no movement of the back plate.

- **Stage III** – Global panel bending occurs. The front plate stretches and the core collapses, transmitting stress to the back plate, which deforms accordingly. The intensity of the transmitted force from the core to the back plate is dependent on the dynamic crush strength of the core, which is in turn dependent on its relative density, cell topology and the base material properties [26]. The amount of panel bending is dependent on the core crush resistance.

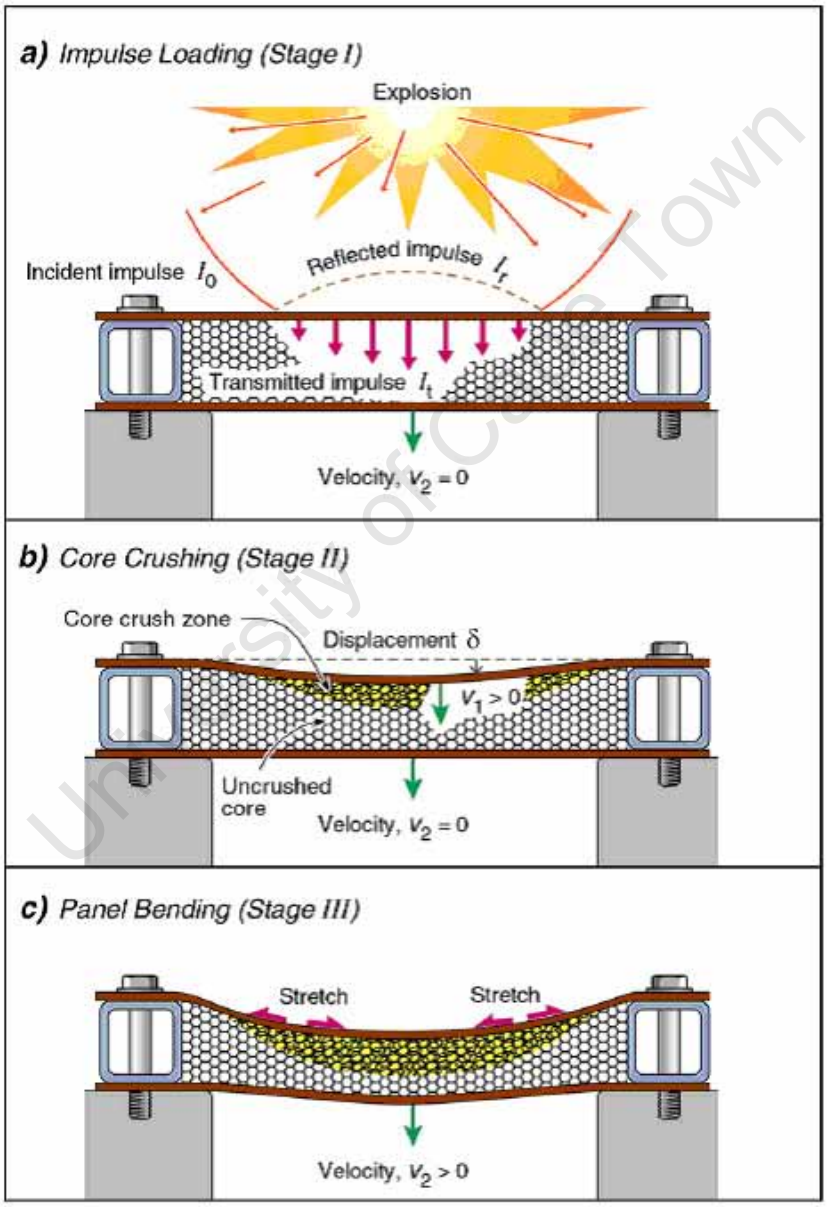

Figure 2-23: The three stages of sandwich panel response to blasting [32]

Photographs of the sandwich panel deformation are shown in Figure 2-24. Cell wall buckling and core densification increased with increasing impulse. Nurick et al [30] observed similar plate and honeycomb failure modes (up to the point of tearing). In addition, at lower specific impulses (up to 21.5kPa.s), the buckling of the cell occurred at the upper segment of the core and the lower segment remained planar and undeformed. This also concurred with the findings of Xue and Hutchinson [50].

Dharmasena et al [32] also performed numerical simulations and obtained good agreement between the simulations and the experimental results. However, core debonding from the front plate, which is shown in the experimental photographs in Figure 2-24, was not captured by the simulation. The sandwich panel had lower back plate deflection than the solid plate. However, after complete core crushing, the advantages of the sandwich panel (as compared to the solid plate) are diminished.

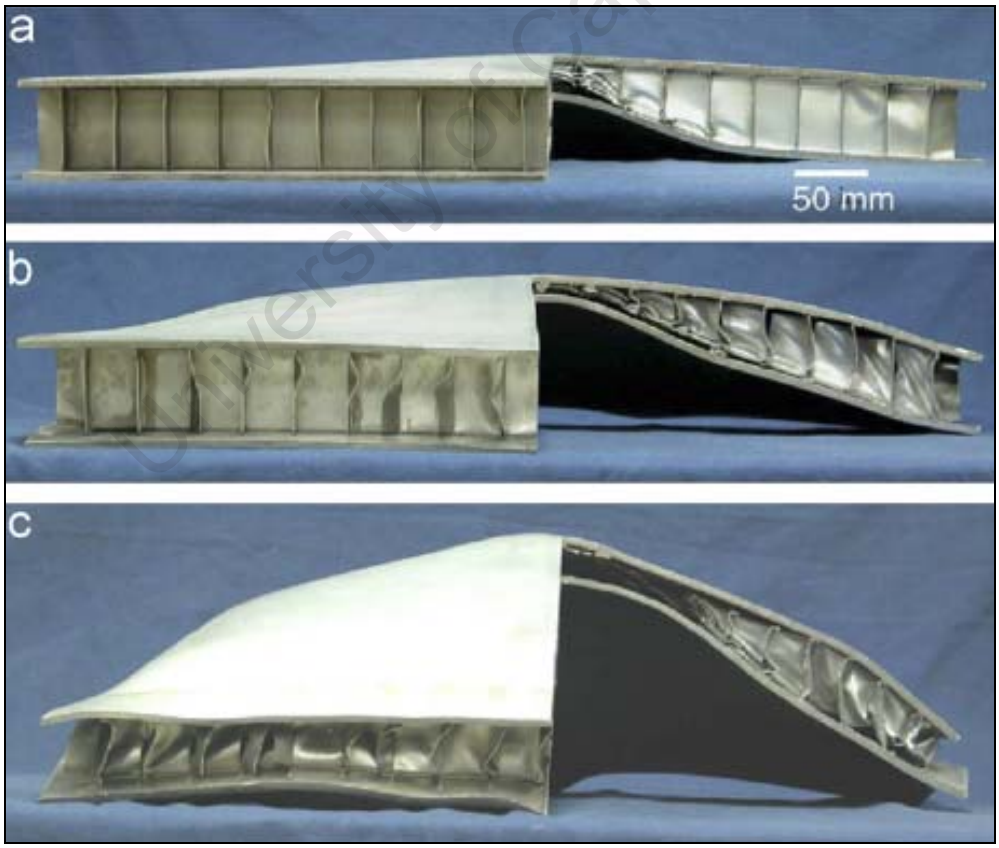

Figure 2-24: Photographs of half sectioned square honeycomb sandwich panels subjected to impulse loads of (a) 21.5kPa.s, (b) 28.4kPa.s and (c) 33.7kPa.s [32]

2.8.2 Previous experimentation on honeycomb sandwich panels

Nurick et al [30] investigated the behaviour of clamped circular aluminium honeycomb sandwich panels subjected to intense air blast. The sandwich panel consisted of 1.6mm mild steel face plates sandwiching a 13mm thick aluminium honeycomb core. The circular exposed area has a diameter of 106mm. Stand-off distances of 150mm and 13mm were chosen to create the assumed uniform and localised loading (see Section 2.6.3). The explosive PE4 was used to generate the blast. The applied impulse was measured by the ballistic pendulum. The response of the plates was compared to that using an air-gap core of the same thickness.

The graph comparing the back plate deflections of the sandwiches with air and aluminium honeycomb cores is shown in Figure 2-25. The results showed that at impulses above 20Ns, the back plate of the honeycomb sandwich panel deformed less than that of the air-gap sandwich panel. The honeycomb core absorbed energy through micro-buckling and global bending. Conversely, at impulses lower than 20Ns, the air-gap sandwich panel exhibited lower back plate deformation than the honeycomb sandwich panel, as shown in Figure 2-25. This was because of the load transfer from the front plate through the honeycomb core to the back plate, which did not occur in the case of the air-gap.

Another interesting point to note was that under localised loading, the honeycomb torn at impulse as low as 10.9Ns. Once the honeycomb reached full densification or is torn, the honeycomb is no longer useful for limiting force transfer. In this case, the area of honeycomb contributing to energy absorption was not at the maximum. Based on this and the plate deformations, it was clear that the sandwich performed better under uniform loading than localised loading.

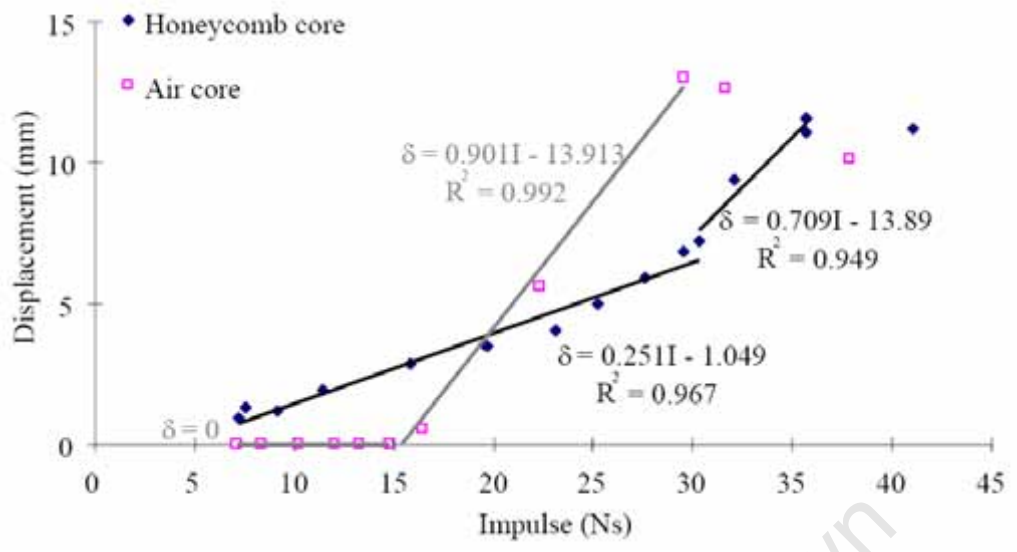

Figure 2-25: Graph of back plate displacement versus impulse for the uniformly loaded mild steel sandwiches with air and aluminium honeycomb cores [30]

2.8.3 Preliminary finite element simulations

Finite element simulations were performed by Karagiozova et al [31] based on the experimental data from Nurick et al [30], up to the point of tearing. The Y cross-section described in Section 2.2.5 was used to calculate the density of the honeycomb core. The core was modelled as a solid whose properties mimic those of the hexagonal cells. The blast loading was simulated by representative pressure-time histories. The simulation was first validated using the experimental results, which compared reasonably well [31]. Thereafter simulations were performed to investigate the effects of core thickness, load duration and panel flexibility.

- **Effect of core thickness**

Karagiozova [51] explained that the sandwich panel can be represented by two semi-rigid plates (i.e. the mild steel face plates) sandwiching a softer material (i.e. the alminium honeycomb core). Before densification, the stress transmitted to the softer material follows the shape of the stress-strain curve as shown in Figure 2-26, which is a simplified representation of Figure 2-13. As the strain increases so the stress increases along the plateau line. Provided that the applied impulse produces strain within the plateau region, the stress transferred stays equal to the plateau stress of the

material. However, if the applied impulse produces greater strain than the densification strain, then the stress transferred jumps directly from the plateau stress to a much higher magnitude stress. Due to the plateau stress and the densification characteristics of the softer material, a shock wave may be produced in the core.

For aluminium honeycomb, densification takes place at approximately 70-75% strain, regardless of the core thickness [26, 37]. Therefore, using a thicker core physically delays the onset of densification. Consequently, using a thicker core decreases the back plate deformation.

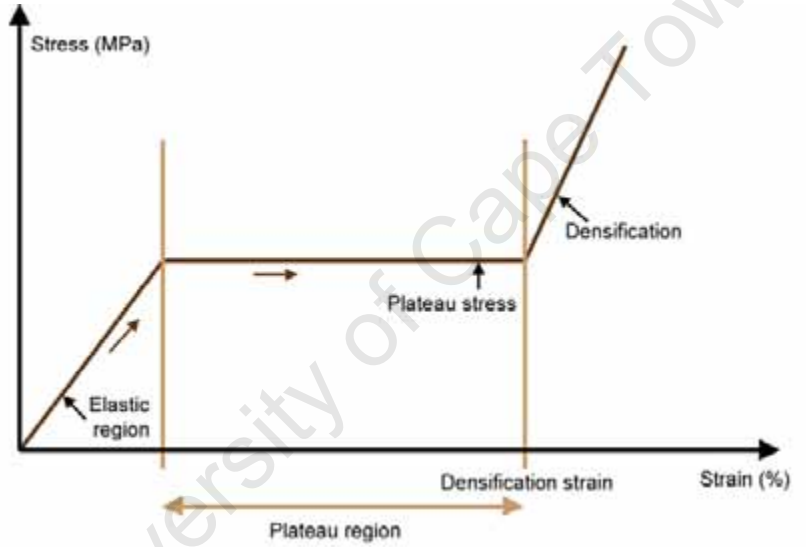

Figure 2-26: Simplified engineering stress-strain graph for a typical aluminium honeycomb

- **Effect of load duration**

The applied impulse is a function of the integral of pressure with respect to time, as shown in Eq 2.6 [31]. This can be represented by the idealised triangular pressure-time history in Figure 2-27, where the area under the curve is the applied impulse. Keeping the applied impulse constant and shortening the time will result in a peak pressure increase. As pressure increases so velocity increases. As can be seen in Eq 2.7 [31], stress transferred is a function of velocity. Therefore making the load duration shorter increases the plate deformation.

$$I = \pi R_p^{\,2} t_0 \int_0^{R_p} p(r_0) dr_0 \qquad \text{Eq 2.6}$$

$$\sigma = \sigma_p + \Delta\sigma \qquad \Delta\sigma = \rho_c (V_f - V_b)^2 / \varepsilon_D \qquad \text{Eq 2.7}$$

Where I is the applied impulse; r_0 is the current radius; R_p is the plate radius; p is pressure; t is time; σ is stress; ρ_c is density of the core; V is velocity and ε is strain.

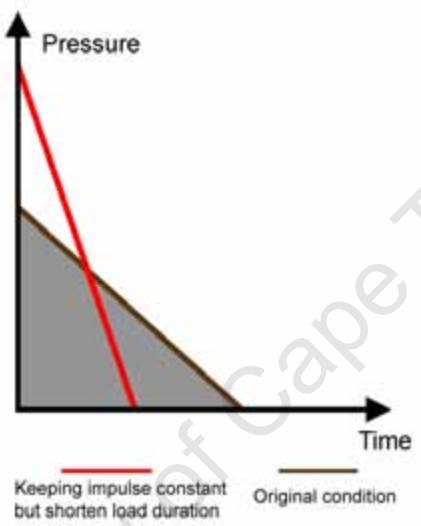

Figure 2-27: Pressure-time history showing the effect of load duration variation

2.8.4 Deformation and failure of blast-loaded metallic sandwich panels

Zhu et al [34] investigated the blast resistance of square sandwich panels with metallic face sheets and honeycomb cores subjected to explosion. The face sheets were made of annealed aluminium alloy, and the HexWeb® aluminium honeycomb core had hexagonal cells. The square panel had an exposed area of 250x250mm and a 12.5mm thick core. TNT was detonated at a stand-off distance of 200mm in free air to produce the blast loading. The applied impulse was measured by the ballistic pendulum.

The study investigated the effect of foil thickness, cell size, mass of charge, relative density of the core, and the face-sheet thickness. The results focused on the back plate response. It showed that increasing the face-sheet thickness decreased the back plate

deflection, but also increased the weight of the panel. It was also found that increasing the foil thickness and increasing the honeycomb relative density both decreased the back plate deflection. Increasing the cell size increased the back plate deflection; and this effect is especially noteworthy for panel with thinner face sheet.

3 - MATERIAL CHARACTERISATION

This chapter introduces the materials used. These include the mild steel face plates and the aluminium honeycomb cores.

3.1 MILD STEEL

The Zwick Universal 1484 Testing Machine in the Centre for Materials Engineering at the University of Cape Town (UCT) was used to perform tensile testing on mild steel specimens.

The tensile specimens were cut from the five mild steel sheets used, labelled A, B, C_3, C_5 and D. Sheet A has a nominal thickness of 1.0mm, whereas the rest of the sheets are 1.6mm thick. A strain rate of $10^{-3}s^{-1}$ was chosen. Heavy duty grips for flat samples were used to accommodate for the plain end specimens. The tests were performed at room temperature.

The specimens were rectangular in cross-section with a “dog-bone” shape. An engineering drawing has been included in Appendix B. The nominal gauge length was 80mm, and the nominal gauge width was 12.5mm. The tensile specimens for sheets C_3 and C_5 were not supplied by the manufacturer. A plate from each sheet was laser cut to produce four specimens. These tensile specimens have a nominal gauge length of 60mm.

3.1.1 Results & Calculations

The results are shown in Figure 3-1 and summarized in Table 3-1. The engineering stress-strain curves of each sheet have been included in Appendix C.

Assuming the mild steel to be rigid-viscoplastic, the constitutive Cowper-Symonds relation was used for the computation of the static yield stresses:

$$\frac{\sigma'_0}{\sigma_0} = 1 + \left(\frac{\dot{\varepsilon}}{D}\right)^{\frac{1}{q}} \qquad \textbf{Eq 3.1}$$

Where σ'_0 is the quasi-static yield stress; σ_0 is the static yield stress; $\dot{\varepsilon}$ is the strain rate; D and q are material constants with values of $40s^{-1}$ and 5 respectively.

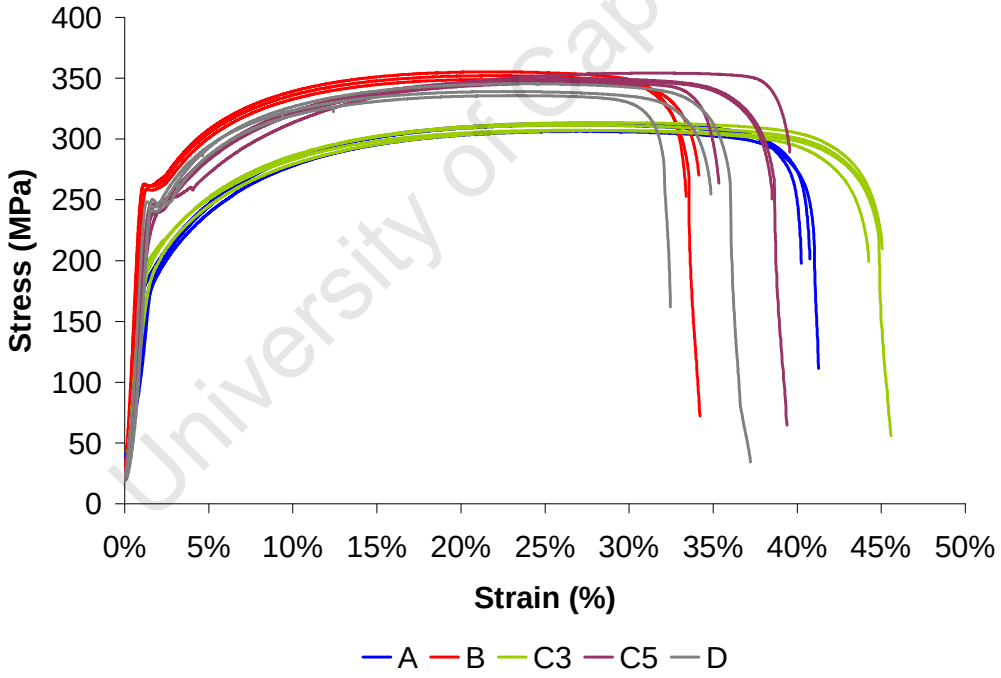

Figure 3-1: Engineering stress-strain curves of all mild steel sheets

Table 3-1: Information of mild steel sheets A, B, C_3, C_5 and D

Specimen Number	Thickness mm	Width mm	Cross-sectional Area m^2	Quasi-static stress MPa	Static Stress MPa	Final Elongation %
A-1	1.00	12.60	1.26E-05	190.11	169.76	37%
A-2	0.98	12.57	1.23E-05	189.50	169.22	38%
A-3	0.98	12.60	1.23E-05	184.08	164.38	35%
Mean average	**0.99**	**12.59**	**1.24E-05**	**187.90**	**167.78**	**37%**
B-1	1.59	12.55	2.00E-05	258.77	231.07	32%
B-2	1.57	12.58	1.98E-05	261.52	233.53	33%
B-3	1.56	12.57	1.96E-05	262.91	234.77	31%
Mean average	**1.57**	**12.57**	**1.98E-05**	**261.07**	**233.12**	**32%**
C_3-1	1.60	12.64	2.02E-05	206.19	184.12	42%
C_3-2	1.62	12.64	2.05E-05	201.58	180.00	42%
C_3-3	1.58	12.44	1.97E-05	195.39	174.48	43%
C_3-4	1.60	12.60	2.02E-05	193.63	172.90	42%
Mean average	**1.60**	**12.58**	**2.01E-05**	**199.20**	**177.87**	**42%**
C_5-1	1.60	12.56	2.01E-05	239.65	214.00	31%
C_5-2	1.60	12.60	2.02E-05	243.57	217.50	27%
C_5-3	1.62	12.44	2.02E-05	245.61	219.32	35%
C_5-4	1.60	12.50	2.00E-05	245.74	219.44	36%
Mean average	**1.61**	**12.53**	**2.01E-05**	**243.64**	**217.56**	**32%**
D-1	1.60	12.50	2.00E-05	254.11	226.91	37%
D-2	1.60	12.50	2.00E-05	248.92	222.28	31%
D-3	1.60	12.50	2.00E-05	244.19	218.05	34%
Mean average	**1.60**	**12.50**	**2.00E-05**	**249.07**	**222.41**	**34%**

3.1.2 Discussion

Sheets A and C_3 resulted in similar stress-strain curves, as shown in Figure 3-1. Sheet B, C_5 and D resulted in different stress-strain curve shape to sheets A and C_3, as shown in Figure 3-1. The distinct upper and lower yield points are evident. The quasi-static yield stresses of sheets B, C_5 and D are approximately 30% higher than that of sheets A and sheet C3. As a result, the static stresses of sheets B, C_5 and D are also approximately 30% higher than that of sheets A and C_3.

3.2 ALUMINIUM HONEYCOMB GEOMETRIC SPECIFICATIONS

This section catalogues the geometry information of the aluminium honeycombs. Three types of aluminium honeycombs were used. They were of thicknesses 13mm, 29mm and 150mm. All three types of specimens were examined under the Leica Stereo Microscope at the Centre of Materials Engineering at the UCT.

The 13mm and 29mm thick honeycombs were originally 14mm and 30mm thick honeycomb sheets manufactured with thin (0.5mm) aluminium skins. Redux 609 adhesive bonded the core to the skins. It is a blue flexible film containing cotton scrim for extra support. After careful removal of the aluminium skins, traces of Redux 609 and the cotton scrim were left on the honeycomb specimens. However, this was found to have little influence on the material behaviour [30]. Conversely, the 150mm thick honeycomb sheet was supplied without the adhesively bonded skins. Therefore, no adhesive was visible on this type of honeycomb.

3.2.1 Results

Figure 3-2 to Figure 3-4 show micrographs and photographs of the 13mm, 29mm and 150mm thick honeycombs, respectively. The relative density of each honeycomb was calculated using Eq 2.1. A summary of the measured dimensions and the calculated values is presented in Table 3-2.

Table 3-2: A summary of the honeycomb geometric information

Core thickness (mm)	Cell size *S* (mm)	Single wall length, *l* (mm)	Double wall length, *c* (mm)	Single wall thickness, *h* (mm)	Double wall thickness, *2h* (mm)	Branch angle, a (^{0})	Relative density (%)	Density (kg/m^3)
13	5.69	4	2.75	0.08	0.18	90^0	3.59%	96.21
29	6.43	3.83	3.39	0.07	0.16	106^0	3.09%	82.81
150	10.22	6.6	4.5	0.11	0.25	96^0	2.95%	79.06

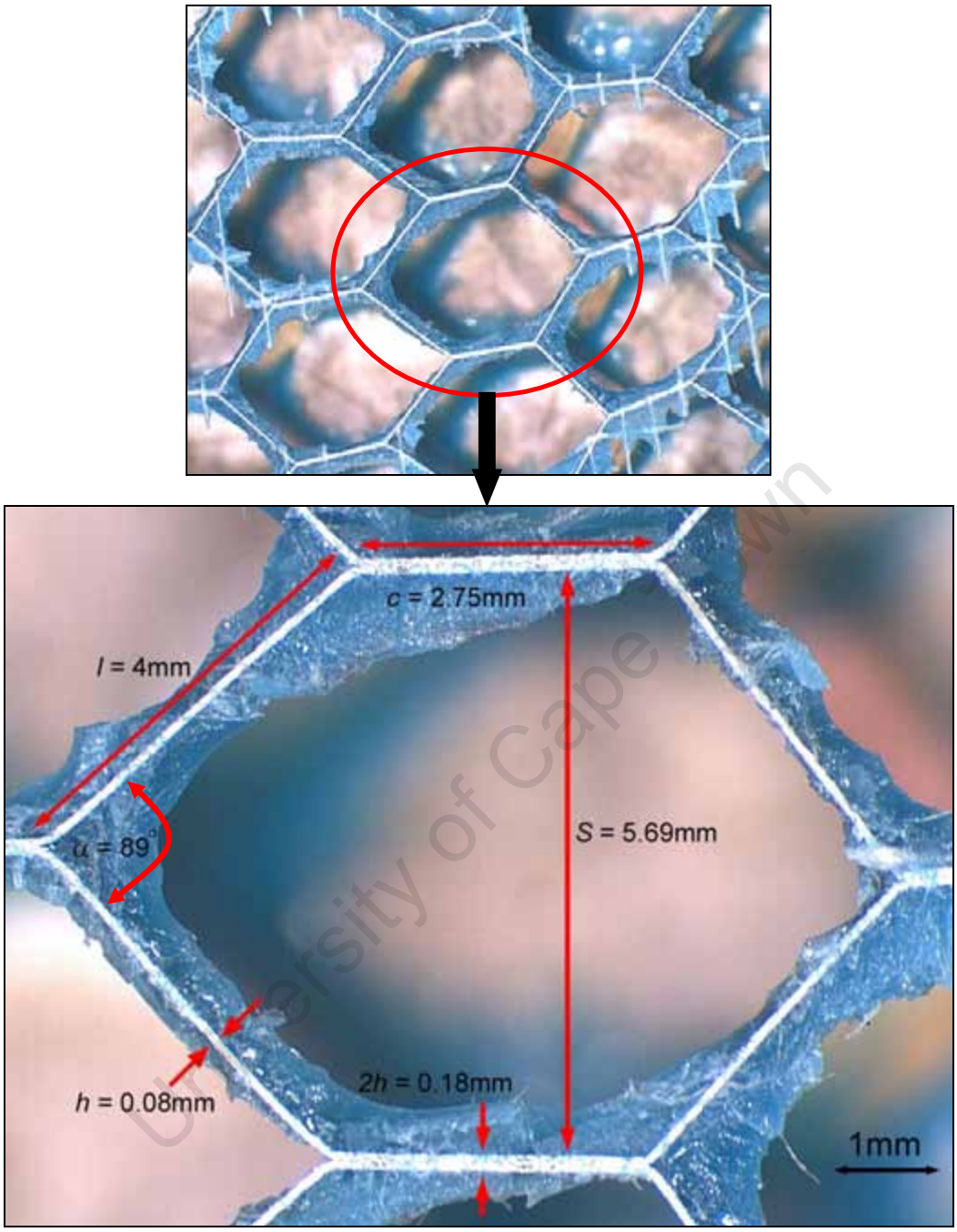

Figure 3-2: Micrographs of the 13mm thick honeycomb, showing a group of cells (top) and the enlargement of a single cell (bottom)

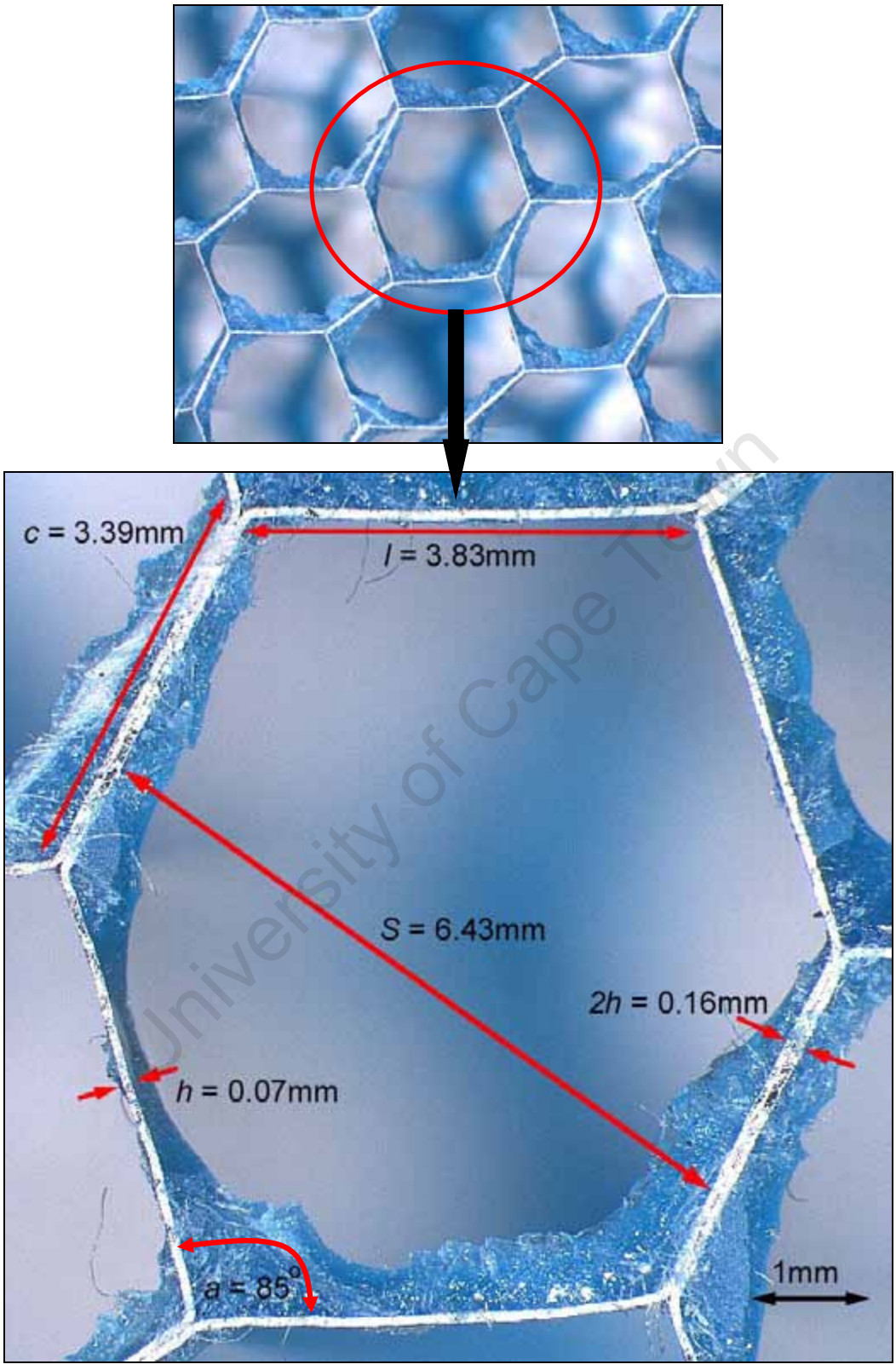

Figure 3-3: Micrographs of the 29mm thick honeycomb, showing a group of cells (top) and the enlargement of a single cell (bottom)

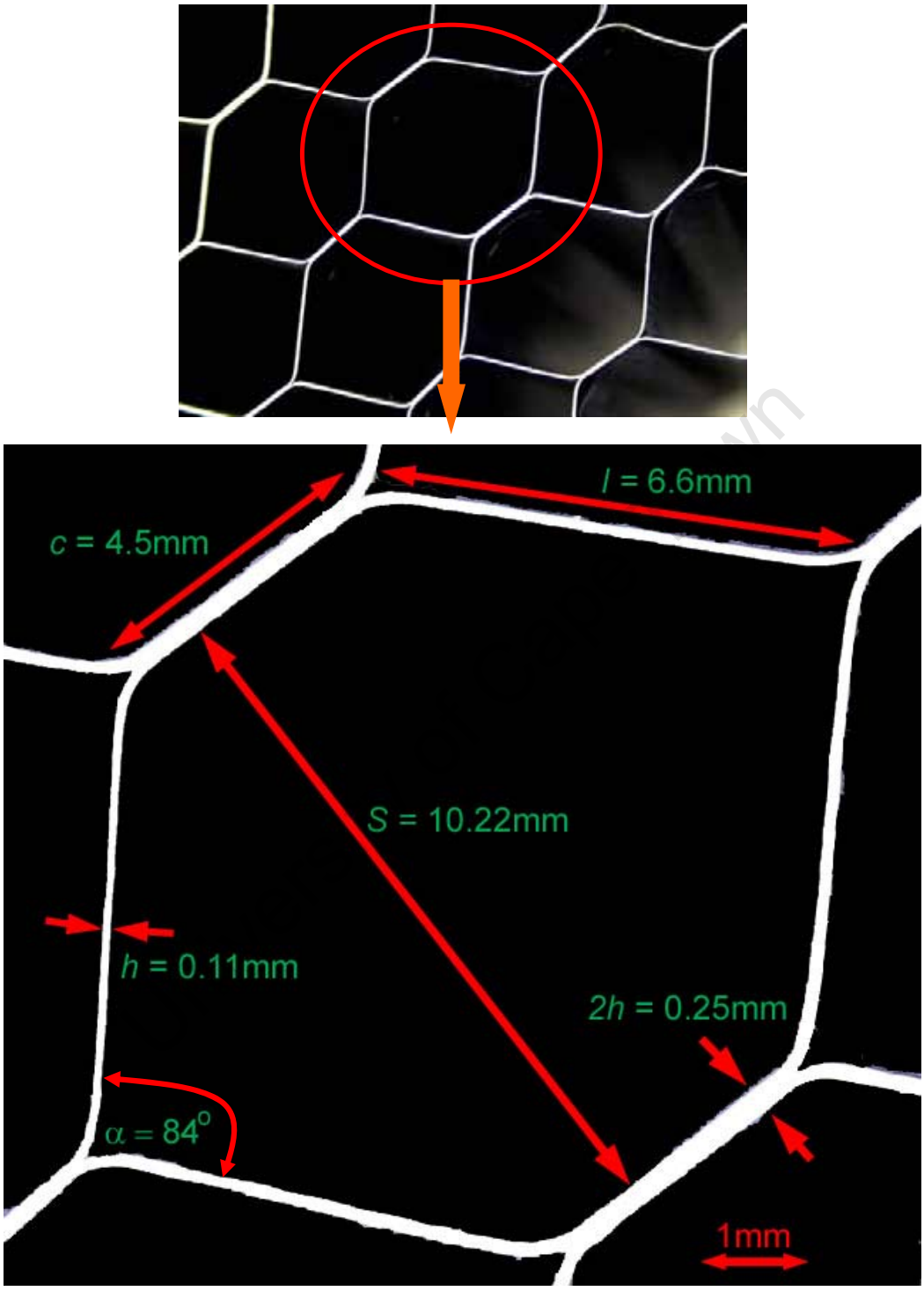

Figure 3-4: Photographs of the 150mm thick honeycomb, showing a group of cells (top) and the enlargement of a single cell (bottom)

3.2.2 Discussion

The influence of branch angle and foil thickness on the crush strength of honeycombs is shown in Figure 2-4. The distribution in the observed branch angles (90-106^{o}) and the single wall thickness (0.07-0.11mm), may have an effect on the crush strengths of the three thickness honeycombs. The intensity of the effect was accounted for by performing quasi-static crush tests, which is presented in Section 3.

It can be seen from the group of cells in Figure 3-2 and Figure 3-3 that within the 13mm and 29mm thick honeycombs there are slight variations in cell shape. The branch angles for both the 13mm and 29mm thick honeycombs each vary by approximately 2%. The distortion is due to the lateral expansion during manufacturing. It is assumed that the global effect of this variation is minor [26].

3.3 ALUMINIUM HONEYCOMB MATERIAL CHARACTERISATION

The Zwick Universal 1484 Testing Machine was used to perform compression tests on the aluminium honeycombs. None of the test specimens were restricted from expanding radially during crushing. A cross-head speed of 1mm/min was used.

3.3.1 Results

The results are summarized in Table 3-3. The force-displacement graph is plotted in Figure 3-5, with enlargement of the peak force and the onset of the plastic deformation sections also shown. Typical engineering stress-strain curves are shown in Figure 3-6 for each honeycomb type. It should be noted that the stress-strain graph have been normalised to exclude the pre-load. The individual curves for each test are included in Appendix C.

Table 3-3: Results of aluminium honeycomb specimens

Honeycomb thickness (mm)	Test	Peak Stress (MPa)	Plateau Stress (MPa)	Onset of densification (% Strain)	Energy absorbed (MJ)	Energy absorbed per unit volume (MJ/m^3)
13mm	1	4.54	2.61	67%	173	1.61
	2	4.42	2.42	67%	165	1.44
	3	4.47	2.59	68%	174	1.52
	Average	**4.48**	**2.54**	**68%**	**171**	**1.52**
29mm	1	3.75	1.75	71%	321	1.26
	2	4.43	1.69	71%	309	1.21
	3	4.44	1.74	72%	325	1.27
	Average	**4.21**	**1.73**	**72%**	**318**	**1.25**
150mm	1	5.82	2.18	77%	2239	1.68
	2	5.66	2.25	74%	2202	1.67
	3	5.54	2.26	72%	2139	1.63
	Average	**5.67**	**2.23**	**74%**	**2193**	**1.66**

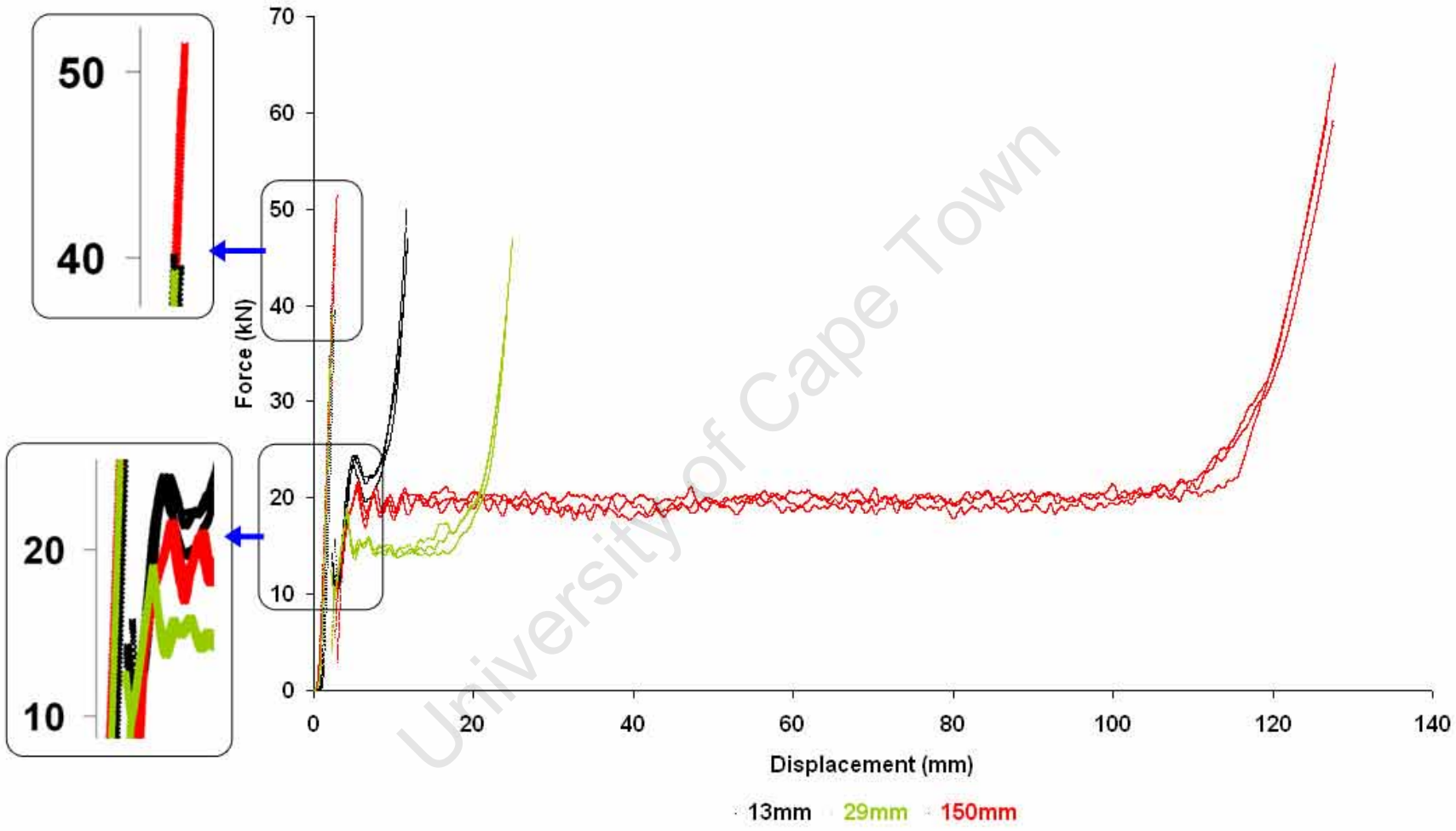

Figure 3-5: Graph of force versus displacement curves for honeycomb compression tests

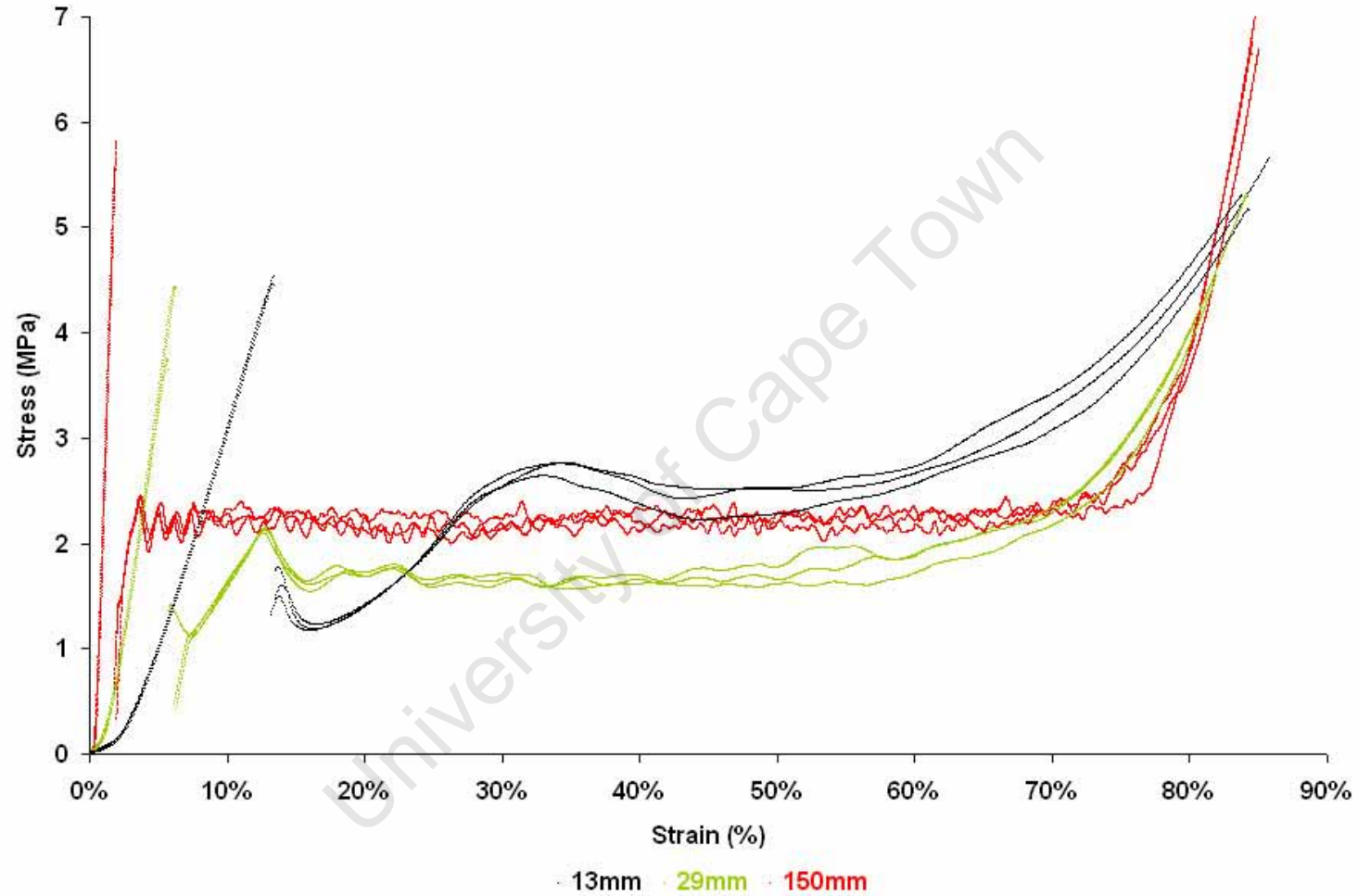

Figure 3-6: Graph of engineering stress-strain curves of compressed aluminium honeycombs of different thickness

3.3.2 Discussion

The energy absorbed by the honeycomb is the area under the force-displacement curves up to the onset of densification (Figure 3-5). These are calculated for each honeycomb and listed in Table 3-3. The honeycombs absorb the energy by folding the cell walls. The thicker the honeycomb the more energy it can absorb. This is just as expected and explained in Section 2.8.3.

Alternatively, the energy absorbed by the honeycomb per unit volume is the area under the stress-strain curve up to the onset of densification (Figure 3-6). These are also calculated and shown in Table 3-3. For honeycombs of equal compressive area, the energy absorbed per unit volume normalises the core thickness. Therefore the energy absorbed per unit volume is entirely dependent on the cell geometries and the material properties of the base material.

It is observed that the 150mm thick honeycomb has the highest peak stress, while the 13mm and 29mm thick honeycombs have similar peak stress values. Furthermore, the 13mm and 150mm thick honeycombs have similar plateau stress values and much higher than the plateau stress of the 29mm thick honeycomb.

As mentioned in Section 3.2.2, the distribution in the observed branch angles (90-106^{o}) and the single wall thickness (0.07-0.11mm), may have an effect on the crush strengths of the three thickness honeycombs. Assuming a similar relationship to that shown in Figure 2-4, the 16^{o} distribution in branch angle would have little influence on crush strength. The variation in foil thickness from 0.07 to 0.11mm would be expected to almost double the crush strength of the honeycombs. However, it is evident from the quasi-static crush tests that no such strength effect is observed. This may be that the effect of the foil thickness being influenced by the effect of varying cell sizes (5.69-10.22mm). The crush strength increases with decreasing cell size, as mentioned in Section 2.2.4. However, more investigation is recommended to quantify the effect of varying cell size on the crush strength; and to understand the influence of

varying cell sizes poses on that of foil thickness and branch angle. However, this was beyond the scope of the present work.

4 - BLAST TESTING DETAILS

The experiments were performed in the Blast Impact and Survivability Research Unit (BISRU) blast chamber at the University of Cape Town (UCT).

The experimental procedure was similar to that used by Nurick et al [6, 26]. All experiments were performed at a stand off distance 150mm (see Section 2.6.3). A photograph of the complete experimental setup on the ballistic pendulum is shown in Figure 4-1. The blast loading is created from the pressure wave generated by the explosion, which is produced by detonating a charge (in this study PE4 is used).

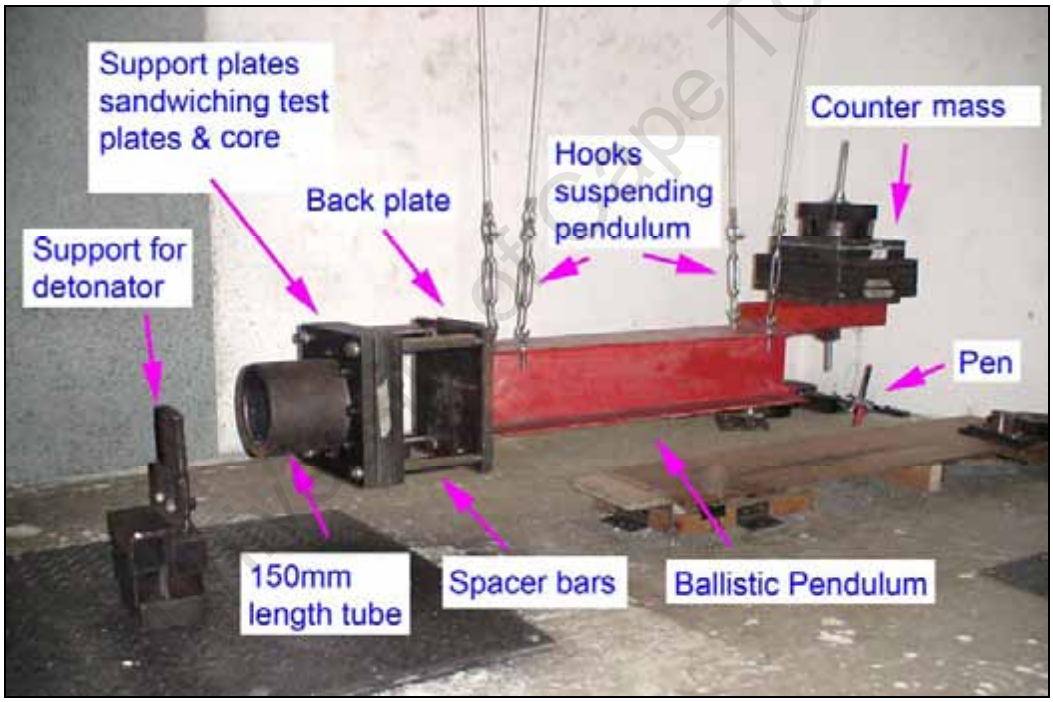

Figure 4-1: Photograph of the blast experiment setup

4.1 BALLISTIC PENDULUM

The ballistic pendulum at UCT is an I-beam suspended by four spring steel cables from a concrete slab ceiling in the blast chamber. Adjustable screws are fitted at the attachment of the spring steel cables, as shown in Figure 4-2. The pendulum is levelled by adjusting the screws and checked by a spirit-level. During the blast event, momentum is transferred to the pendulum causing it to swing. The swing of the pendulum is measured and the impulse is calculated based on the geometry of the pendulum. The calculations are shown in Appendix A.

The test rig is attached to the front end of the pendulum, while counter balancing masses are attached to the back end. This is to ensure that all four spring steel cables carry approximately equal loads, thus the impulse is applied through the centroid of the pendulum. The spacer rods allow the plates to deform without having any contact with the I-beam.

A pen is attached to the bottom of the pendulum at the back. The pen draws strokes on the tracing paper as the pendulum swings, recording the oscillation amplitude required to calculate the impulse. The measurements of the ballistic pendulum have been included in Appendix A.

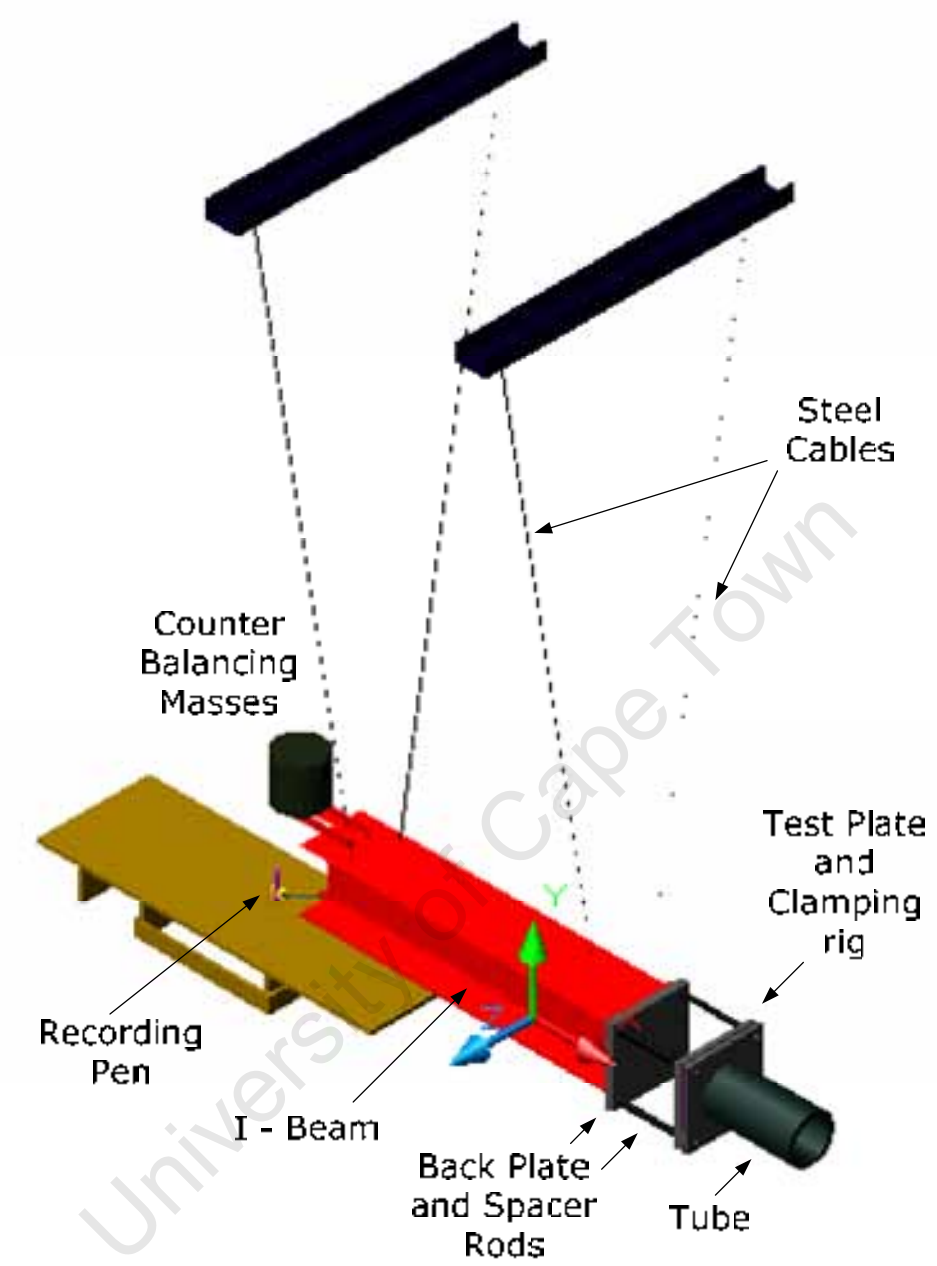

Figure 4-2: 3D schematic of the ballistic pendulum [44]

4.2 TEST PANELS

Tests were performed on four main types of sandwich panel, as described below. Unless specified, all test panels had 1.6mm thick mild steel face plates.

- ***Single* (S13, S29 and S29-1) sandwich panel** (shown in Figure 4-3) – The sandwich consisted of a mild steel plate, a honeycomb core, and another mild steel plate. The S13 test series uses a 13mm thick honeycomb. The S29 test series uses a 29mm thick honeycomb. The S29-1 test series uses a 29mm thick honeycomb with 1.0mm thick mild steel plates.
- **S150 sandwich panel** (shown in Figure 4-4) – This sandwich panel is the same as the *Single* sandwich. Due to practical difficulties, the S150 panels could not be attached to the pendulum, hence the panel was placed vertically on a support and the blast was directed downwards. The applied impulse was then estimated from the impulse versus charge mass relationship of PE4, obtained from the other test results.
- **D29/13 sandwich panel** (shown in Figure 4-5) – This panel consisted of a mild steel plate, a 29mm thick honeycomb, a mild steel plate, a 13mm thick honeycomb, and another mild steel plate.
- **D13a/13 sandwich panel** (shown in Figure 4-6) – The sandwich consisted of a mild steel plate, a 13mm thick air gap, a 13mm thick honeycomb core and another mild steel plate.

All sandwich panels except S150 were attached to the ballistic pendulum. In this study, the test plate upon which the blast wave impinged is referred to as the *front plate;* and the test plate closer to the I-beam is the *back plate*.

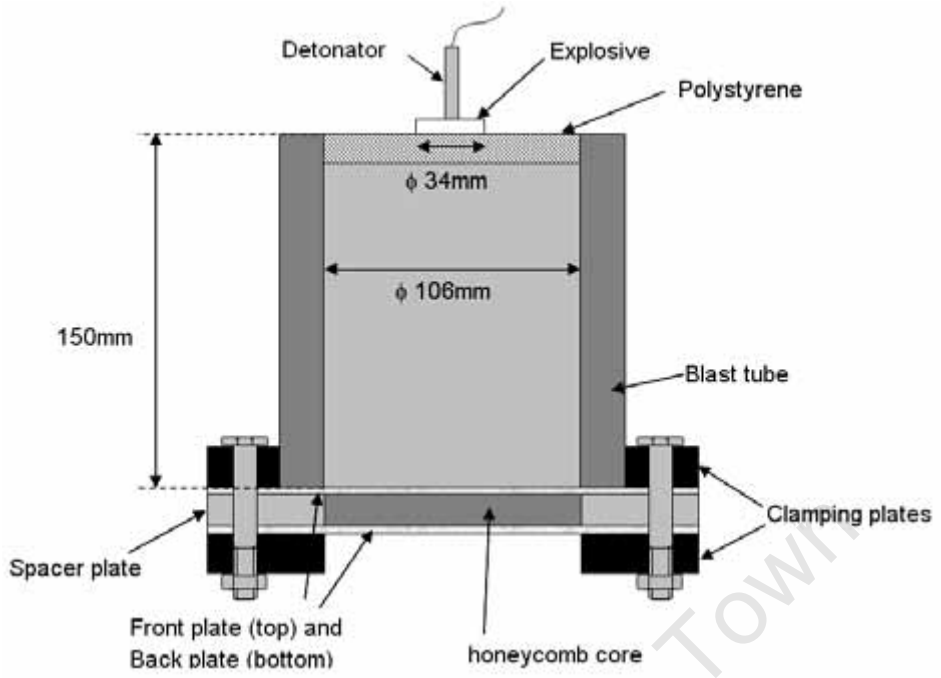

Figure 4-3: Schematic of the *Single* (S13, S29 and S29-1) sandwich panel

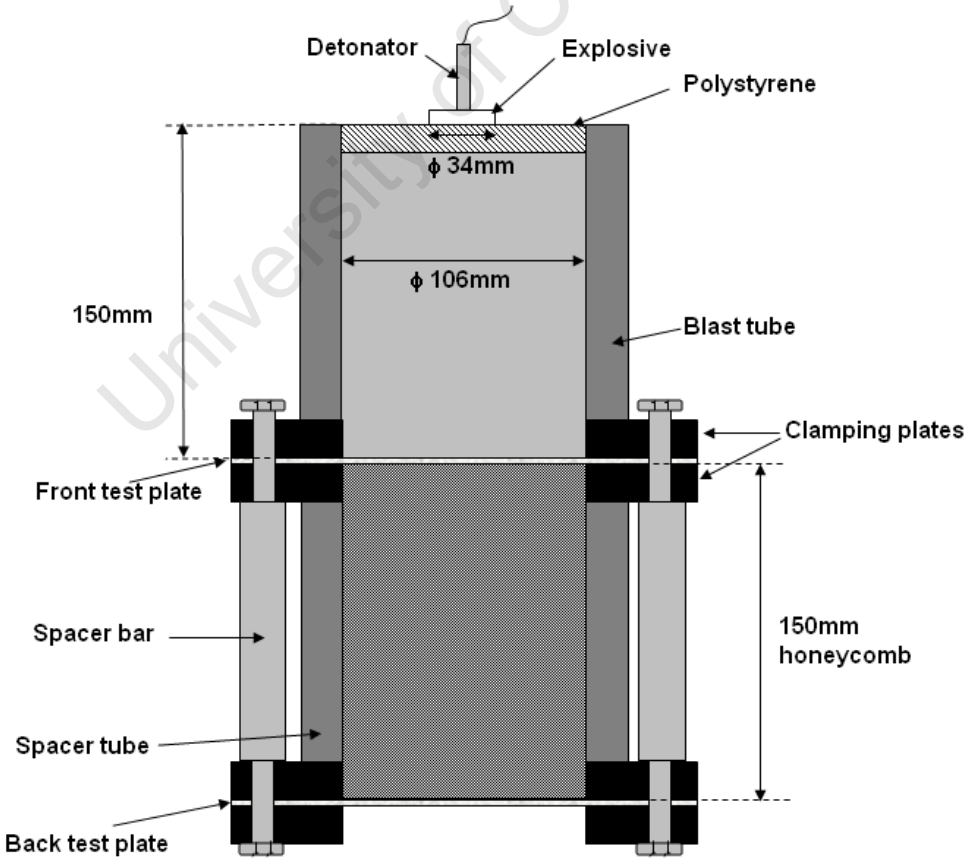

Figure 4-4: Schematic of the S150 sandwich panel

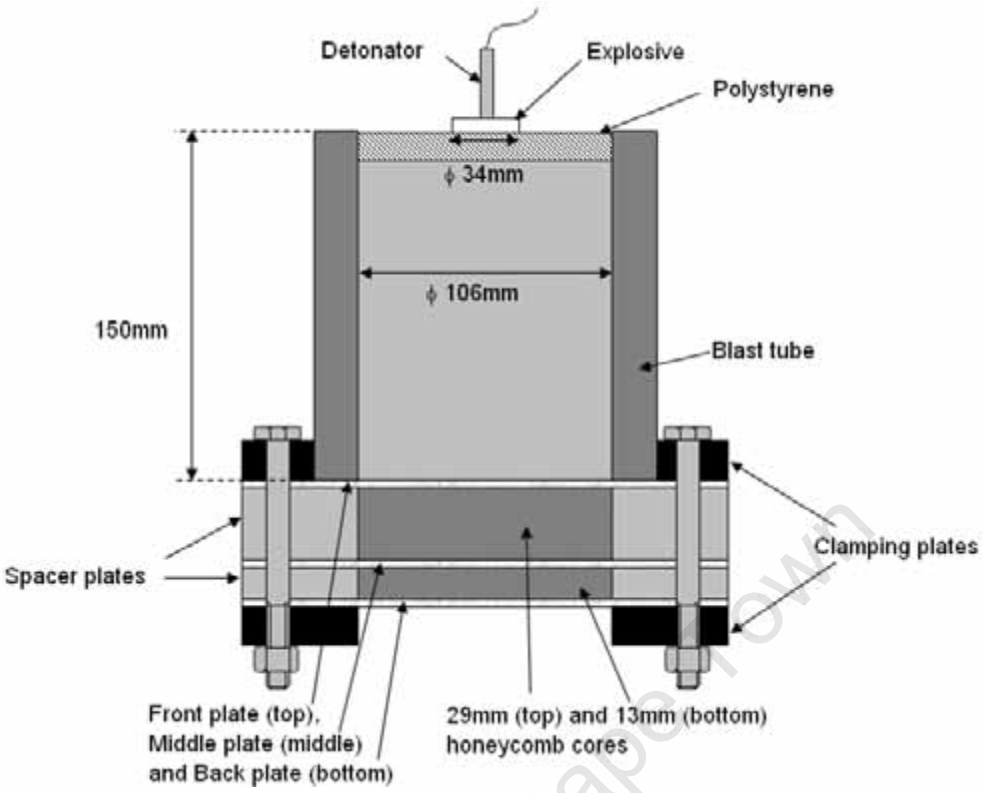

Figure 4-5: Schematic of the D29/13 sandwich panel

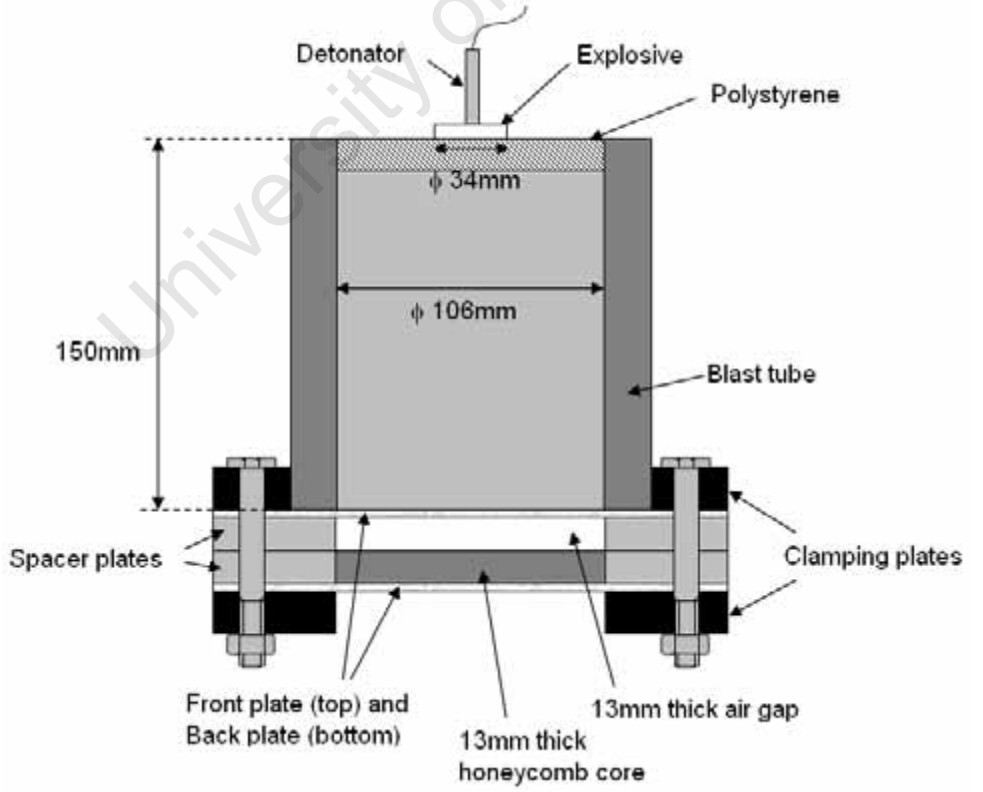

Figure 4-6: Schematic of the D13a/13 sandwich panel

Table 4-1 displays the details of the test series. Other than test series S29-1, all the test series made use of 1.6mm thick mild steel plates. A total of 61 experiments were performed for this study. The numbers of experiments performed for each sandwich panel are indicated in the brackets.

Table 4-1: Summary of all test series

		Honeycomb Core Thickness (mm)				
		13	29	150	29/13	13a/13
Plate Thickness (mm)	1.0		S29-1 (9)			
	1.6	S13 (16) [30]	S29 (25)	S150 (7)	D29/13 (10)	D13a/13 (10)
Experiment info		Previous	Experiments performed for this study			

Note 1: The letter "a" stand for air gap core

Note 2: The numbers of experiments performed for each sandwich panel are indicated in the brackets

4.3 EXPLOSIVE AND POLYSTYRENE

The explosive used is PE4. Wharton et al [52] recorded the properties of PE4 as shown in Table 4-2:

Table 4-2: Properties of PE4 [52]

RDX and Lithium grease	88% RDX and 12% Lithium grease
Density	1.6 (gcm^{-3})
$TNT_{equivalent}$	130% (by ballistic mortar tests)
Detonation velocity	8200 (ms^{-1})

The explosive was shaped into a disc of 34mm load diameter and attached onto a polystyrene pad as shown in Figure 4-7. The mass of explosive used was increased by increasing only the load height. A 1g leader of explosive attached the detonator to the main charge.

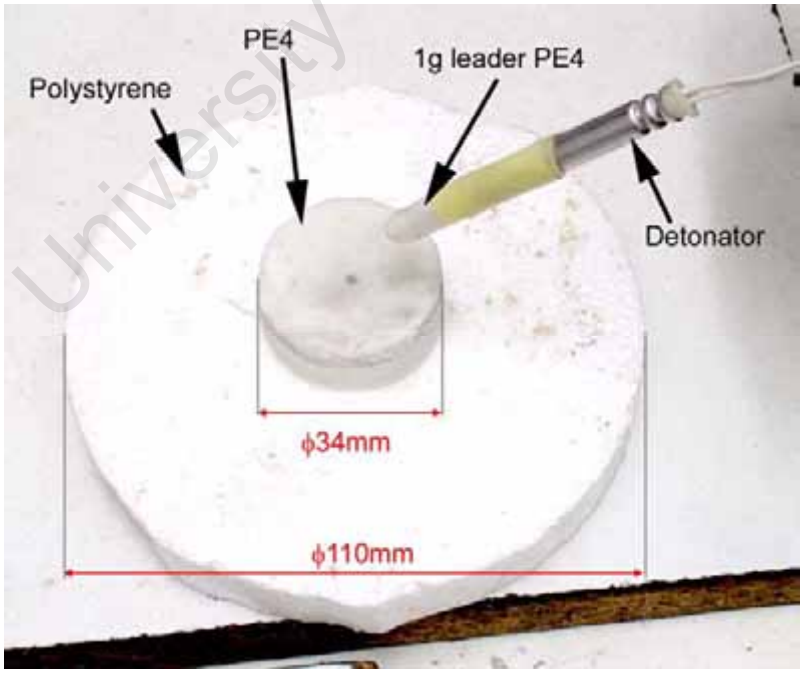

Figure 4-7: Photograph of a typical explosive charge used during testing

4.4 TEST MATRIX

Corresponding to the test configurations on Figure 4-3 to Figure 4-6, all tests are summarized in Table 4-1 and Table 4-3. They include the experiments carried out in this study and test series S13 for result comparisons.

By comparing different test series, the influence of various parameters can be determined, namely:

- **Varying core thickness** – Comparing S13, S29 and S150 (i.e. 13mm, 29mm and 150mm);
- **Varying face sheet thickness** – Comparing S29 and S29-1 (i.e. 1.6mm and 1.0mm);
- **Varying the core arrangement** – Investigating D29/13 and D13a/13 (29mm honeycomb plus a middle plate plus 13mm honeycomb; and 13mm air gap plus 13mm honeycomb).

Table 4-3: Test overview

Stand-off distance (mm)	Blast operation	Plate thickness (mm)	Setting	Core (mm)	Charge mass (g)																										Series name
150	Uniform loading	1.0	h/comb	29	2		3	4			6			8		10		12	13	14											S29-1
		1.6	h/comb	13	2	2.5	3	4				6.5		8		10		12	13	14	15		16			20	22	24			S13 [30]
				29	2		3	4	5		6		7	8	9	10		12		14	15	15.5	16	17	18	20	22	24			S29
				150														12					16		18	20		24	34		S150
				29/13							6					10		12		14	15					20	22	24	34	40	D29/13
			air-h/c	13/13				4			6		7	8		10	11	12		14			16			20					D13a/13

4.5 EXPERIMENTAL MEASUREMENTS

Honeycomb deflection and crush distances were measured for every honeycomb, as shown in Figure 4-8 and Figure 4-9 respectively. It was ensured that measurements were taken on the material and not through the gap of the cell. For the mid-span crush distance, four points were taken to obtain the average at this radius. The same was done for the outer-span. Note that the terms “mid-point” and “centre” are used to differentiate honeycomb deflection and crushing respectively, but they both describe the centre of circle.

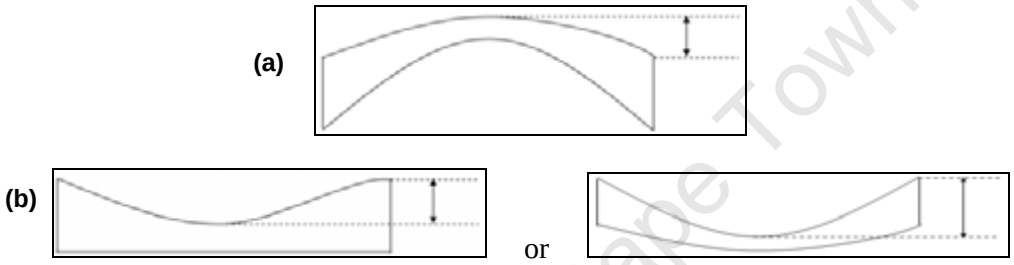

Figure 4-8: Mid-point deflection on the front surface (a); and the back surface (b) of the honeycomb

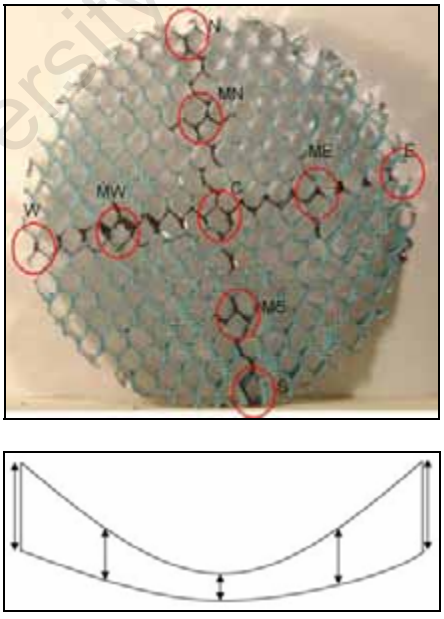

Figure 4-9: Crush distances measured across the diameter of a honeycomb

5 - BLAST TEST RESULTS

The specimens are named according to the test series and the mass of explosives used. The notations are listed below:

M = mass charge, *excluding* the 1g leader charge attached to the detonator;

R = repeat test;

f = front plate;

m = middle plate;

b = back plate;

h = honeycomb core;

For example **S29M22f** means the specimen is from test series S29, subjected to 22g explosives; the photo is showing the front plate.

S29-1M06h means the specimen is from test series S29-1, subjected to 6g explosives; the photo is showing the honeycomb.

Summaries of the material properties and experimental setup, as well as the experimental results are shown in Table 5-1 to Table 5-10. The experimental results are listed according to the test series and are listed in order of decreasing charge mass. The charge masses listed do not include the 1g leader charge. All tests used 150mm stand-off distance and 34mm charge diameter.

Table 5-1: Sandwich schematics and material properties of test series S150

S150 sandwich schematics			
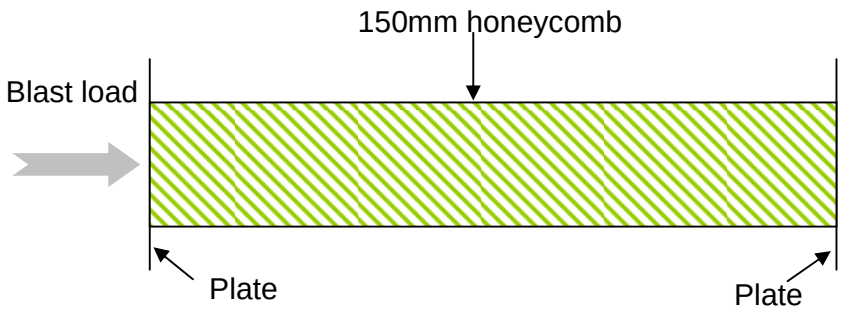			
Face plates material properties			
Front plate		Back plate	
Sheet	C_5	Sheet	B
Thickness	1.6mm	Thickness	1.6mm
Quasi-static yield stress	243.64MPa	Quasi-static yield stress	261.07MPa
Static stress	217.56MPa	Static stress	233.12MPa
Final elongation	32% strain	Final elongation	32% strain
Core material properties			
Thickness		150mm	
Density		79.06Kg/m^3	
Relative density		2.95%	
Plateau stress		2.23MPa	
Onset of densification		74% strain	

Table 5-2: Results of test series S150

Date	Test Number	Plate Thickness (mm)	Charge Mass (g)	Impulse (Ns)	Plate mid-point deflection				Plate failure mode		Dimensionless Impulse (Front plate only)
					Front plate		Back plate		Front plate	Back plate	
					(mm)	d/H	(mm)	d/H			
2007-08-09	S150M34	1.6	34	40.45	20.23	12.64	4.62	2.89	II	I	49.31
2007-08-09	S150M24	1.6	24	36.45	21.04	13.15	4.38	2.74	II	I	44.44
2007-08-10	S150M20	1.6	20	33.17	25.01	15.63	3.52	2.20	II	I	40.44
2007-08-14	S150R18	1.6	18	31.17	23.18	14.49	3.89	2.43	II	I	38.00
2007-08-10	S150M18	1.6	18	31.17	23.00	14.38	1.70	1.06	I (thinning)	I	38.00
2007-08-10	S150M16	1.6	16	28.93	20.70	12.94	1.76	1.10	I (thinning)	I	35.27
2007-08-10	S150M12	1.6	12	23.73	15.94	9.96	1.13	0.71	I	I	28.93

Date	Test Number	Charge Mass (g)	Impulse (Ns)	Honeycomb crush distance			H/c mid-point deflection	
				Outer-span (mm)	Mid-span (mm)	Center (mm)	Front surface (mm)	Back surface (mm)
2007-08-09	S150M34	34	40.45	90.73	100.76	100.81	18.81	5.03
2007-08-09	S150M24	24	36.45	75.62	83.98	87.51	20.91	3.23
2007-08-10	S150M20	20	33.17	19.80	29.50	35.85	23.01	3.87
2007-08-14	S150R18	18	31.17	23.16	33.25	35.92	18.67	4.08
2007-08-10	S150M18	18	31.17	2.14	12.19	23.14	21.16	1.99
2007-08-10	S150M16	16	28.93	1.50	10.26	20.50	18.77	1.81
2007-08-10	S150M12	12	23.73	1.20	8.56	17.20	14.68	1.47

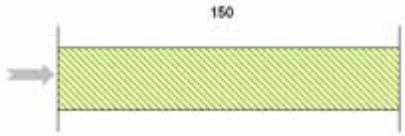

Table 5-3: Sandwich schematics and material properties of test series S29

S29 sandwich schematics			
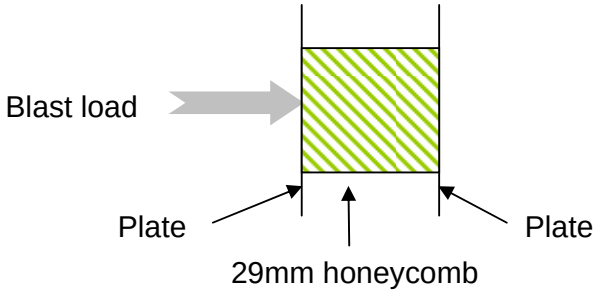			
Material properties			
Face plates		Face plates of repeat tests	
Sheet	B	Sheet	D
Thickness	1.6mm	Thickness	1.6mm
Quasi-static yield stress	261.07MPa	Quasi-static yield stress	249.07MPa
Static stress	233.12MPa	Static stress	222.41MPa
Final elongation	32% strain	Final elongation	34% strain
Core material properties			
Thickness		29mm	
Density		82.81Kg/m^3	
Relative density		3.09%	
Plateau stress		1.73MPa	
Onset of densification		72% strain	

Table 5-4: Results of test series S29

Date	Test Number	Plate Thickness (mm)	Charge Mass (g)	Impulse (Ns)	Plate mid-point deflection				Plate failure mode		Dimensionless Impulse (Front plate only)
					Front plate		Back plate		Front plate	Back plate	
					(mm)	d/H	(mm)	d/H			
2007-05-31	S29M24	1.6	24	36.75	18.83	11.77	21.47	13.42	II	II*	43.28
2007-06-01	S29M22	1.6	22	36.79	23.53	14.71	12.65	7.91	II	I	43.33
2007-05-31	S29M20	1.6	20	34.36	23.31	14.57	12.22	7.64	II	I	40.46
2007-06-01	S29M18	1.6	18	31.30	26.35	16.47	3.88	2.43	II*	I	36.86
2007-10-19	S29RM17	1.6	17	31.16	23.45	14.66	3.25	2.03	I (thinning)	I	37.58
2007-10-16	S29RM16	1.6	16	31.69	23.22	14.51	3.10	1.94	I (thinning)	I	38.21
2007-06-01	S29M16	1.6	16	29.15	22.52	14.08	2.73	1.71	I (thinning)	I	34.33
2007-10-19	S29RM15.5	1.6	15.5	29.73	23.45	14.65	3.31	2.07	I (thinning)	I	35.85
2007-05-31	S29M15	1.6	15	28.06	21.03	13.14	2.66	1.66	I (thinning)	I	33.05
2007-10-16	S29RM15	1.6	15	25.48	21.23	13.27	3.18	1.99	I (thinning)	I	30.73
2007-06-01	S29M14	1.6	14	27.77	19.89	12.43	2.56	1.60	I	I	32.71
2007-10-16	S29RM14	1.6	14	24.85	20.67	12.92	2.97	1.85	I (thinning)	I	29.97
2007-06-01	S29M12	1.6	12	25.50	18.23	11.39	2.45	1.53	I	I	30.04
2007-10-16	S29RM12	1.6	12	25.37	19.00	11.88	2.91	1.82	I	I	30.59
2007-06-01	S29M10	1.6	10	21.50	16.58	10.36	2.37	1.48	I	I	25.33
2007-10-16	S29RM10	1.6	10	19.85	15.60	9.75	2.41	1.51	I	I	23.93
2007-10-16	S29RM09	1.6	9	19.59	14.80	9.25	2.40	1.50	I	I	23.63
2007-05-31	S29M09	1.6	9	18.97	15.42	9.64	2.25	1.41	I	I	22.34
2007-06-02	S29M08	1.6	8	17.55	12.18	7.61	1.96	1.23	I	I	20.67
2007-10-19	S29RM07	1.6	7	15.41	12.08	7.55	1.95	1.22	I	I	18.59
2007-06-02	S29M06	1.6	6	14.90	8.59	5.37	1.70	1.06	I	I	17.55
2007-10-19	S29RM05	1.6	5	10.60	8.37	5.23	1.56	0.98	I	I	12.78
2007-06-02	S29M04	1.6	4	11.31	5.80	3.63	1.56	0.98	I	I	13.32
2007-05-31	S29M03	1.6	3	8.70	4.13	2.58	1.10	0.69	I	I	10.25
2007-05-31	S29M02	1.6	2	5.34	0.42	0.26	0.50	0.31	I	I	6.29

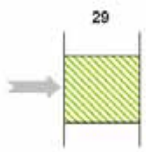

Table 5-4 (continue): Results of test series S29

Date	Test Number	Charge Mass (g)	Impulse (Ns)	Honeycomb crush distance			H/c mid-point deflection	
				Outer-span (mm)	Mid-span (mm)	Center (mm)	Front surface (mm)	Back surface (mm)
2007-05-31	S29M24	24	36.75	24.07	26.18	25.78	11.94	15.68
2007-06-01	S29M22	22	36.79	21.82	25.46	26.74	20.41	11.50
2007-05-31	S29M20	20	34.36	21.69	25.86	26.80	18.82	11.50
2007-06-01	S29M18	18	31.30	7.31	16.87	24.17	24.95	4.40
2007-10-19	S29RM17	17	31.16	1.13	11.29	20.38	21.97	2.23
2007-10-16	S29RM16	16	31.69	1.85	11.27	21.19	21.36	2.03
2007-06-01	S29M16	16	29.15	3.44	13.39	21.95	20.47	1.87
2007-10-19	S29RM15.5	15.5	29.73	1.40	11.49	19.97	20.82	2.66
2007-05-31	S29M15	15	28.06	3.05	12.55	19.36	18.99	2.27
2007-10-16	S29RM15	15	25.48	1.19	10.43	17.94	19.66	2.65
2007-06-01	S29M14	14	27.77	2.98	11.13	18.36	18.00	2.29
2007-10-16	S29RM14	14	24.85	1.77	10.73	17.81	19.13	2.67
2007-06-01	S29M12	12	25.50	2.60	9.45	15.87	16.59	2.93
2007-10-16	S29RM12	12	25.37	0.40	9.16	16.07	18.20	2.44
2007-06-01	S29M10	10	21.50	2.39	9.07	13.74	14.92	2.91
2007-10-16	S29RM10	10	19.85	1.01	8.36	13.25	14.42	2.18
2007-10-16	S29RM09	9	19.59	1.04	6.67	12.48	13.27	2.01
2007-05-31	S29M09	9	18.97	2.20	8.50	12.72	13.46	2.79
2007-06-02	S29M08	8	17.55	1.99	7.58	11.32	11.42	2.69
2007-10-19	S29RM07	7	15.41	0.59	5.84	8.75	11.15	1.85
2007-06-02	S29M06	6	14.90	1.75	5.36	8.58	9.04	2.34
2007-10-19	S29RM05	5	10.60	0.31	3.92	7.00	7.67	1.14
2007-06-02	S29M04	4	11.31	1.62	3.77	5.00	5.61	1.79
2007-05-31	S29M03	3	8.70	1.57	2.60	3.62	3.70	1.94
2007-05-31	S29M02	2	5.34	0.89	0.63	0.98	0.98	1.10

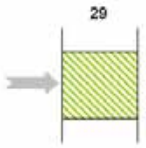

Table 5-5: Sandwich schematics and material properties of test series S29-1

S29-1 sandwich schematics	
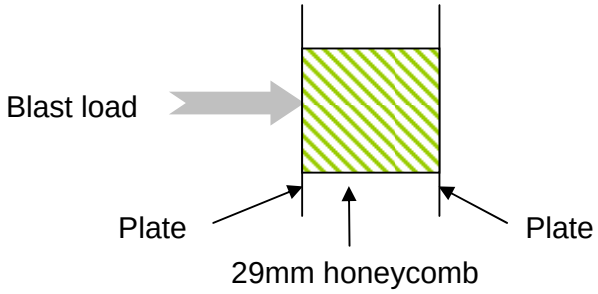	
Face plate material properties	
Sheet	A
Thickness	1.0mm
Quasi-static yield stress	187.90MPa
Static stress	167.78MPa
Final elongation	37% strain
Core material properties	
Thickness	29mm
Density	82.81Kg/m^3
Relative density	3.09%
Plateau stress	1.73MPa
Onset of densification	72% strain

Table 5-6: Results of test series S29-1

Date	Test Number	Plate Thickness (mm)	Charge Mass (g)	Impulse (Ns)	Plate mid-point deflection				Plate failure mode		Dimensionless Impulse (Front plate only)
					Front plate		Back plate		Front plate	Back plate	
					(mm)	d/H	(mm)	d/H			
2007-06-02	S29-1M14	1.0	14	25.59	24.41	24.41	20.54	20.54	II	II*	85.95
2007-06-23	S29-1M13	1.0	13	24.93	21.25	21.25	14.40	14.40	II	I	83.72
2007-06-02	S29-1M12	1.0	12	23.70	25.95	25.95	5.83	5.83	II*	I	79.59
2007-06-02	S29-1M10	1.0	10	20.86	22.88	22.88	5.19	5.19	I (thinning)	I	70.05
2007-06-04	S29-1M08	1.0	8	18.56	19.83	19.83	4.70	4.70	I (thinning)	I	62.34
2007-06-04	S29-1M06	1.0	6	14.18	15.81	15.81	4.25	4.25	I	I	47.63
2007-06-04	S29-1M04	1.0	4	9.76	10.51	10.51	3.60	3.60	I	I	32.78
2007-06-04	S29-1M03	1.0	3	7.57	6.53	6.53	3.19	3.19	I	I	25.42
2007-06-04	S29-1M02	1.0	2	5.93	2.88	2.88	2.38	2.38	I	I	19.90

Date	Test Number	Charge Mass (g)	Impulse (Ns)	Honeycomb crush distance			H/c mid-point deflection	
				Outer-span (mm)	Mid-span (mm)	Center (mm)	Front surface (mm)	Back surface (mm)
2007-06-02	S29-1M14	14	25.59	23.06	25.69	25.47	26.23	13.50
2007-06-23	S29-1M13	13	24.93	23.37	25.93	26.26	22.09	12.23
2007-06-02	S29-1M12	12	23.70	10.77	19.87	24.80	22.52	7.01
2007-06-02	S29-1M10	10	20.86	2.36	12.84	19.15	21.00	3.96
2007-06-04	S29-1M08	8	18.56	2.42	10.79	15.69	17.45	4.18
2007-06-04	S29-1M06	6	14.18	2.15	8.12	11.30	13.81	4.51
2007-06-04	S29-1M04	4	9.76	1.74	4.84	7.06	8.96	3.56
2007-06-04	S29-1M03	3	7.57	1.44	3.40	3.94	5.90	2.77
2007-06-04	S29-1M02	2	5.93	0.91	1.00	1.87	2.83	2.02

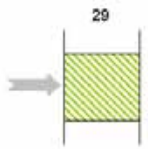

Table 5-7: Sandwich schematics and material properties of test series D29/13

D29/13 sandwich schematics			
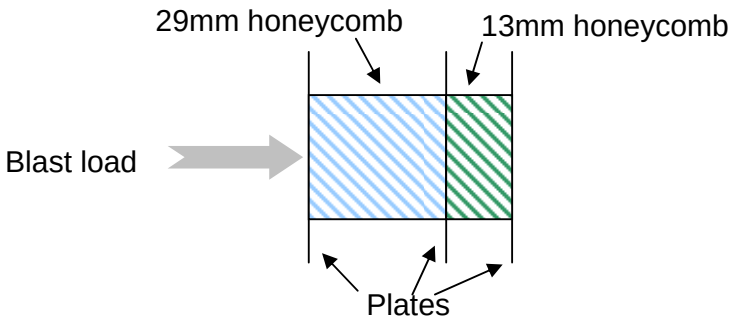			
Face plate material properties			
Sheet		B	
Thickness		1.6mm	
Quasi-static yield stress		261.07MPa	
Static stress		233.12MPa	
Final elongation		32% strain	
Core material properties			
29mm thick honeycomb		13mm thick honeycomb	
Thickness	29mm	Thickness	13mm
Density	82.81Kg/m^3	Density	96.21Kg/m^3
Relative density	3.09%	Relative density	3.59%
Plateau stress	1.73MPa	Plateau stress	2.54MPa
Onset of densification	72% strain	Onset of densification	68% strain

Table 5-8: Results of test series D29/13

Date	Test Number	Plate Thickness (mm)	Charge Mass (g)	Impulse (Ns)	Plate mid-point deflection						Plate deflection-thickness			Dimensionless Impulse (Front plate only)
					Front plate		Middle plate		Back plate		Front plate	Middle plate	Back plate	
					(mm)	d/H	(mm)	d/H	(mm)	d/H	(Ratio)	(Ratio)	(Ratio)	
2007-06-12	D29/13M40	1.6	40	44.97	20.51	12.82	17.48	10.93	6.16	3.85	II	I (thinning)	I	52.97
2007-06-11	D29/13M34	1.6	34	45.85	18.78	11.74	18.00	11.25	7.90	4.94	II	II*	I	53.99
2007-06-05	D29/13M24	1.6	24	38.24	24.31	15.19	12.24	7.65	3.28	2.05	II	I	I	45.04
2007-06-11	D29/13M22	1.6	22	37.94	22.27	13.92	11.98	7.49	3.16	1.98	II	I	I	44.68
2007-06-05	D29/13M20	1.6	20	32.52	25.34	15.84	1.25	0.78	1.20	0.75	II*	I	I	38.30
2007-06-23	D29/13M15	1.6	15	28.91	20.71	12.94	1.02	0.64	0.66	0.41	I (thinning)	I	I	34.05
2007-06-05	D29/13M14	1.6	14	25.48	19.41	12.13	0.60	0.38	0.50	0.31	I	I	I	30.01
2007-06-23	D29/13M12	1.6	12	23.95	17.50	10.94	0.53	0.33	0.21	0.13	I	I	I	28.20
2007-06-23	D29/13M10	1.6	10	21.24	14.43	9.02	0.18	0.11	0.12	0.08	I	I	I	25.01
2007-06-23	D29/13M06	1.6	6	13.91	8.71	5.44	0.08	0.05	0.00	0.00	I	I	I	16.38

Date	Test Number	Charge Mass (g)	Impulse (Ns)	29mm H/c crush distance			13mm H/c crush distance			29mm H/c m-point d		13mm H/c m-point d	
				Outer-span (mm)	Mid-span (mm)	Center (mm)	Outer-span (mm)	Mid-span (mm)	Center (mm)	Front surface (mm)	Back surface (mm)	Front surface (mm)	Back surface (mm)
2007-06-12	D29/13M40	40	44.97	24.86	26.94	27.00	2.59	9.39	10.26	19.94	13.84	12.94	5.23
2007-06-11	D29/13M34	34	45.85	23.94	26.74	27.03	5.67	9.82	10.39	18.71	12.56	12.50	6.85
2007-06-05	D29/13M24	24	38.24	20.61	25.78	26.58	0.78	4.84	8.10	21.19	11.57	11.09	3.77
2007-06-11	D29/13M22	22	37.94	18.97	25.63	26.50	0.61	4.50	7.03	21.03	10.58	10.42	4.18
2007-06-05	D29/13M20	20	32.52	2.68	14.31	24.66	0.17	0.14	0.20	23.80	1.54	0.68	0.87
2007-06-23	D29/13M15	15	28.91	2.11	12.30	19.43	0.07	0.26	0.20	19.28	0.59	0.51	0.54
2007-06-05	D29/13M14	14	25.48	1.88	11.59	20.78	0.19	0.20	0.22	19.55	0.45	0.27	0.59
2007-06-23	D29/13M12	12	23.95	1.19	9.18	16.04	0.22	0.21	0.29	16.18	0.69	0.90	0.73
2007-06-23	D29/13M10	10	21.24	0.90	8.86	14.24	0.16	0.26	0.25	13.55	0.41	0.34	0.46
2007-06-23	D29/13M06	6	13.91	0.42	5.56	8.75	0.18	0.24	0.27	8.58	0.07	0.23	0.08

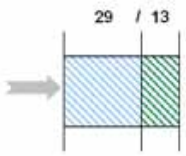

Table 5-9: Sandwich schematics and material properties of test series D13a/13

D13a/13 sandwich schematics	
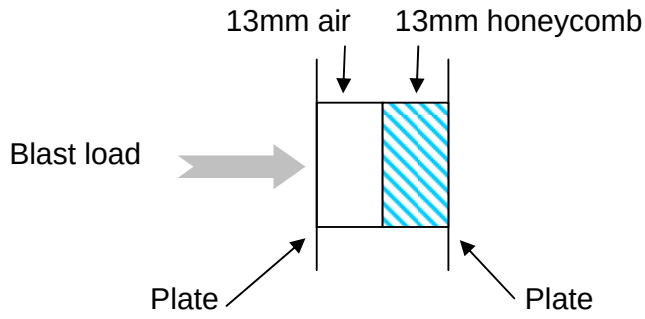	
Face plate material properties	
Sheet	C_3
Thickness	1.6mm
Quasi-static yield stress	199.20MPa
Static stress	177.87MPa
Final elongation	42% strain
Core material properties	
Thickness	13mm
Density	96.21Kg/m^3
Relative density	3.59%
Plateau stress	2.54MPa
Onset of densification	68% strain

Table 5-10: Results of test series D13a/13

Date	Test Number	Plate Thickness (mm)	Charge Mass (g)	Impulse (Ns)	Plate mid-point deflection				Plate failure mode		Dimensionless Impulse (Front plate only)
					Front plate		Back plate		Front plate	Back plate	
					(mm)	d/H	(mm)	d/H			
2007-08-01	D13a/13M20	1.6	20	36.45	18.55	11.59	21.33	13.33	II	II	49.15
2007-08-01	D13a/13M16	1.6	16	30.51	22.71	14.19	10.68	6.68	II	I	41.13
2007-08-01	D13a/13M14	1.6	14	28.01	23.43	14.64	5.51	3.44	II*	I	37.77
2007-08-01	D13a/13M12	1.6	12	26.02	20.68	12.93	1.95	1.22	I (thinning)	I	35.08
2007-08-14	D13a/13M11	1.6	11	22.28	18.72	11.70	0.75	0.47	I (thinning)	I	30.03
2007-08-01	D13a/13M10	1.6	10	22.02	18.01	11.26	0.54	0.34	I	I	29.69
2007-08-01	D13a/13M08	1.6	8	19.07	15.03	9.39	0.48	0.30	I	I	25.72
2007-08-14	D13a/13M07	1.6	7	17.44	13.84	8.65	0.15	0.09	I	I	23.51
2007-08-01	D13a/13M06	1.6	6	14.78	12.51	7.82	0.10	0.06	I	I	19.93
2007-08-01	D13a/13M04	1.6	4	10.55	9.46	5.91	0.00	0.00	I	I	14.23

Date	Test Number	Charge Mass (g)	Impulse (Ns)	Honeycomb crush distance			H/c mid-point deflection		H/c crush radius (mm)
				Outer-span (mm)	Mid-span (mm)	Center (mm)	Front surface (mm)	Back surface (mm)	
2007-08-01	D13a/13M20	20	36.45	10.30	Torn	Torn	Torn	Torn	53
2007-08-01	D13a/13M16	16	30.51	4.45	9.93	11.36	18.01	9.16	53
2007-08-01	D13a/13M14	14	28.01	2.17	6.59	Torn	13.85	4.67	45
2007-08-01	D13a/13M12	12	26.02	0.00	1.33	8.80	9.22	1.02	32
2007-08-14	D13a/13M11	11	22.28	0.00	1.13	7.10	7.67	0.64	30
2007-08-01	D13a/13M10	10	22.02	0.00	0.61	7.27	7.56	0.27	30
2007-08-01	D13a/13M08	8	19.07	0.00	0.00	4.20	4.34	0.36	24
2007-08-14	D13a/13M07	7	17.44	0.00	0.00	2.96	3.45	0.29	20
2007-08-01	D13a/13M06	6	14.78	0.00	0.00	1.77	1.84	0.40	15
2007-08-01	D13a/13M04	4	10.55	0.00	0.00	0.00	0.00	0.00	0

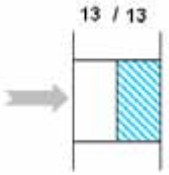

6 - OBSERVATIONS

This chapter reports the post-test observations made on the mild steel plates and the aluminium honeycombs subjected to blasting.

6.1 PLATE DEFORMATION PROFILE

The mid-plate deflection increased with increasing impulse. All plates exhibited a deformation profile characterised by a global dome, as shown in Figure 6-1. This is typically associated with uniformly distributed loading and was also observed by Jacob et al [46] for stand-off distance greater than the plate radius (see Section 2.6.3).

Figure 6-1: A large global dome profile is observed throughout all test series. Specimen S29-1M10, S29-1 sandwich, charge mass = 10g, impulse = 20.86Ns, front (bottom) and back (top) plates.

6.2 THINNING

As mentioned in Section 2.7, as plate deflection increases with increasing impulse the plate is stretched until thinning results at the boundary prior to tearing. Thinning was observed for face plates of all five test series. In particular, thinning occurred for impulses ranging from 18 to 31Ns, depending upon panel configuration. The panels with thin (1mm) face plates exhibited thinning at the bottom of the impulse range (18-21Ns). An example of thinning is shown in Figure 6-2.

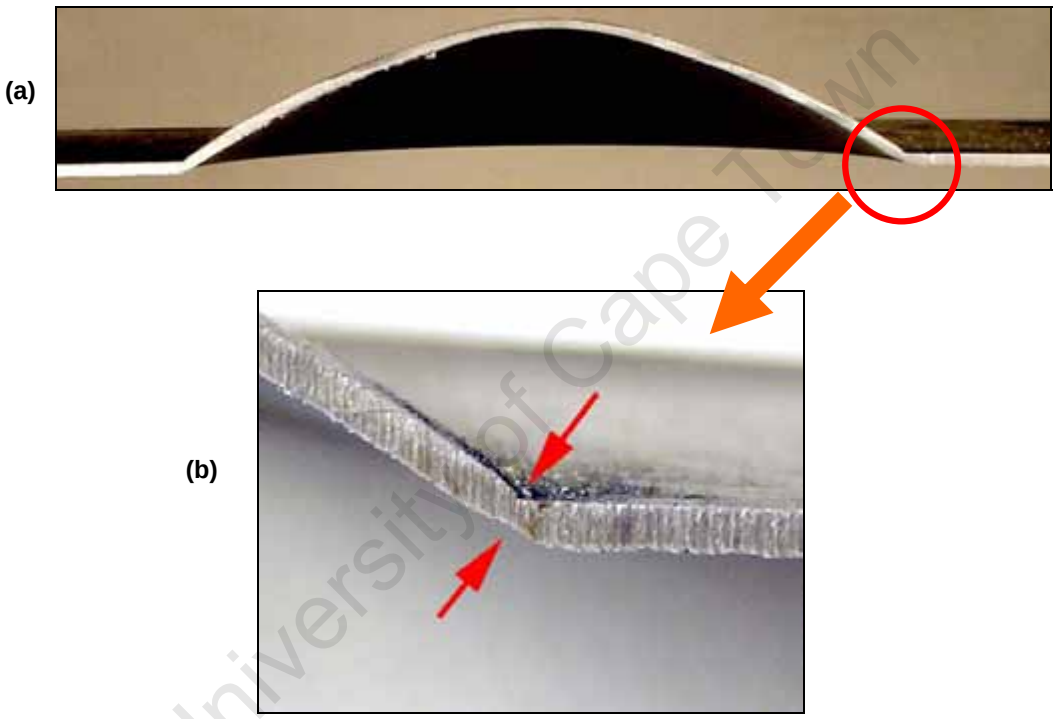

Figure 6-2: Specimen deformation profile (a); and enlargement (b) of the thinning edge. Specimen D13a/13M12f, D13a/13 sandwich, charge mass = 12g, impulse = 26.02Ns, front plate

6.3 TEARING

Plate deflection increases with increasing impulse. At sufficiently large impulse the plate deflection reaches a threshold and tearing occurs. Initially, partial tearing occurs along the boundary, which is classified as Mode II* failure (see Section 2.7).

Tearing was observed for all test series. With increasing impulse, tearing occurred first on the front plates, then on the middle plate (if there was one), then on the back plates. An example of tearing is shown in the photograph in Figure 6-3. As impulse was further increased, complete tearing occurred and the torn section looked like a circular cap. This is classified as Mode II failure; a photograph of a plate exhibiting Mode II failure is shown in Figure 6-4. It is noted that the adhesive pattern of the honeycomb leave imprints on the test plates at higher impulses.

Figure 6-3: Tearing along the boundary is observed on specimen D13a/13M14f, D13a/13 sandwich, charge mass = 14g, impulse = 28.01Ns, front plate

(a)

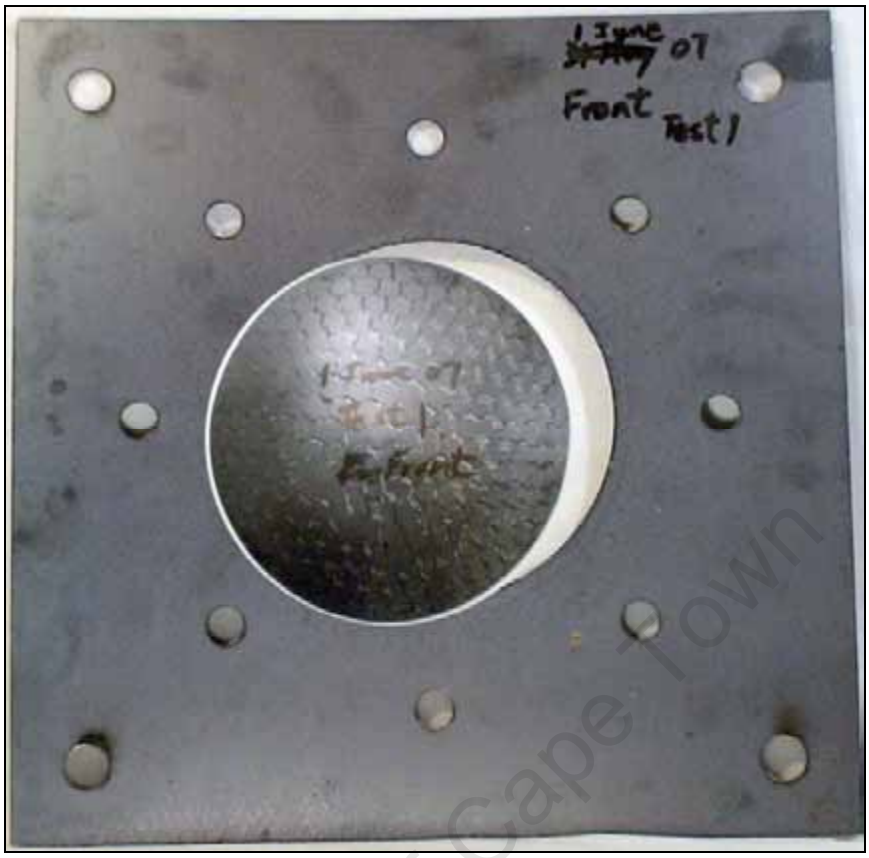

(b)

Figure 6-4: Complete tearing exhibited on specimen S29M22f, S29 sandwich, charge mass = 22g, impulse = 36.79Ns, front plate. The back view (a) and the side view (b)

6.4 HONEYCOMB DEFORMATION PROFILE

Depending on the impulse magnitude, the honeycomb dissipates energy via two mechanisms: crushing of the honeycomb cells and global bending of the core (see Section 2.3). An example of the buckling pattern is shown in Figure 6-5. In addition, peeling at the double wall portion (see Section 2.2.3) has been noted in all the test series, an example is shown in Figure 6-6.

Figure 6-5: Honeycomb crushing is observed on blast specimen – D29/13M24h(29), D29/13 sandwich, charge mass = 24g, impulse = 38.24Ns, 29mm honeycomb

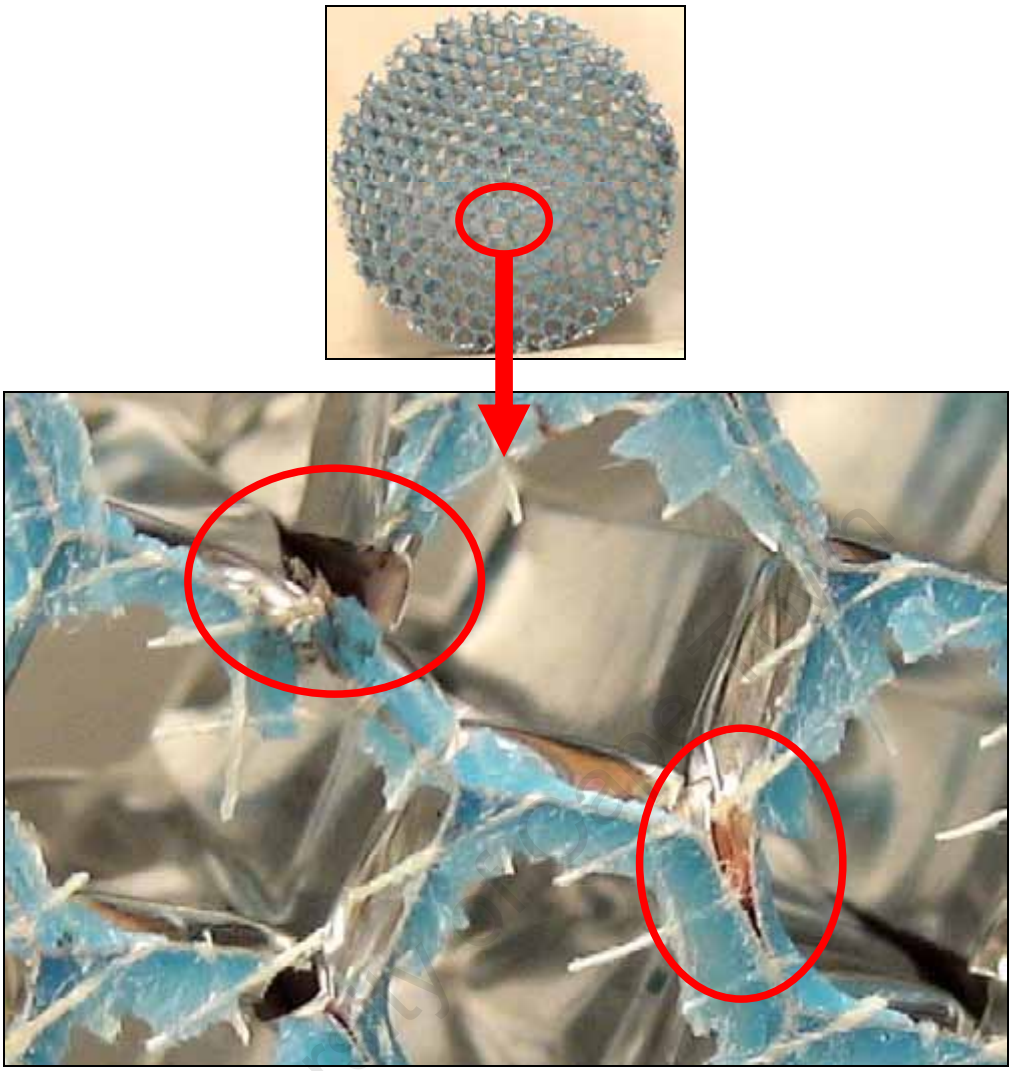

Figure 6-6: Peeling off at the double wall portion. Specimen S29-1M06h, S29-1 sandwich, charge mass = 6g, impulse = 14.18Ns, honeycomb peeling

The overall profile of the deformed core follows the plate deflection profile. In all cases, the core centre crushes the most. A photograph showing the global bending of an entire core is shown in Figure 6-7.

Figure 6-7: Global bending observed in specimen S29M24h, S29 sandwich, charge mass = 24g, impulse = 36.75Ns, honeycomb profile

The honeycomb cores from panels in test series D13a/13 exhibited more localised deformation profiles, as shown in Figure 6-8. The spacing of the air gap allows only the top portion of the dome to deform into the honeycomb. Thus only the central region of the honeycomb is utilised in the absorption of the blast energy. Consequently the honeycomb only deforms in the area of contact and displays a similar failure mode to that under localised loading conditions.

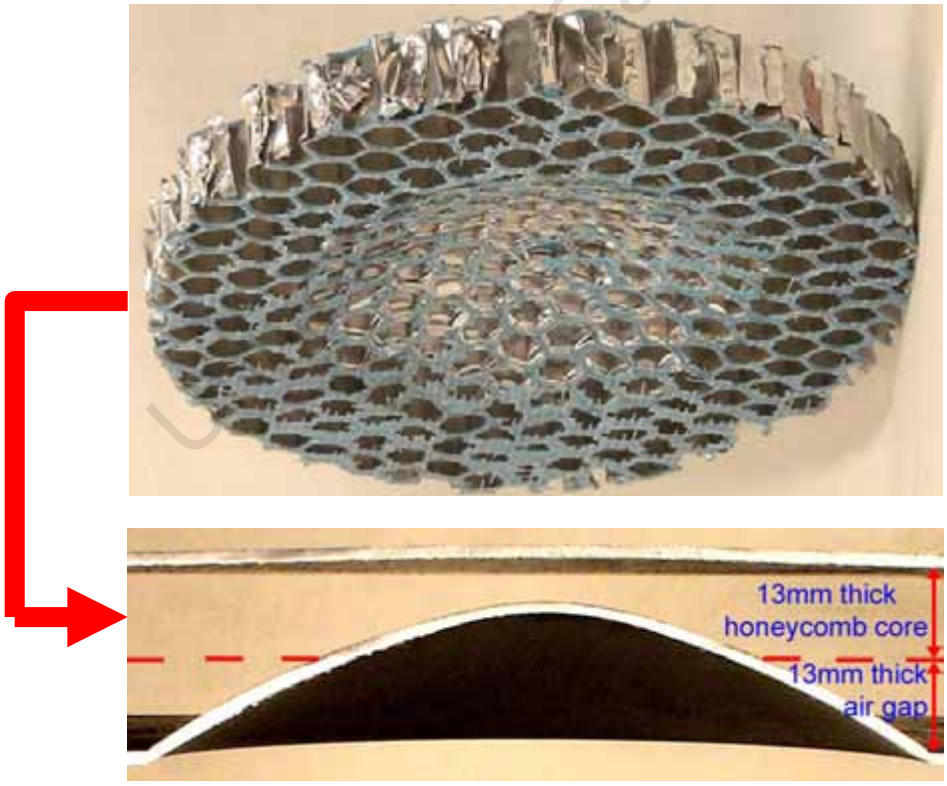

Figure 6-8: Localised deformation observed in D13a/13 sandwich. Specimen D13a/13M12, charge mass = 12g, impulse = 26.02Ns

7 - ANALYSIS OF RESULTS

This chapter examines the relationship between impulse and charge mass for all the tests. It also analyses each test series. The comparison between the test series is discussed in Chapter 8.

For easier recognition of data points and test series, a systematic graphing system is used. Each test series is colour coded with a single colour scheme. In addition, the shapes of the data points are unified to represent specific results. The details are summarized in Table 7-1.

Table 7-1: Summary of coding for graphs

Test series	Colour code	Plate deflection		Honeycomb crush distance			Honeycomb mid-point deflection		Dimensionless impulse
		Front	Back	Center	Mid-span	Outer-span	Front surface	Back surface	
S13	Other (black)	▲	△	+	×	×			◆
S150	Red	■	□	+	×	×	●	○	◆
S29	Green	■	□	+	×	×	●	○	◆
S29-1	Purple	■	□	+	×	×	●	○	◆
D29/13	Blue	■	□	+	×	×	●	○	◆
D13a/13	Brown	■	□	+	×	×	●	○	◆

In those cases where curves have been drawn through the test data, the appropriate best fit regression analysis has been adopted. In the face plate deflection graphs the onset of plate tearing has been indicated by grey circles.

7.1 RELATIONSHIP BETWEEN IMPULSE AND CHARGE MASS

All charge masses used in the current study are plotted in Figure 7-1. There are two parts to the curve. Firstly, at relatively low charge masses, it shows that the impulse increases linearly with increasing charge mass. This linearly increasing relationship has been noticed by researchers before [45, 53].

The second part is that after the linearly increasing trend, the impulse start to "tail-off" (i.e. less increase in impulse). Above 35Ns, there is no increase in impulse with increasing mass of explosive.

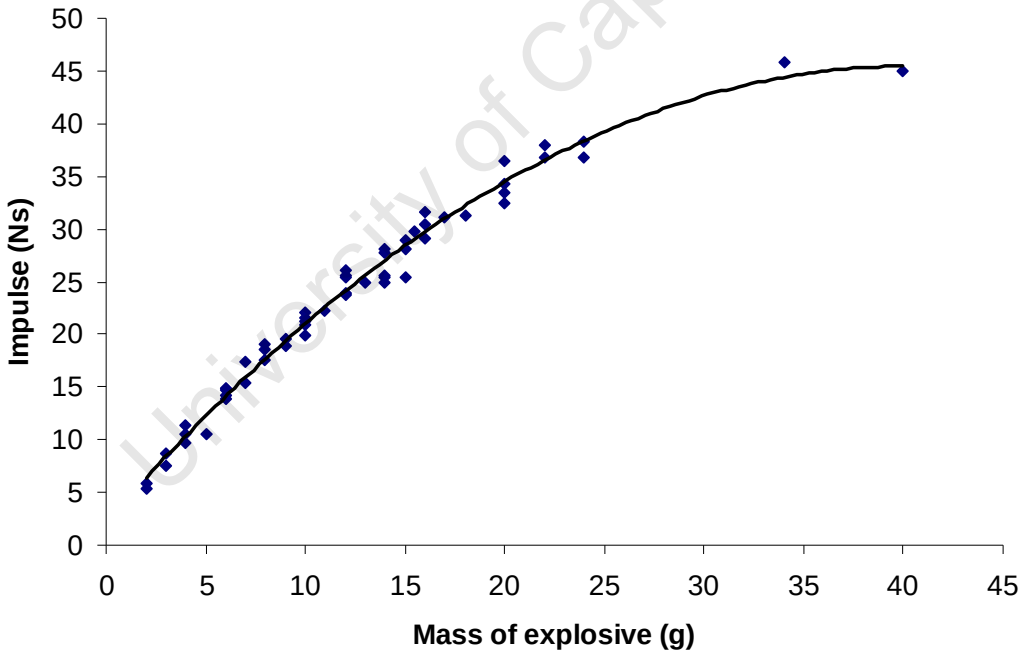

Figure 7-1: Graph of impulse versus charge mass for all tests.

The change in the increase of impulse is due to the effective mass of explosive phenomenon, reported by Kennedy [54]. For a constant charge diameter, there is a

corresponding maximum effective charge height. This charge dimension will produce the maximum plate velocity, after which the velocity reaches an asymptotic limit despite any increase in charge mass.

Figure 7-2 illustrates the effective mass of explosive for a charge diameter *d*. The 30^o lateral edges, which are the expected un-reactive explosive, are discounted. The effective mass of explosive is indicated by the grey region, and the maximum height of the effective mass is indicated as h_E. Consequently, charge heights beyond this maximum height will not contribute towards the applied impulse.

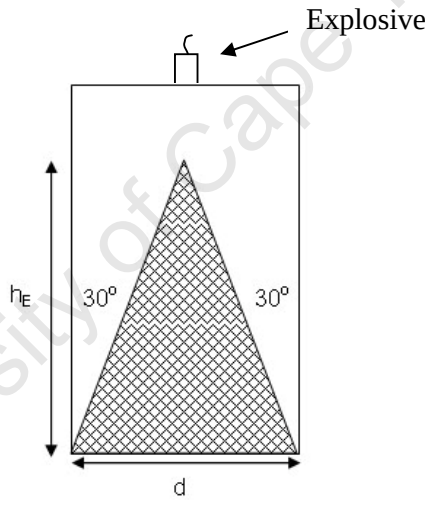

Figure 7-2: Illustration of the effective mass of explosive. The unshaded region is completely discounted in calculating the effective charge mass.

In this study, a constant charge diameter of 34mm was used. Therefore the maximum charge height is calculated as *29.44mm*, which is *42.77g* of charge mass. This is outside the range of this study; but it can be seen that at 40g of charge mass the linearly increasing trend starts to approach the maximum limit.

7.2 ANALYSIS OF SANDWICH PANELS

In order to better understand the response of the panels and to fully explain the effect of core densification, analysis is performed in the order of test series S13, S150 and S29. Series S13 shows the effect of densification and eliminates front plate tearing until much higher impulse. Series S150 shows effect of front plate tearing with no core densification. Series S29 exhibits both the front plate tearing and densification phenomena. Observations from series S13 and S150 will be used to interpret the behaviour of the S29 panels.

7.2.1 Analysis of test series S13

These test results were obtained from work reported by Nurick et al [30] using the same test procedure implemented in this research. The core thickness was 13mm. The relevant information for this test series is listed in Appendix D [30, 31].

The front plate responds in the same way as a clamped single circular plate subjected to uniformly distributed blast loading [2, 28]. Teeling-Smith and Nurick [2], as shown in Figure 7-3, predicted a maximum mid-point plate deflection of approximately 30mm for a 1.6mm thick monolithic circular plate subjected to uniformly distributed blast loading. This indicates that if the core thickness is lower than 30mm, contact between the front plate and the back plate will occur prior to front plate tearing. In the current investigation, a relatively small core thickness (i.e. 13mm) is used. Photographs of the face plates are shown in Figure 7-4. The face plate deflection-impulse graph is shown in Figure 7-5, with the onset of core densification during quasi-static compression superimposed on the graph. After complete core densification at the centre, the front plate deflection is obstructed by the back plate, as visible in Figure 7-4 for 30.3Ns. Therefore less front plate deflection is observed than that of the same thickness monolithic blast loaded plate.

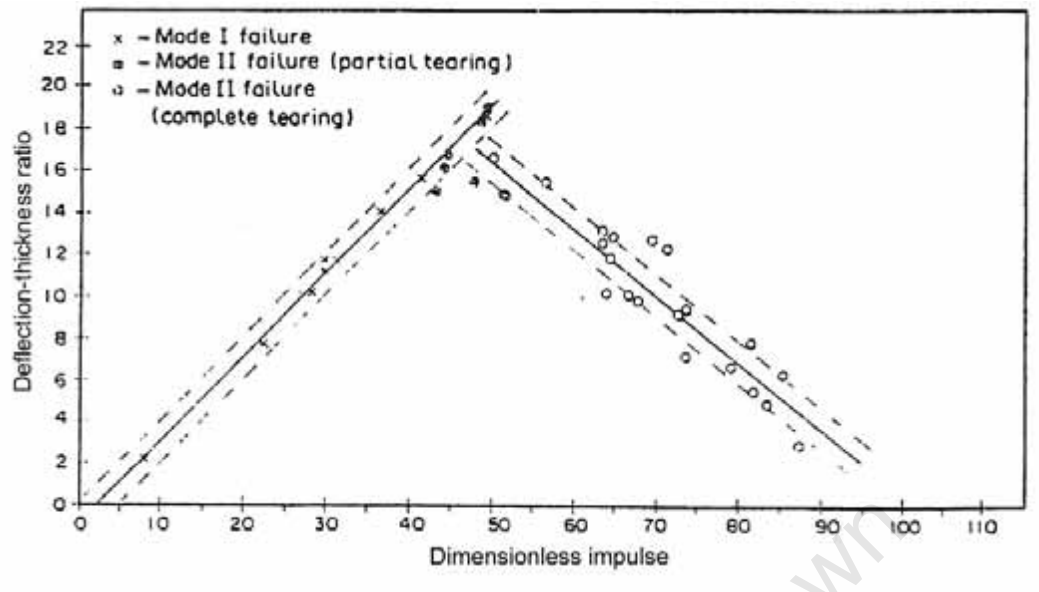

Figure 7-3: Graph of deflection-thickness ratio versus dimensionless impulse for monolithic circular plates [2]

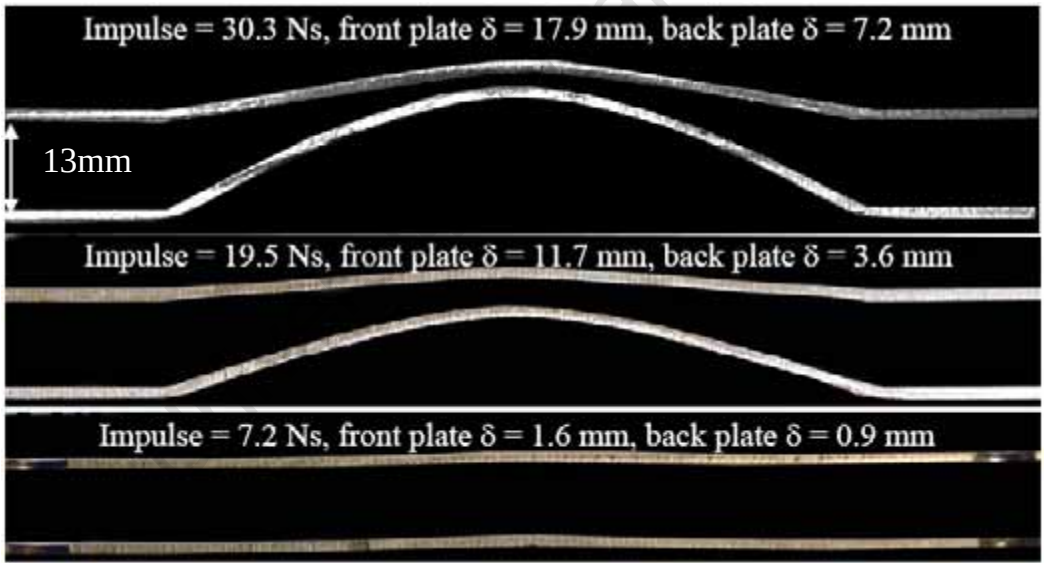

Figure 7-4: Photographs of the face plates cross-section from S13 [30]

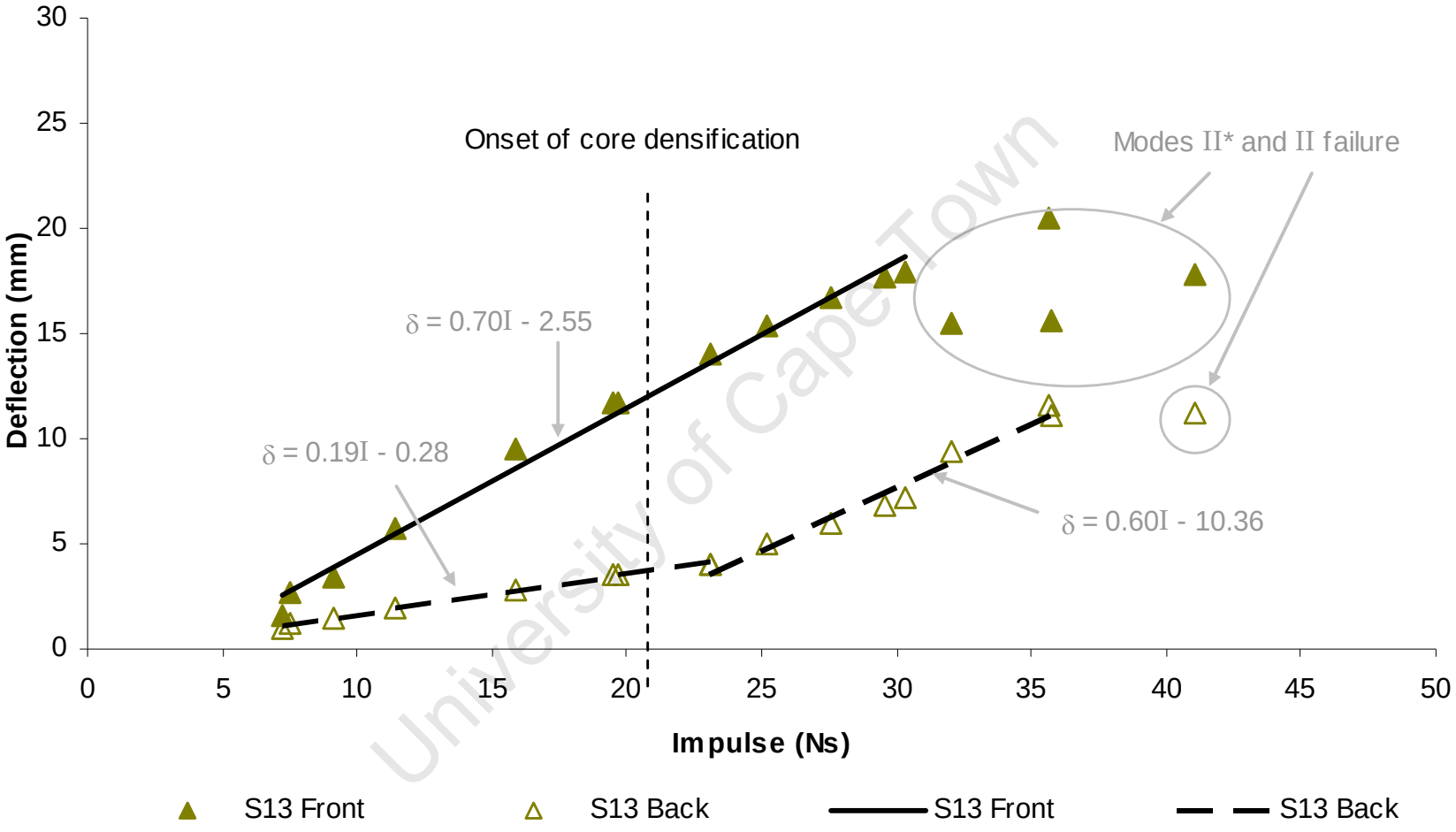

Figure 7-5: Graph of face plate deflection versus impulse of S13

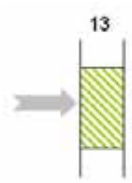

Photographs of the cores are shown in Figure 7-6 to demonstrate the change in centre crush distance. The core crushing-impulse graph is shown in Figure 7-7, with the onset of densification during quasi-static compression superimposed on the graph. At approximately 23Ns the centre of the core experiences a gradient decrease, as shown in Figure 7-7. This is due to complete core densification in the centre region. This means that the centre of the core reaches the maximum crushing limit and no further crushing is possible with increasing impulse. Furthermore, at approximately 31Ns, the outer-span of the core experiences an increase in the gradient, as shown in Figure 7-7. This is due to the front plate tearing.

From the above, it becomes clear that in core crushing, a gradient increase is due to front plate tearing; and a gradient decrease is due to the complete core densification.

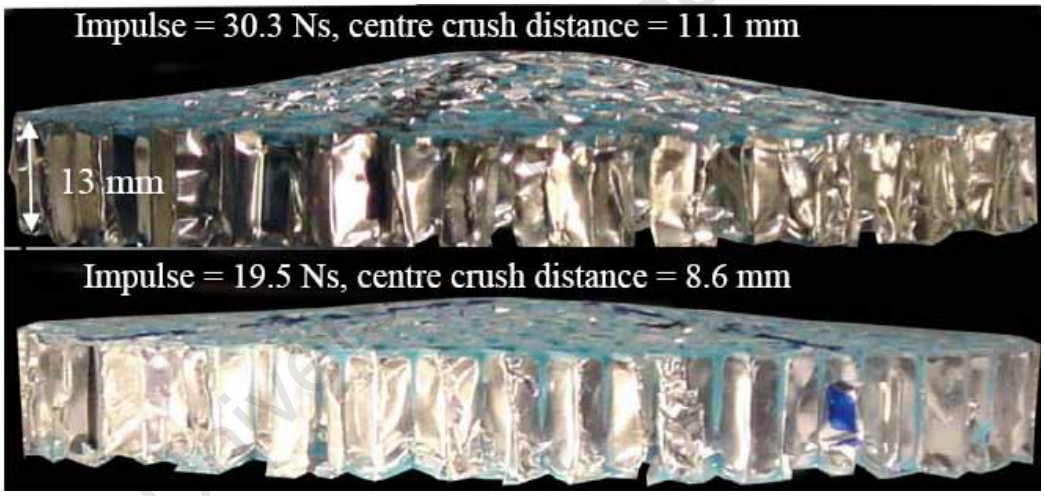

Figure 7-6: Photographs of honeycomb cores from S13 [30]

The back plate also responds in a similar way as a clamped single circular plate subjected to uniformly distributed blast loading. However, the load transfer to the back plate is regulated by the core. The onset of core densification (at approximately 21Ns) allows higher stresses to be transferred to the back plate and a gradient increase in the back plate deflection is observed, as shown in Figure 7-5.

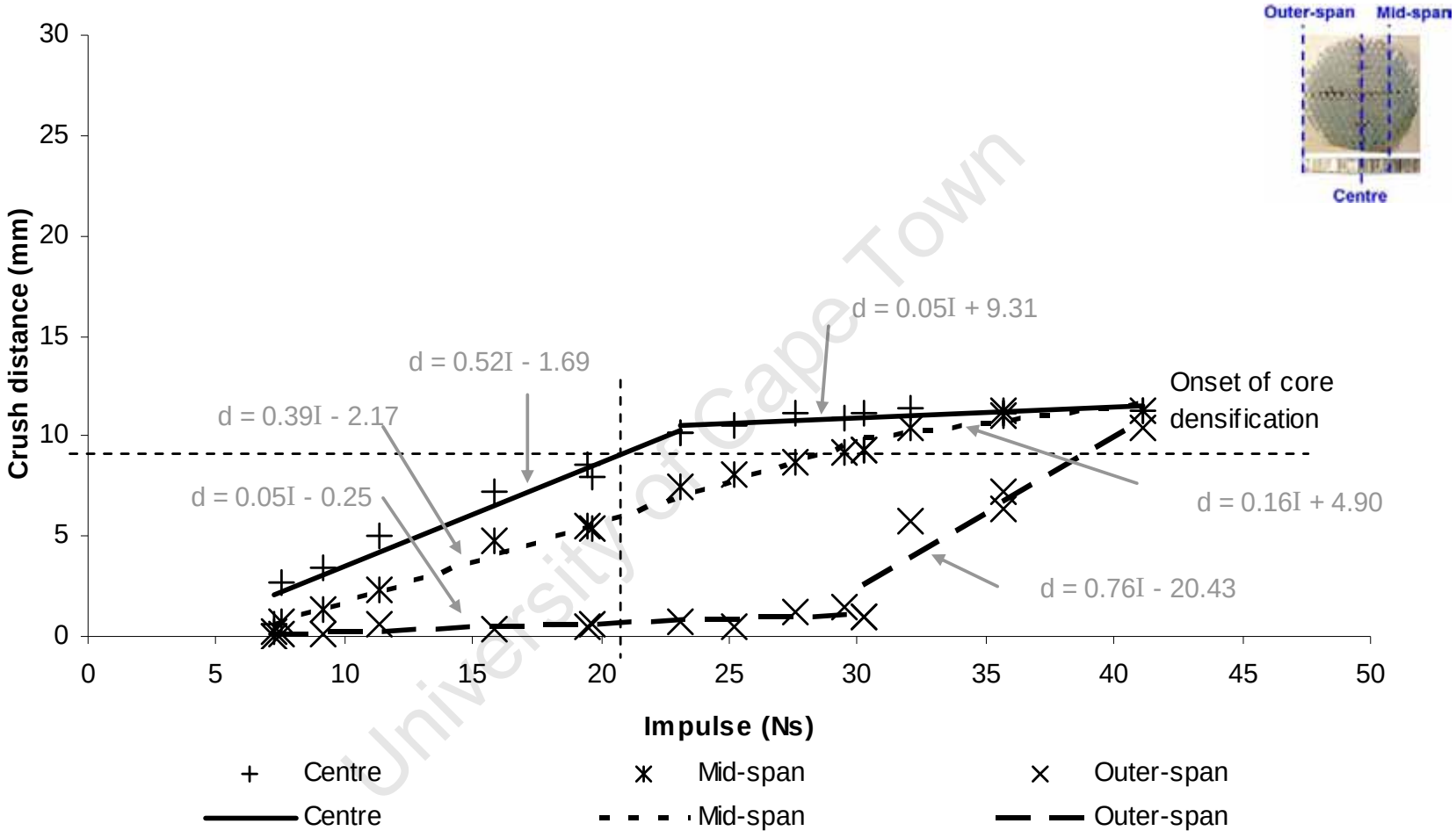

Figure 7-7: Graph of core crush distance versus impulse of S13

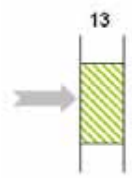

7.2.2 Analysis of test series S150

The experimental results of test series S150 are shown in Table 5-1 and Table 5-2. The face plate deflection-impulse graph is shown in Figure 7-8. The core crushing-impulse graph is shown in Figure 7-9, with the quasi-static onset of core densification superimposed on the graph.

The front plate deflects in the same way as a clamped single circular plate subjected to uniformly distributed loading [2, 28]. The plate deflection increases with increasing impulse thereafter tearing occurs and the deflection starts to decrease with increasing impulse, as shown in Figure 7-8.

The onset of core densification in the quasi-static axial compression tests occurred at 112mm crush distance (i.e. 74% strain). From Figure 7-9, it is evident that none of the S150 tests produced densification of the core, for impulses up to 40.5Ns.

A sharp increase in the core crushing gradients is observed at 31Ns, as shown in Figure 7-9. Photographs of core crushing from and after 31Ns are shown in Figure 7-10. Because no densification takes place, the only factor that influenced the gradient change is the front plate tearing. The torn front plate has kinetic energy which causes further crushing of the core. Higher impulses cause the residual velocity of the torn fragment to increase [55] and this increased the percentage crush. The core crushing increased at a faster rate with increasing impulse after tearing.

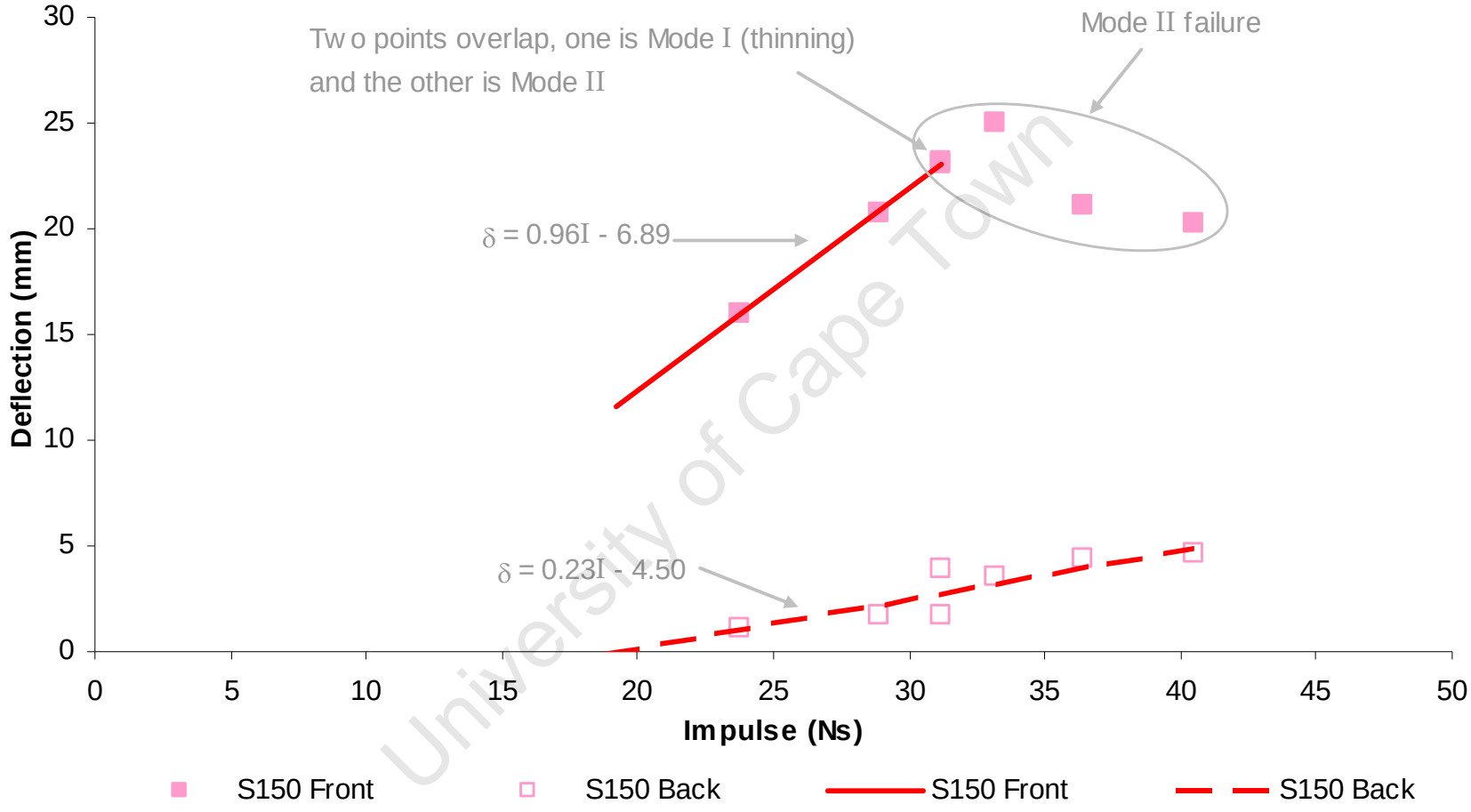

Figure 7-8: Graph of face plate deflection versus impulse of S150

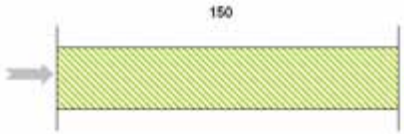

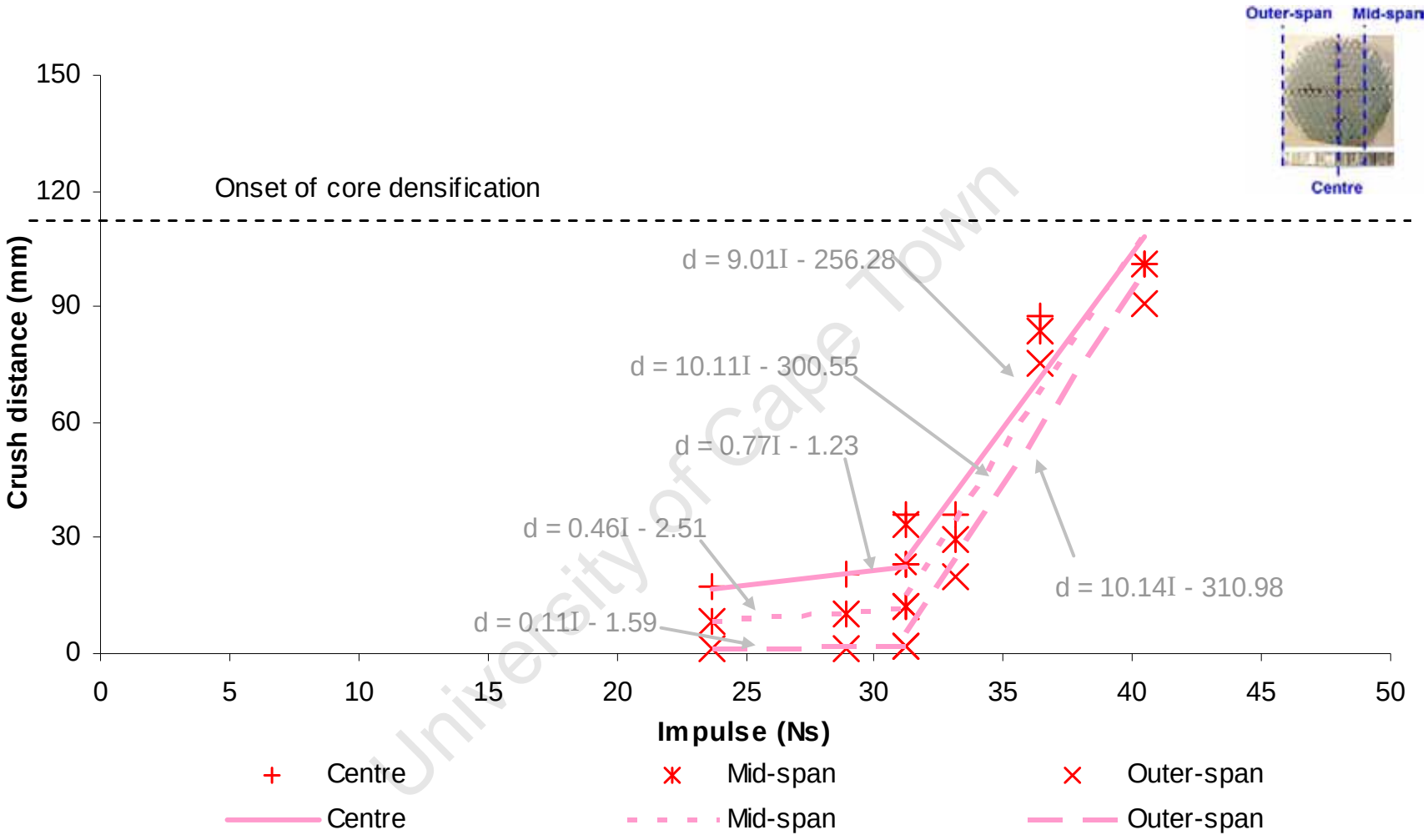

Figure 7-9: Graph of core crush distance versus impulse of S150

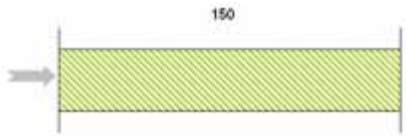

Figure 7-10: Photographs of the honeycomb cores from S150

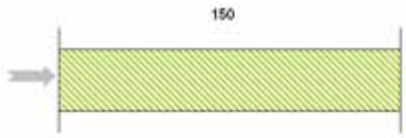

A photograph of the back plate deflections from S150 tests are shown in Figure 7-11. The back plate also responds in a similar way to a clamped single circular plate subjected to uniformly distributed blast loading. The load transferred to the back plate is regulated by the core (see Section 2.3.3). In this case, no core densification takes place therefore no dramatic increase in the back plate deflection gradient is observed, as shown in Figure 7-8.

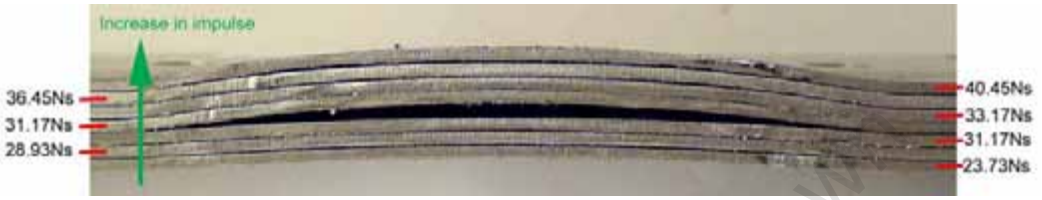

Figure 7-11: Photograph of the back plate deflections from S150

Lastly, the interaction between the mid-point deflections of the face plates and that of the core is shown in Figure 7-12. The front plate deforms into the core and the core transfers the load to the back plate. Therefore the deflection trend of the front surface of the core follows the deformation trend of the front plate. In addition, the back plate deformation profile follows the deflection of the back surface of the core.

It is noted that the front plate deflection is generally higher than the deformation of the front surface of the core. This may be due to the elastic spring back of the core after the clamp is released. However, further study is needed to investigate the effect of spring back of the core.

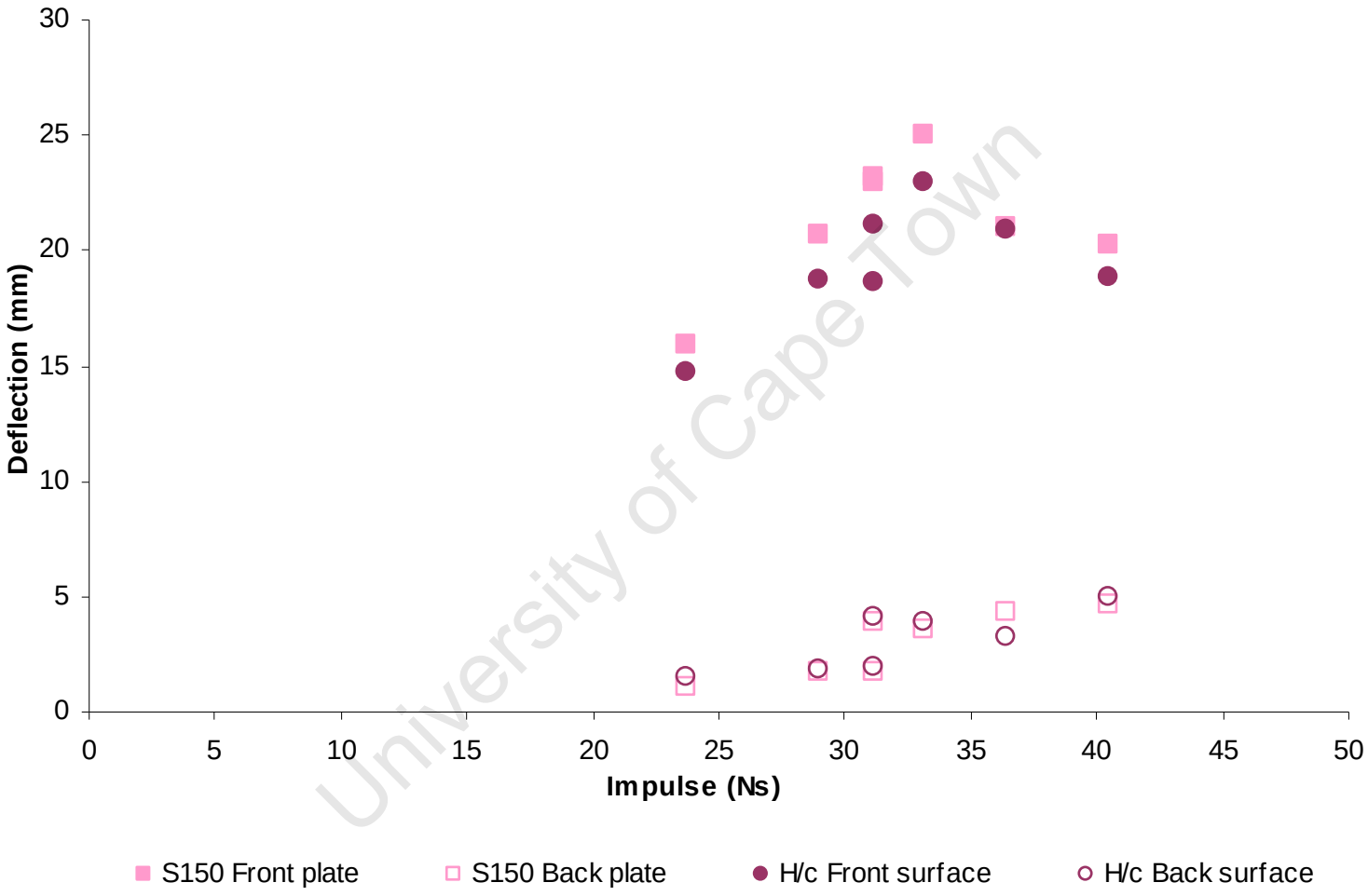

Figure 7-12: Graph of mid-point deflection of face plates and core versus impulse of S150

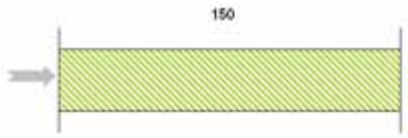

7.2.3 Analysis of test series S29

The relevant experimental results for test series S29 are listed in Table 5-3 and Table 5-4. The face plate deflection-impulse graph and the core crushing-impulse graph are shown in Figure 7-13 and Figure 7-14, respectively. The onset of core densification obtained from quasi-static compression test is superimposed on both graphs.

Just as in test series S150, the front plate deflection is similar to that of a clamped monolithic circular plate subjected to uniformly distributed blast loading [2, 28]. The torn front plate has kinetic energy which causes further core crushing. The core crushing increased at a faster rate with increasing impulse after front plate tearing. Therefore when the front plate tears (at approximately 31Ns), a gradient increase is observed in the crushing of the mid-span and outer-span of the core, as shown in Figure 7-14.

The back plate deflection is dependent on the load transferred via the core (see Section 2.3.3). Core densification appears to begin at approximately 30Ns, as shown in Figure 7-14. Higher stresses are transferred to the back plate, and the back plate deflection increases rapidly, as shown in Figure 7-13.

The interactions between the sandwich components (i.e. front plate, honeycomb core and back plate) are shown in Figure 7-15. The deflection of the front surface of the honeycomb follows a similar trend to that of the front plate; and the deflection of the back plate correlates with that of the back surface of the honeycomb.

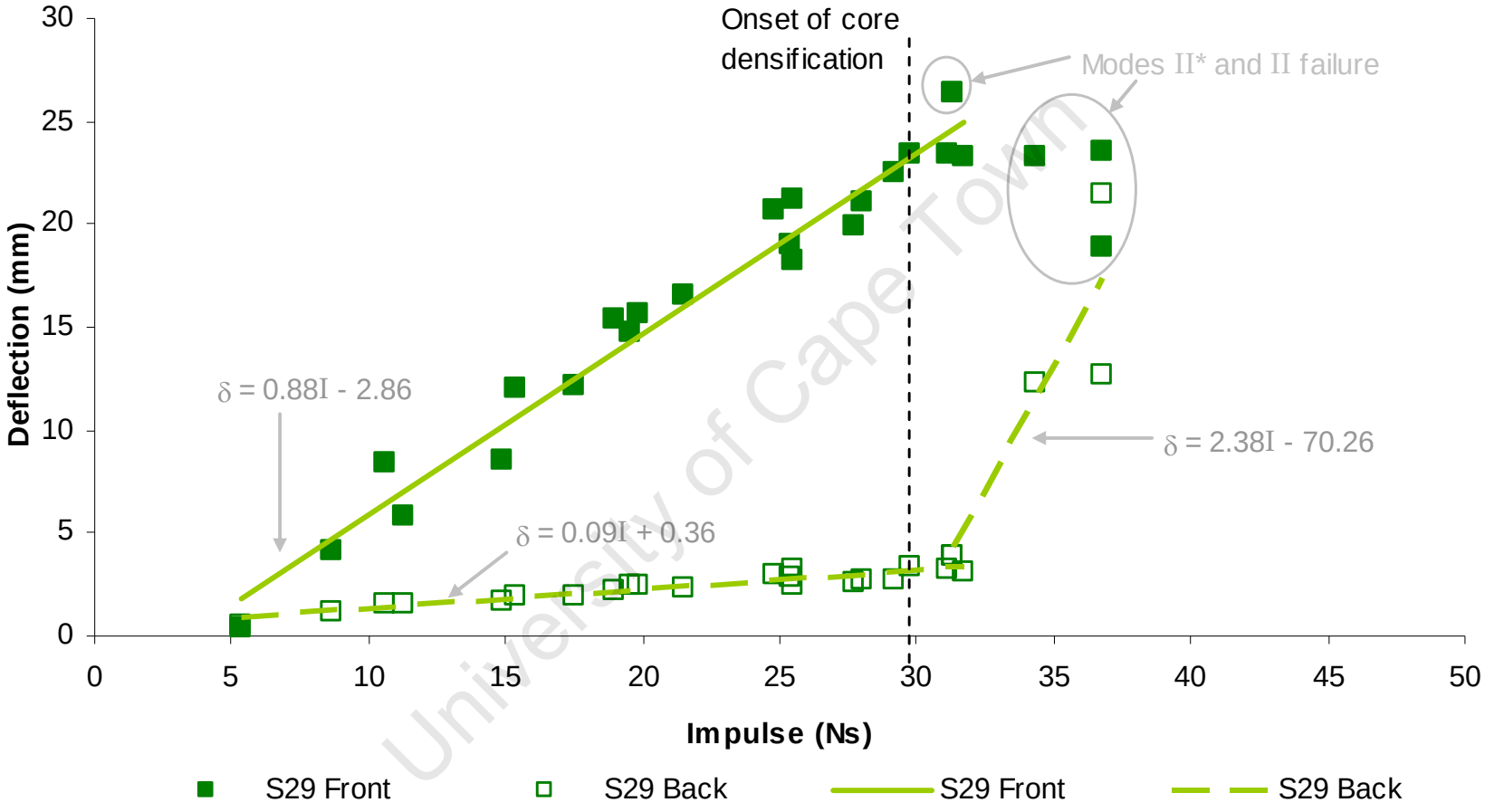

Figure 7-13: Graph of face plate mid-point deflection versus impulse of S29

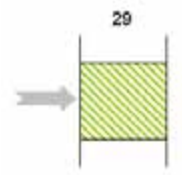

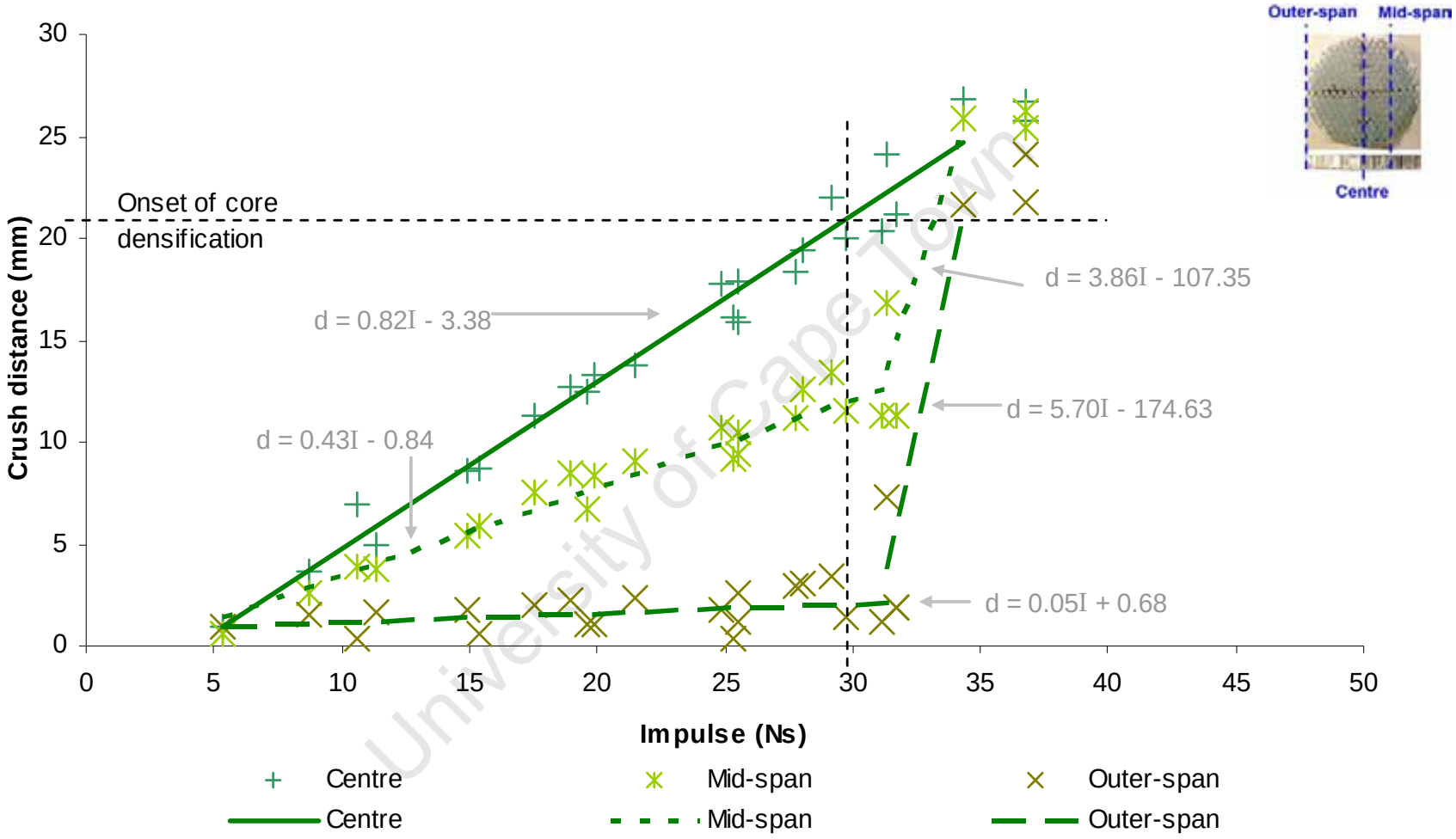

Figure 7-14: Graph of honeycomb crush distance versus impulse of S29

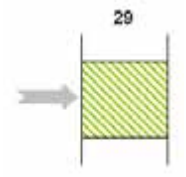

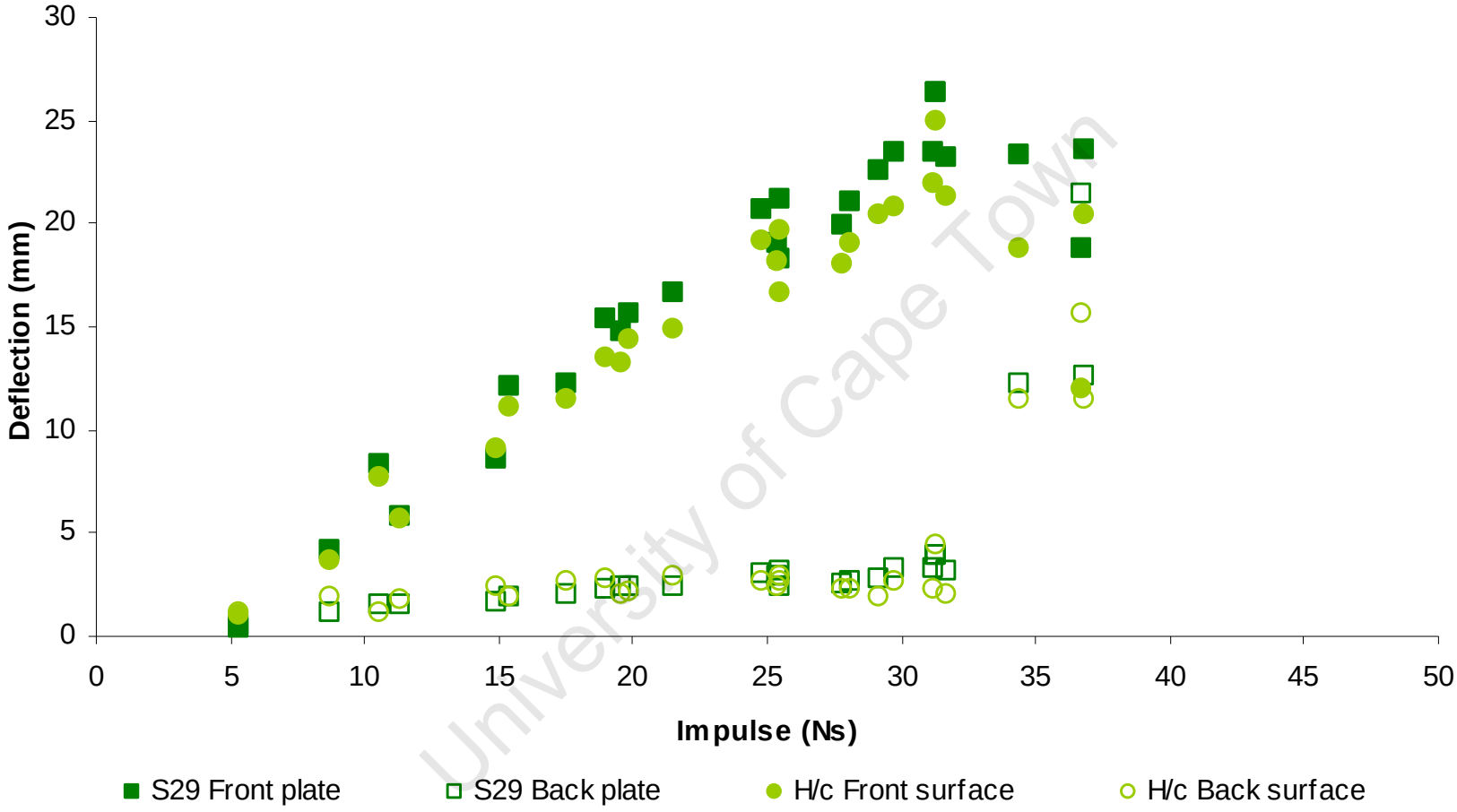

Figure 7-15: Graph of mid-point deflection of plate and honeycomb versus impulse of S29

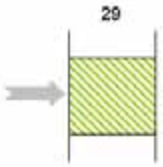

7.2.4 Analysis of test series S29-1

The experimental results of test series S29-1 are shown in Table 5-5 and Table 5-6. These panels had lower thickness (1.0mm) face plates. The graph of face plate deflection-impulse and the graph of core crushing-impulse are shown in Figure 7-16 and Figure 7-17, respectively. The onset of core densification is superimposed on both graphs.

The graphs in this test series have similar shapes and stages to those in test series S29; however the thinner face plates have lower tearing threshold impulses. The gradient increases in the crushing of the mid-span and outer-span of the core (see Figure 7-17) are due to the front plate tearing at approximately 24Ns. In addition, the gradient increase in the back plate deflection (see Figure 7-16) is due to the onset of densification at the centre region of the core. The steep rise in the back plate deflection can also be seen in the photograph as shown in Figure 7-18.

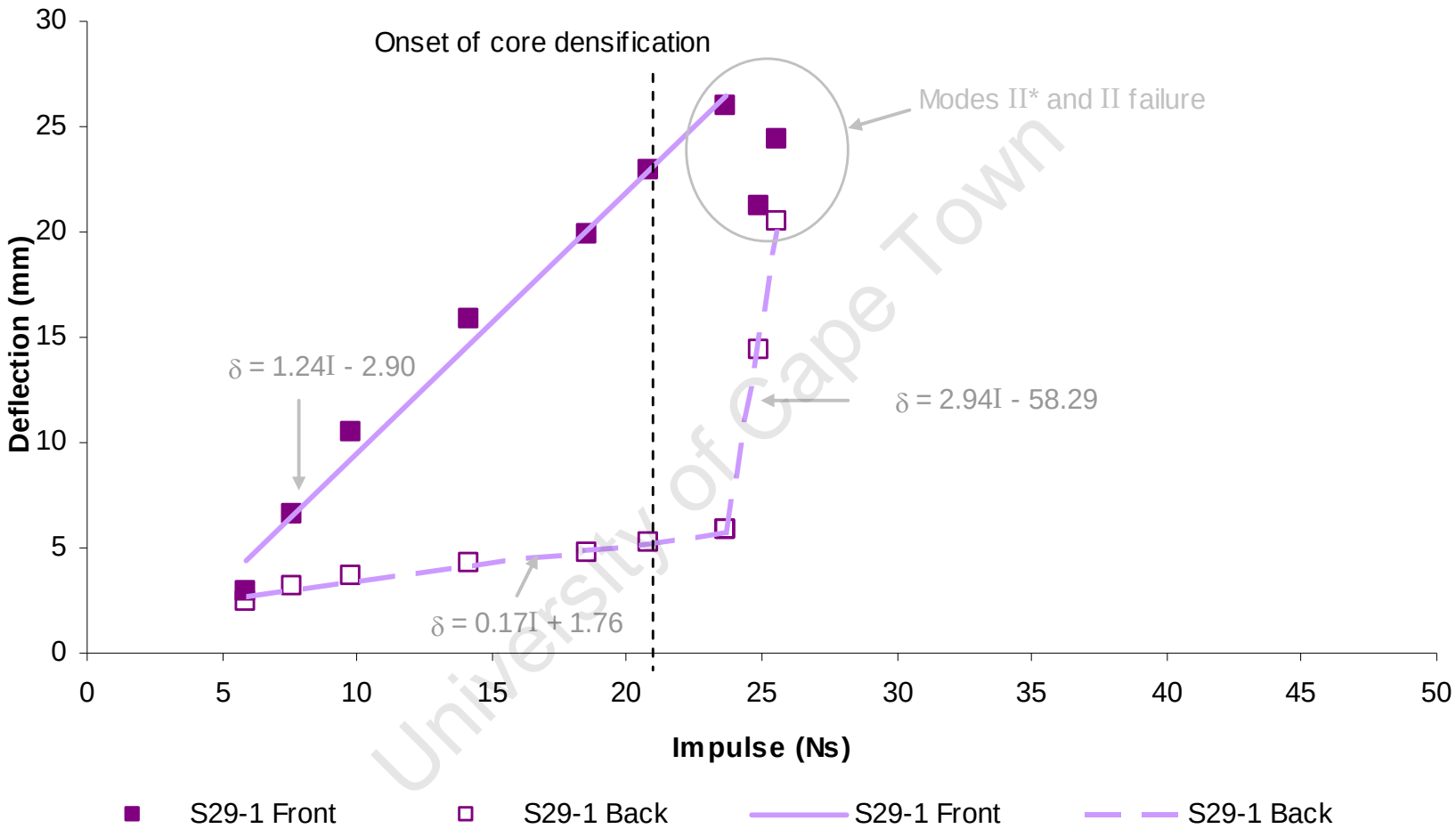

Figure 7-16: Graph of plate deflection versus impulse of S29-1

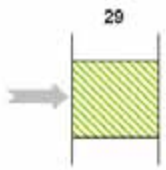

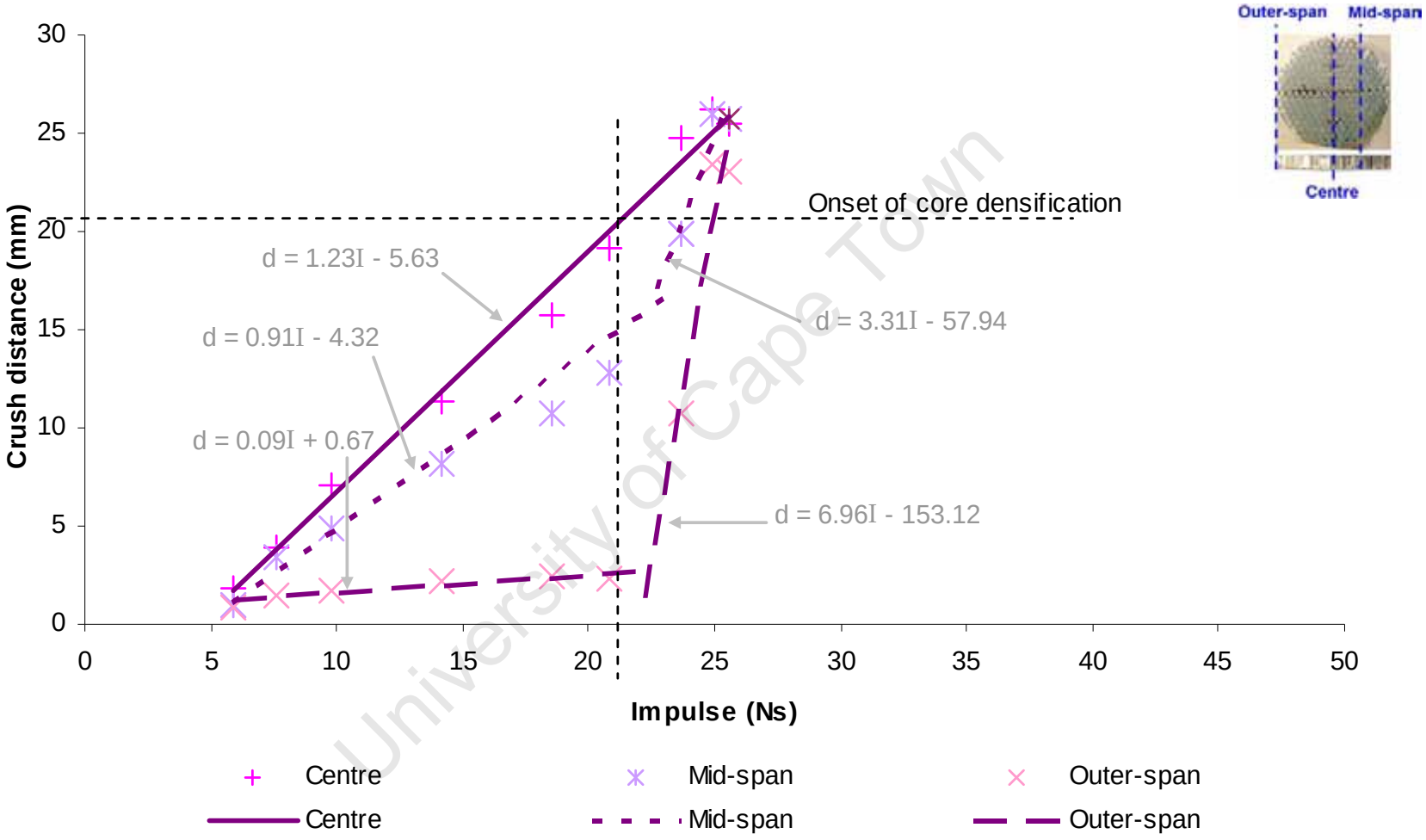

Figure 7-17: Graph of core crushing versus impulse of S29-1

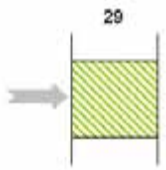

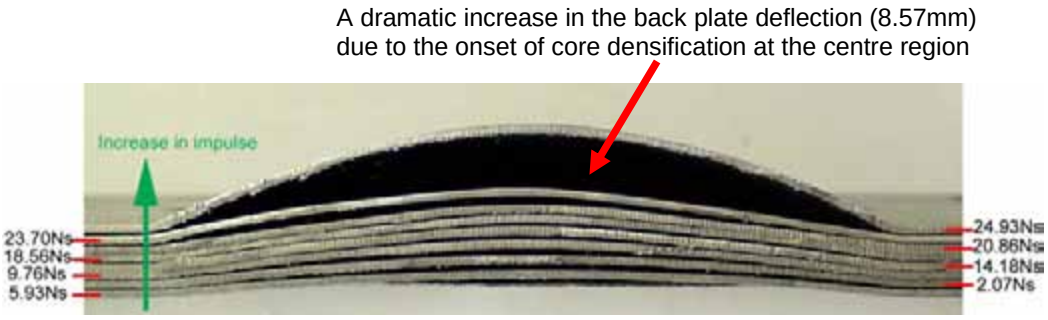

Figure 7-18: Photograph of plate deflection profile of the back plates from S29-1

The deflection of the front surface of the honeycomb follows a similar trend to that of the front plate; and the deflection of the back plate correlates with that of the back surface of the honeycomb. This relationship is demonstrated in a graph of mid-point deflection of face plates and core versus impulse, as shown in Figure 7-19. This relationship between the sandwich panel components is similar to that observed in the S29 panels. However, front plate tearing initiates at a lower impulse for the S29-1 panels (at the same deflection-thickness ratio), and the onset of core densification of the S29-1 panels occur at lower impulse (more on this in Section 8.2).

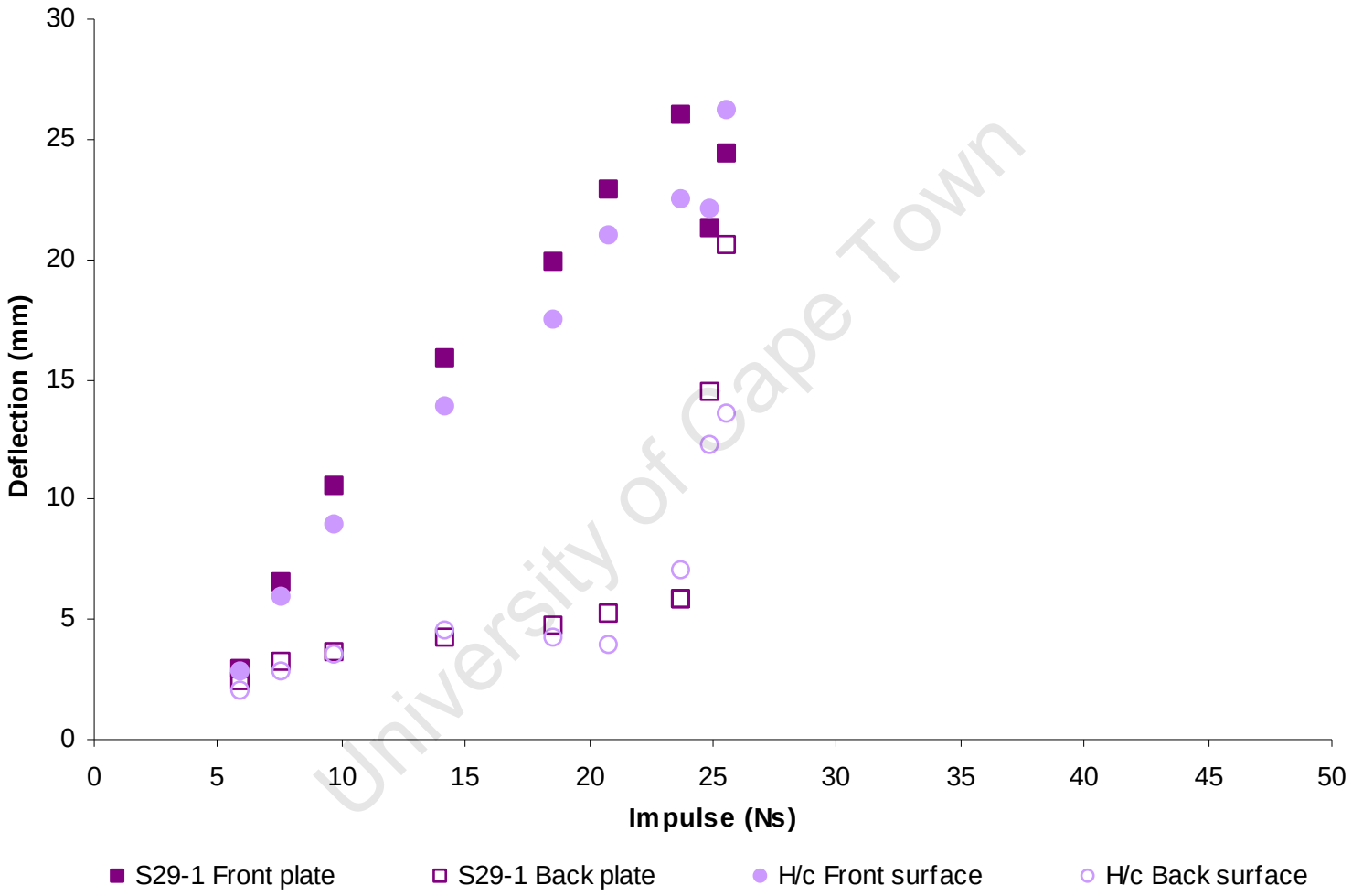

Figure 7-19: Graph of mid-point deflection of face plates and core versus impulse of S29-1

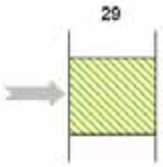

7.2.5 Analysis of test series D29/13

The experimental results for test series D29/13 are shown in Table 5-7 and Table 5-8. These test specimens consisted of a front plate, a 29mm thick honeycomb core, a middle plate, a 13mm thick honeycomb core and a back plate (as shown in Figure 4-5).

It is important to note that the maximum effective charge mass for this load diameter is 42.77g (see Section 7.1). However, at 34g of charge mass, the impulse already starts to reaches a maximum, as shown in Figure 7-1. Therefore a similar impulse is obtained for charge mass 34g and 40g (45.85Ns and 44.97Ns, respectively)

The face plate deflection-impulse graph and the core crushing-impulse graph for test series D29/13 are shown in Figure 7-20 and Figure 7-21, respectively. The onset of core densification is superimposed on both graphs. Test series D29/13 follows similar deformation profiles to that of S29. When complete core densification occurs, a decrease in the crushing gradient is observed (in the 29mm thick core centre and mid-span), as shown in Figure 7-21. Conversely, an increase in the crushing gradient is observed (see Figure 7-21) due to the tearing of the front plate at 32.5Ns.

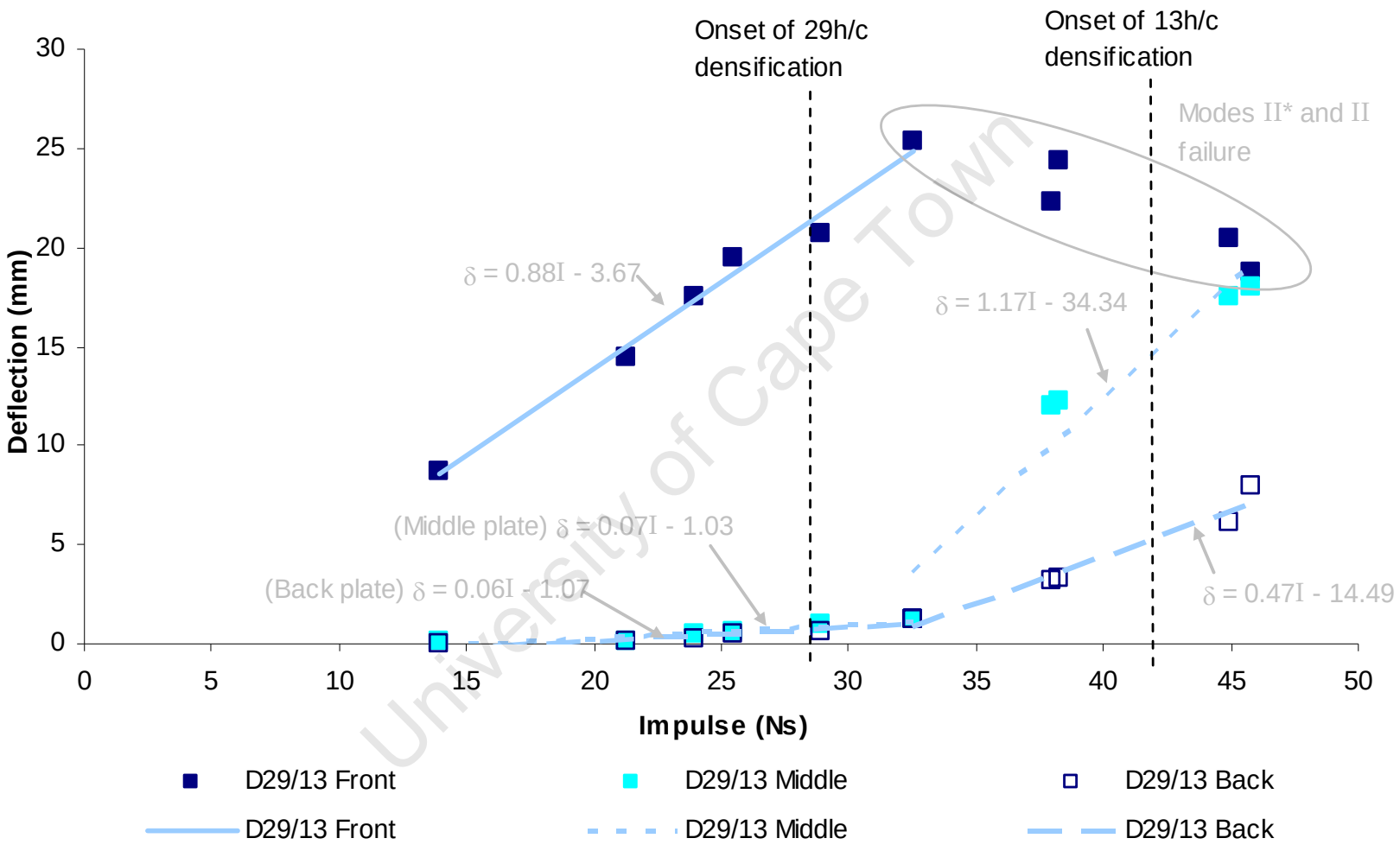

Figure 7-20: Graph of plate deflection versus impulse of D29/13

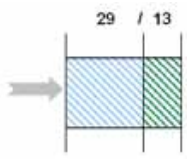

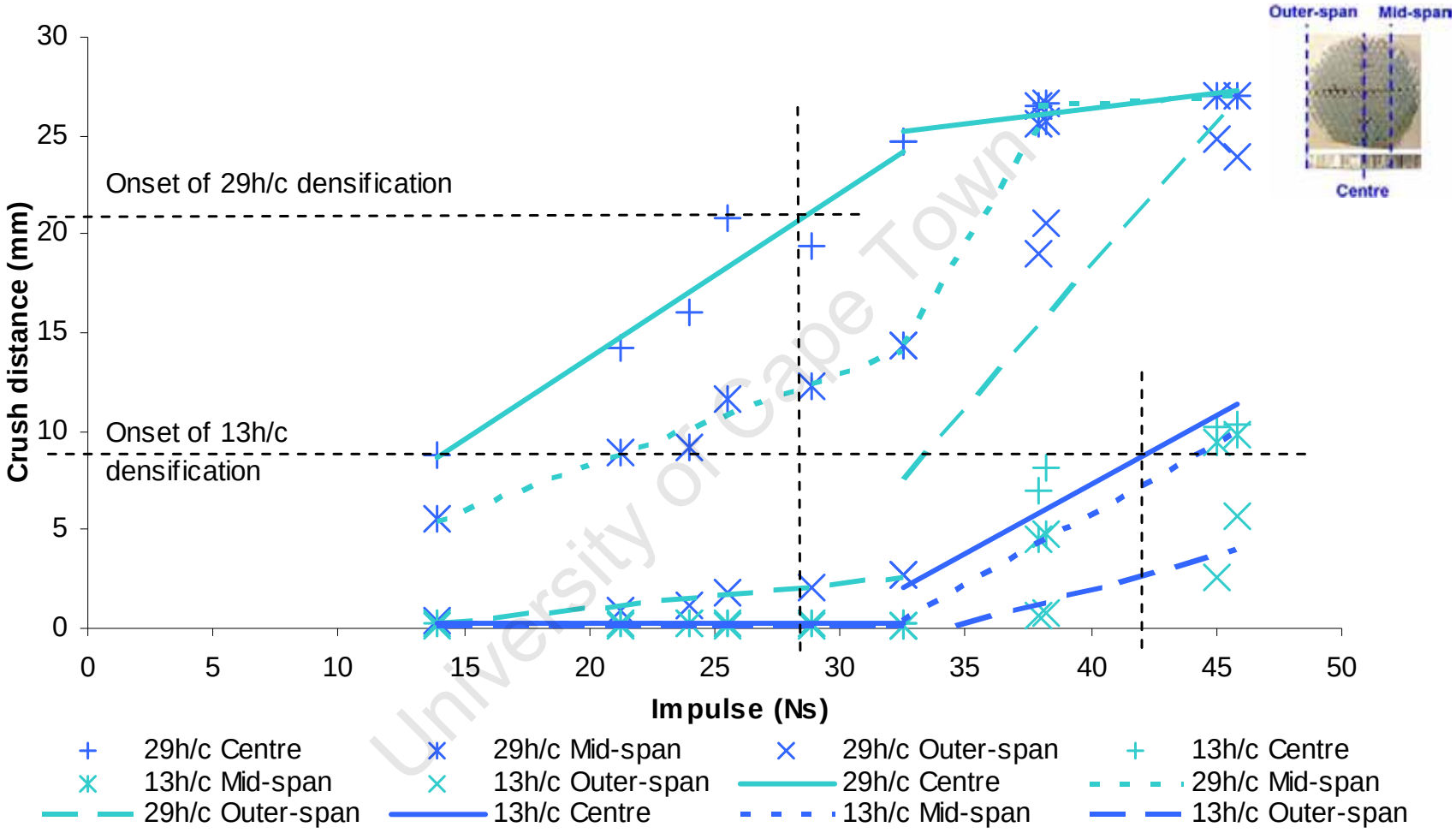

Figure 7-21: Graph of core crushing versus impulse of D29/13

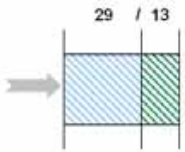

The middle plate and back plate experience deflection gradient increase (see Figure 7-20) due to the onset of core densification of the 29mm thick core. The sudden increase in the deflection of the middle plates from D29/13 tests is visible in the photograph shown in Figure 7-22.

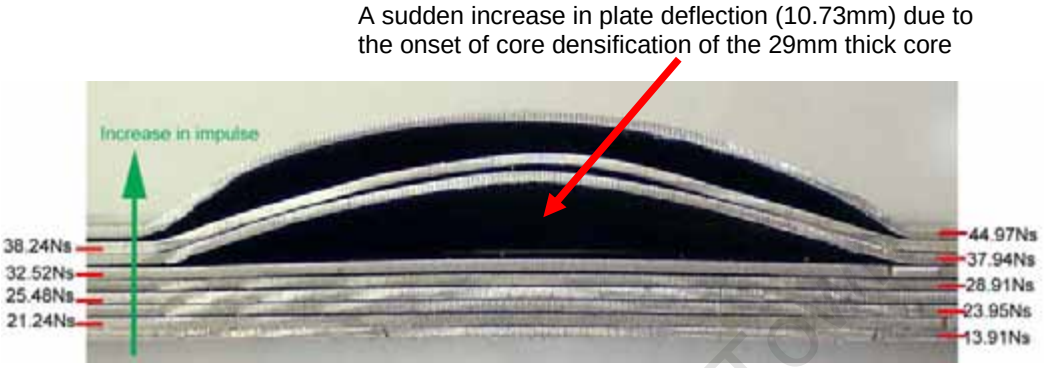

Figure 7-22: Photograph of the deflection profile of the middle plates from D29/13

Once more, just as in the other test series, the front plate deforms into the front surface of the 29mm thick honeycomb, and load is transferred to the middle plate. The middle plate then deflects into the front surface of the 13mm thick honeycomb, which in turn transfers load to the back plate. The mid-point plate deflection and core deformation are shown in Figure 7-23.

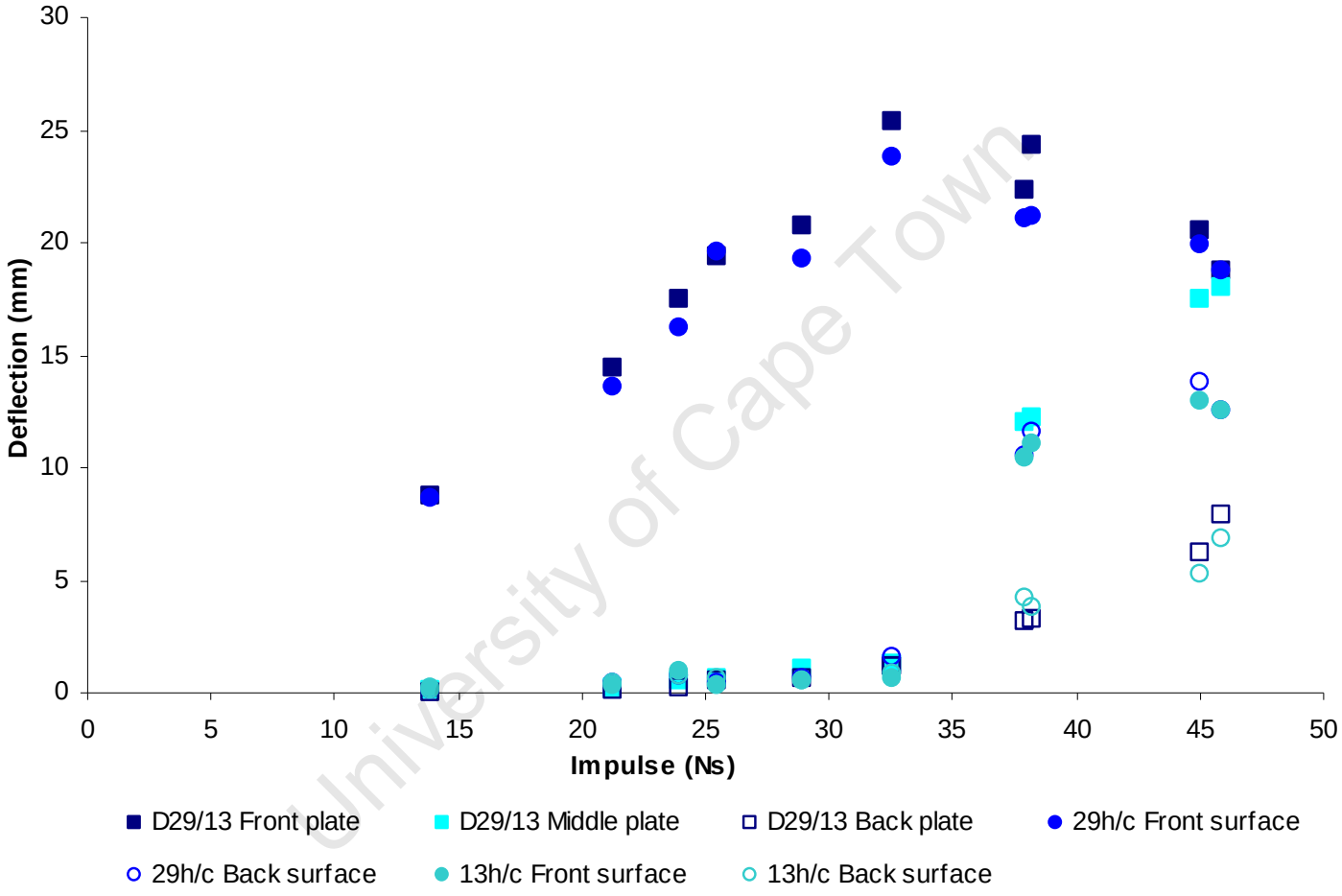

Figure 7-23: Graph of mid-point deflection of face plates and honeycomb core versus impulse of D29/13

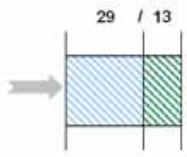

7.2.6 Analysis of test series D13a/13

The experimental results for test series D13a/13 are shown in Table 5-9 and Table 5-10. These test specimens consisted of 1.6mm thick mild steel face plates sandwiching a 13mm thick air gap and a 13mm honeycomb core (as shown in Figure 4-6). Due to the configuration of this test series, the interaction between the plates and the cores in this test series is very different from the test series analysed in the previous sections.

- **Interaction between the sandwich components**

In this sandwich configuration, the front plate deflects into the air gap. The front plate must deform more than 13mm (the air gap depth) before it will contact the honeycomb. When the front plate does contact and deform into the honeycomb, the centre of the honeycomb crushes first (see Figure 6-8), following the front plate profile. As the front plate deflection increases, the area over which honeycomb crushing occurs increases.

The mid-point deflection of the face plates and the honeycomb is shown in Figure 7-24. Unlike the test series analysed in the previous sections, in this case the deflection of the front surface of the honeycomb is much less than the front plate. This is because of the presence of the air gap. The back surface of the honeycomb is constantly in contact with the back plate. Therefore the honeycomb core transfers load to the back plate. The deflection of the back surface of the honeycomb correlates with the deflection of the back plate.

With increasing impulse, the front plate deflection increases and this increases the contact region between the front plate and the front surface of the honeycomb. The increase in the contact region is shown in Figure 7-25.

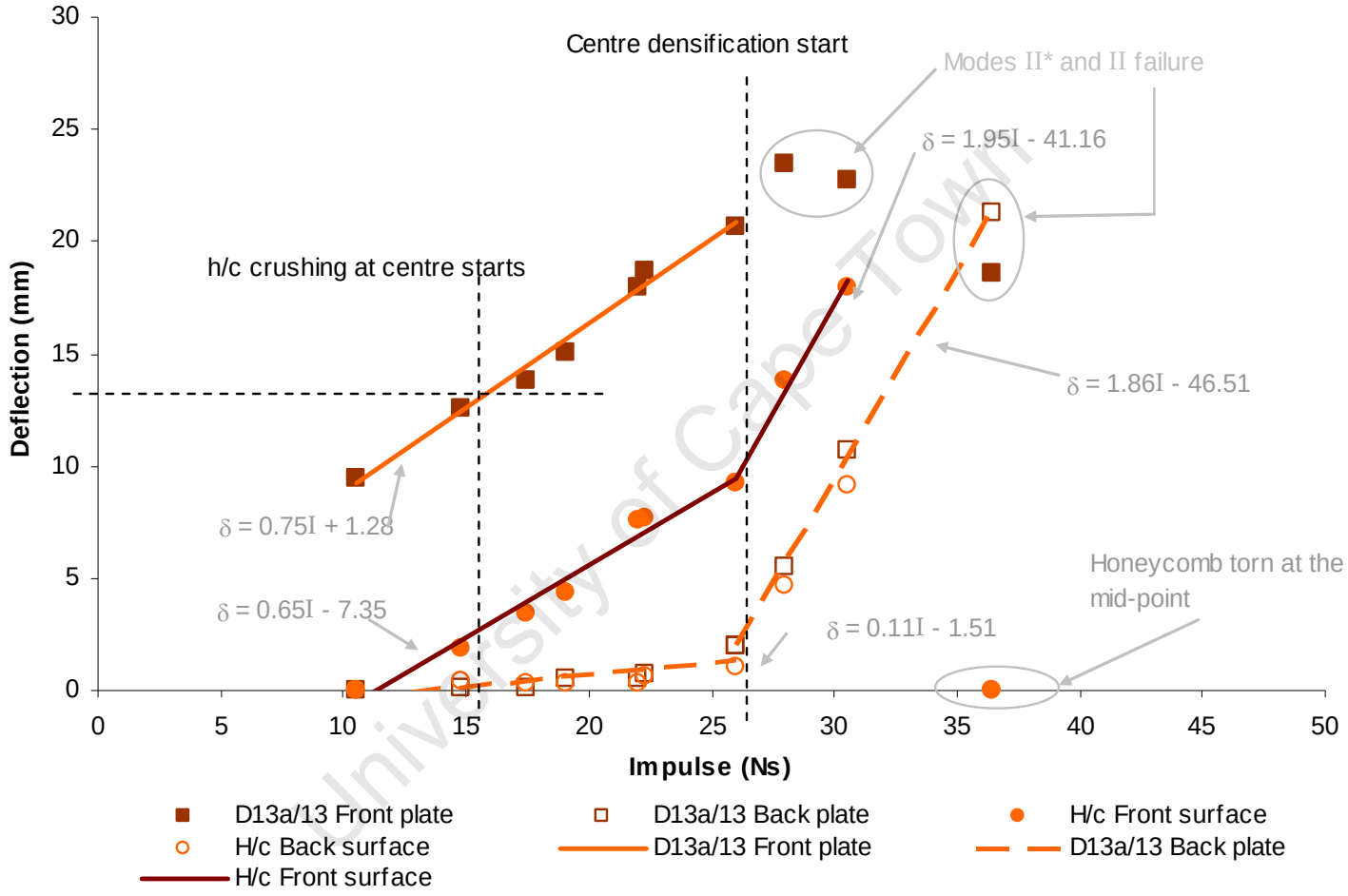

Figure 7-24: Graph of mid-point deflection of face plates and honeycomb versus impulse of D13a/13

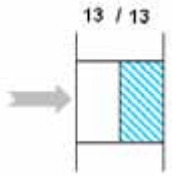

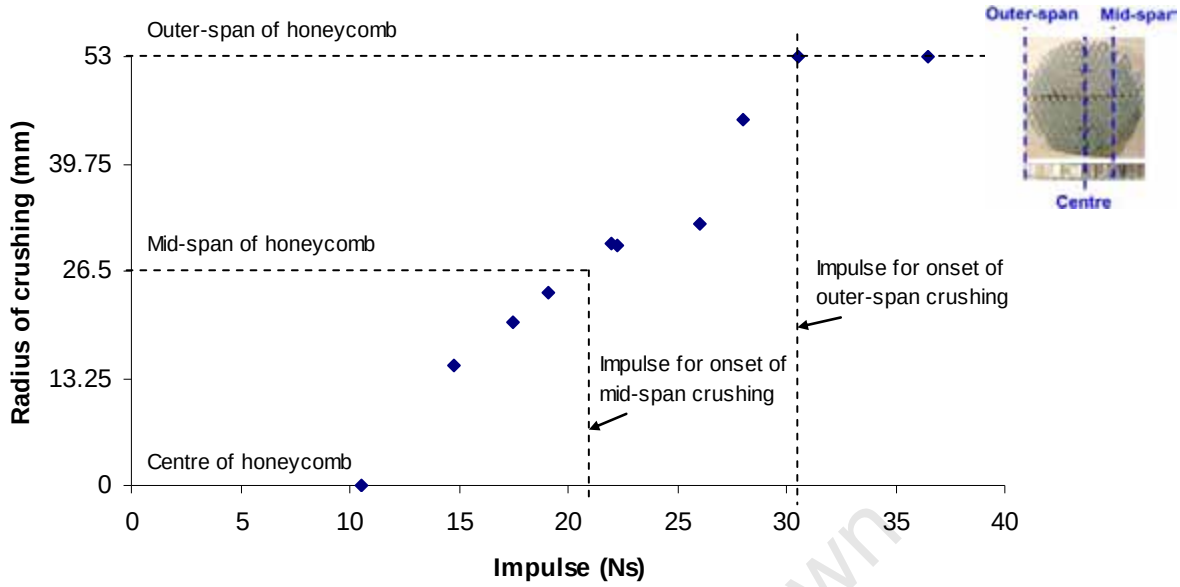

Figure 7-25: Graph of radius of honeycomb crushing versus impulse of D13a/13

It can be seen in Figure 7-24 that the front plate deflects first. Then at approximately 15Ns, the centre of the honeycomb starts to deform, as shown in Figure 7-25. This impulse corresponds to permanent deflection of the front plate of approximately 13mm. At approximately 21Ns, the mid-span of the honeycomb starts to crush, as shown in Figure 7-25. The crushing of the centre region of the honeycombs at higher impulses is visible in the photographs in Figure 7-26. As the impulse increases, there is a clear increase in the area of honeycomb crushing, as evident in Figure 7-25 and Figure 7-26.

- **Deformation of the plates and cores**

The plate deflection-impulse graph and the core crushing-impulse graph are shown in Figure 7-27 and Figure 7-28, respectively. The onset of core densification is superimposed on both graphs. The face plate deflection and the core crushing exhibit the same gradient changes as those test series previously analysed. The gradient increase in the mid-span and outer-span of the honeycomb (see Figure 7-28) are due to the tearing of the front plate. The gradient increase in the back plate deflection (see Figure 7-27) is due to the onset of honeycomb densification at the centre region.

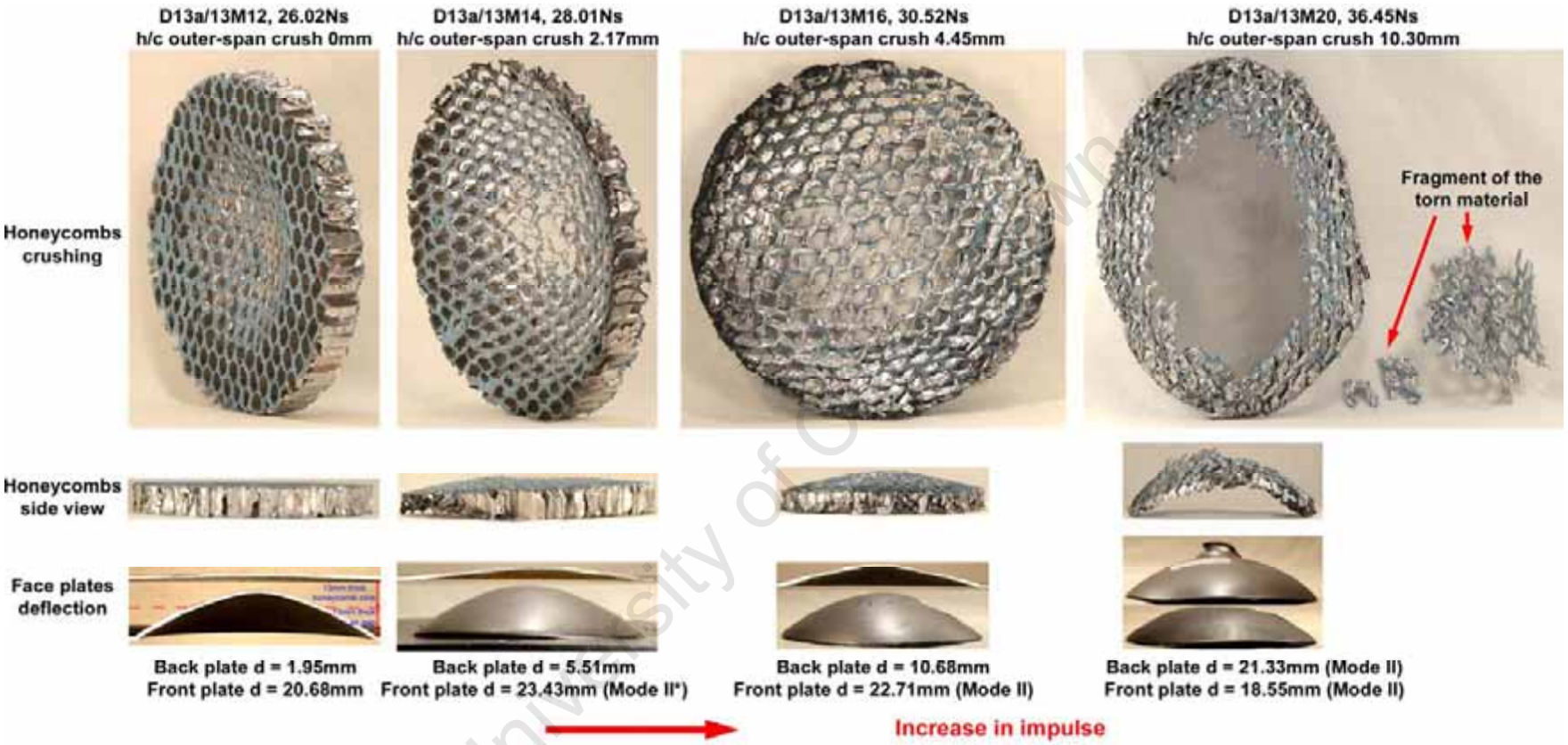

Figure 7-26: Photographs of core crushing and deflection of face plates from D13a/13

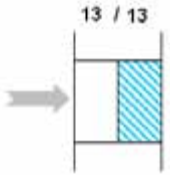

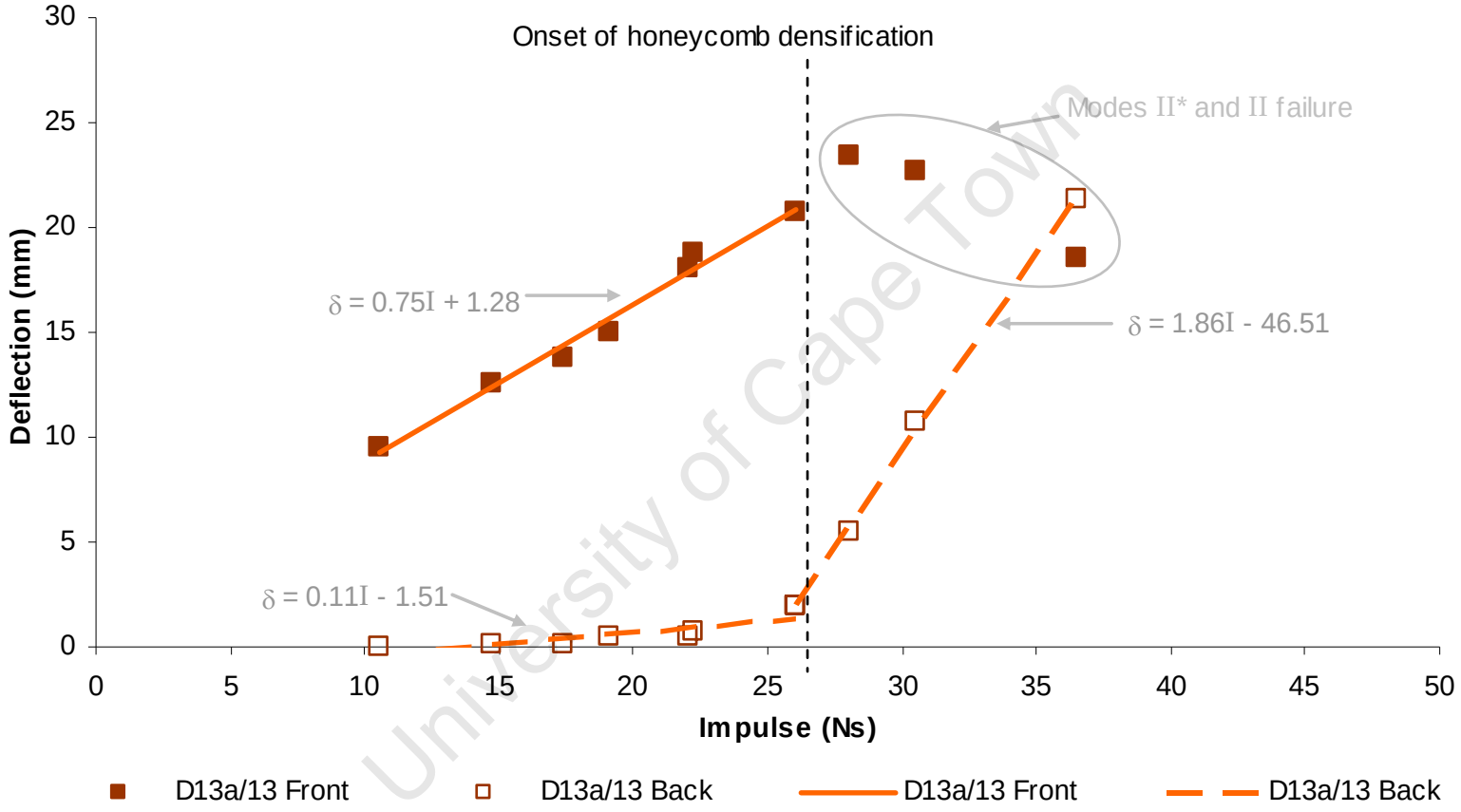

Figure 7-27: Graph of plate deflection versus impulse of D13a/13

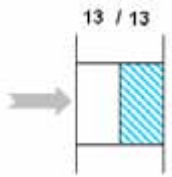

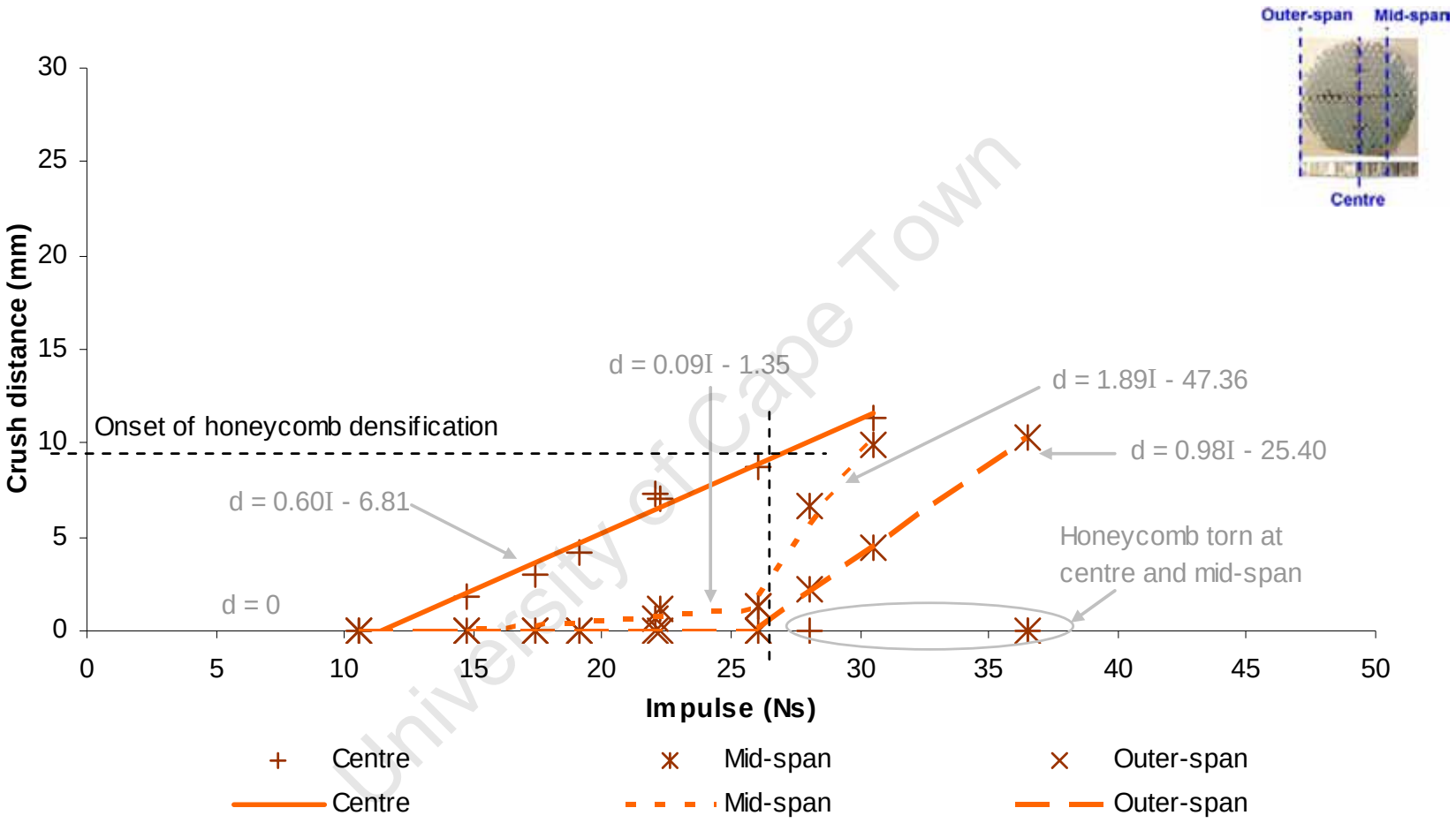

Figure 7-28: Graph of core crushing versus impulse of D13a/13

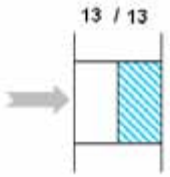

8 - DISCUSSION

This chapter compares the test series to investigate the effect of varying core thickness, face plate thickness, and core arrangement.

8.1 EFFECT OF CORE THICKNESS

This section investigates the effect of the core thickness on the blast response of the sandwich panels. The three test series, namely S13, S29 and S150, used the same face plate thickness but different core thicknesses.

8.1.1 Front plate deflections

Jacob et al [46] proposed the dimensionless damage number for a monolithic circular plate subjected to blast loading:

$$\phi_c = \frac{I\left(1+\ln\left(R_p/R_0\right)\right)}{\pi R_p H^2\sqrt{\sigma_0\rho}}\left(\frac{1}{1+\ln\left(r/R_0\right)}\right) \qquad \textbf{Eq 8.1}$$

This dimensionless damage number normalises the difference in the impulse (I), the plate radius (R_p), the load radius (R_0), the plate thickness (H), the static yield stress of the plate (σ_0), the plate material density (ρ), and the stand-off distance (r).

Jacob et al [46] reported that for a monolithic plate blasted at different stand-off distances (13-300mm) the results are enveloped within the 90% confidence lines of the Nurick and Martin [6] empirical relationship:

$$\frac{\delta}{H} = 0.425\phi_c \qquad \textbf{Eq 8.2}$$

A graph of deflection-thickness ratio versus dimensionless impulse for the front plates of the test series S13, S29 and S150 is shown in Figure 8-1. The data do not include the torn plates (Modes II* and II failure). The Nurick and Martin empirical relationship (Eq 8.2) and the 90% and 99.9% confidence lines are superimposed on Figure 8-1. Most data are enveloped between the empirical relationship and the lower 99.9% confidence line. The 90% confidence lines bracket only most of the S29 data. The rest of the data from S29 and all data from S13 and S150 fall below the lower 90% confidence line. This indicates that the empirical relationship slightly overestimates the front plate deflection of honeycomb sandwich panels. This shows that the honeycomb core provides structural support for the front plate under blasting situations.

Data from series S13 fall on either side of the lower 99.9% confidence line; and at impulses higher than approximately 30Ns the S13 data fall below the line. The S13 data lying outside of the 99.9% confidence line has lower deflection-thickness ratio at higher dimensionless impulses because of the relatively small core thickness of the sandwich panel. As mentioned in Section 7.2.1, the expected maximum deflection of a monolithic circular mild steel plate subjected to uniformly distributed blasting prior to tearing is approximately 30mm [2]. Before S13 core densification, there is no discernable influence of core thickness on the deflection of front plates. However, after core densification, the front plate starts to deform into the back plate. This reduces the front plate deflection to be less than the predicted empirical value. At a deflection of 13mm (8.1 plate thicknesses) the front plate contacts the back plate and the front plate deflections no longer increase linearly with increasing dimensionless impulse.

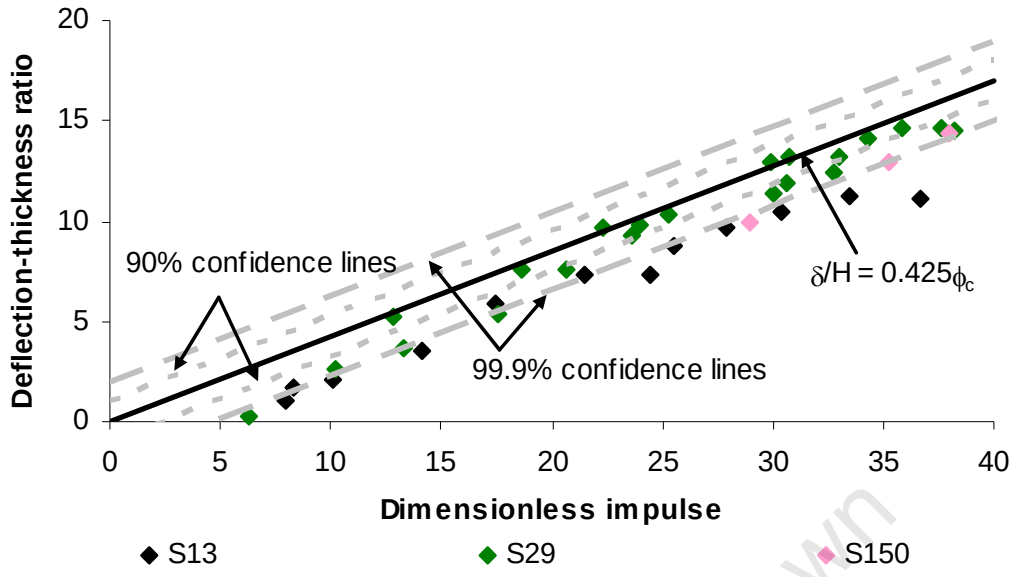

Figure 8-1: Graph of deflection-thickness ratio versus dimensionless impulse of the front plates of S13, S29 and S150

8.1.2 Core crushing

The graph of honeycomb core centre crushing–thickness ratio versus impulse of test series S13, S29 and S150 is shown in Figure 8-2. The core crushing is divided by the original thickness to normalise the effect of core thickness. It can be seen that with increasing core thickness, the ratio of core crushing is dramatically decreased; as might be expected since front plate deformation controls core crushing.

8.1.3 Core crush distance gradient change

The core crushing gradient change is shown in Figure 8-2. There are two scenarios – a gradient increase and a gradient decrease:

- In test series S13, as the centre of the core crushes to the maximum limit, the crushing gradient decreases and the best fit approaches a horizontal line. This shows that core crushing gradient decreases when the core reaches complete densification.

- In test series S150, the core is too thick for densification to occur over the impulse range applied to the front plates. Therefore core crushing gradient increase is due to front plate tearing.

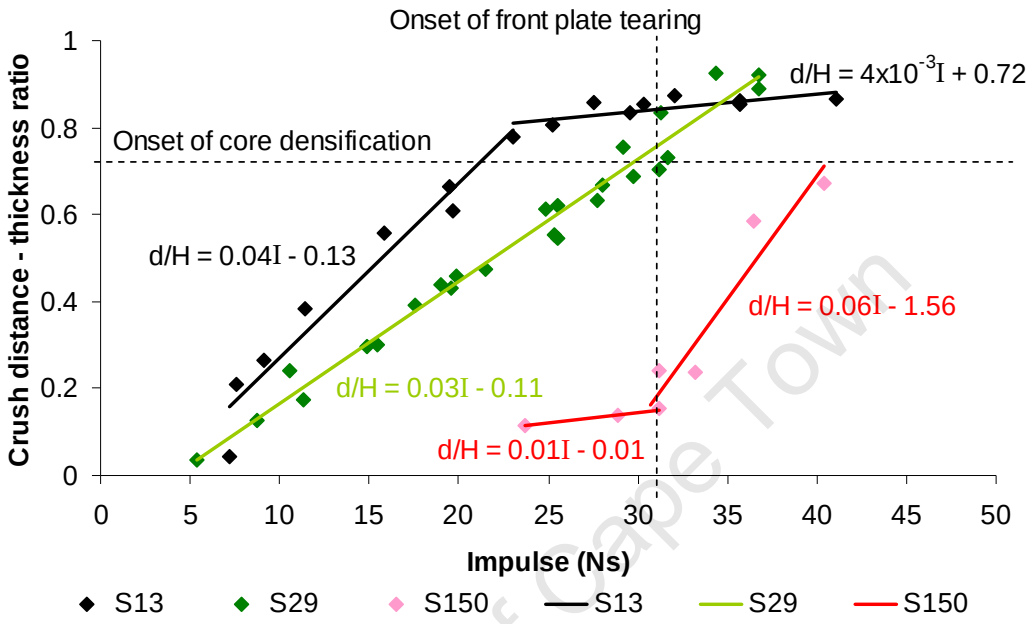

Figure 8-2: Graph of crush distance–thickness ratio versus impulse of the honeycomb core centres of S13, S29 and S150

8.1.4 Back plate deflections

The back plate deflection versus impulse graph of the three test series is shown in Figure 8-3. This graph should be analysed using two factors: the material property of the core (i.e. the plateau stress) and the core thickness.

The plateau stress is influenced by the branch angle and foil thickness (see Section 2.2.2), and is independent of the core thickness. The stress transferred to the back plate is limited to the plateau stress of the honeycomb before the onset of core densification. An increase in plateau stress enables higher stresses to be transferred to the back plate, thereby increasing the back plate deflection.

In the current study, the plateau stresses of the 13mm, 29mm and 150mm thick honeycombs are 2.5MPa, 1.7MPa and 2.2MPa, respectively. Considering only this factor, it is expected that S13 exhibits the highest back plate deflections, S150 showing less back plate deflections, and S29 the least back plate deflections. However, this is not the case as shown in Figure 8-3.

Figure 8-3 shows that the back plates deflect less with increasing in the core thickness. In addition, the deflection curves are shifted to the right; indicating that the thicker core can sustain higher impulses and resulting in less back plate deflection. In S13 and S29 panels, the back plates exhibit a change in deflection gradient. The back plate deflections increase rapidly with increasing impulse in the S13 and S29 panels once the honeycomb centre had densified. In S150 panels, there was no core densification therefore no back plate gradient change occurs. At sufficient impulse, the load transfer through the core is large enough to cause back plate tearing in S13 and S29 panels. In S150 panels, the thicker core does not densify so the lower loads result in smaller deflections on the back plate and no tearing occurs.

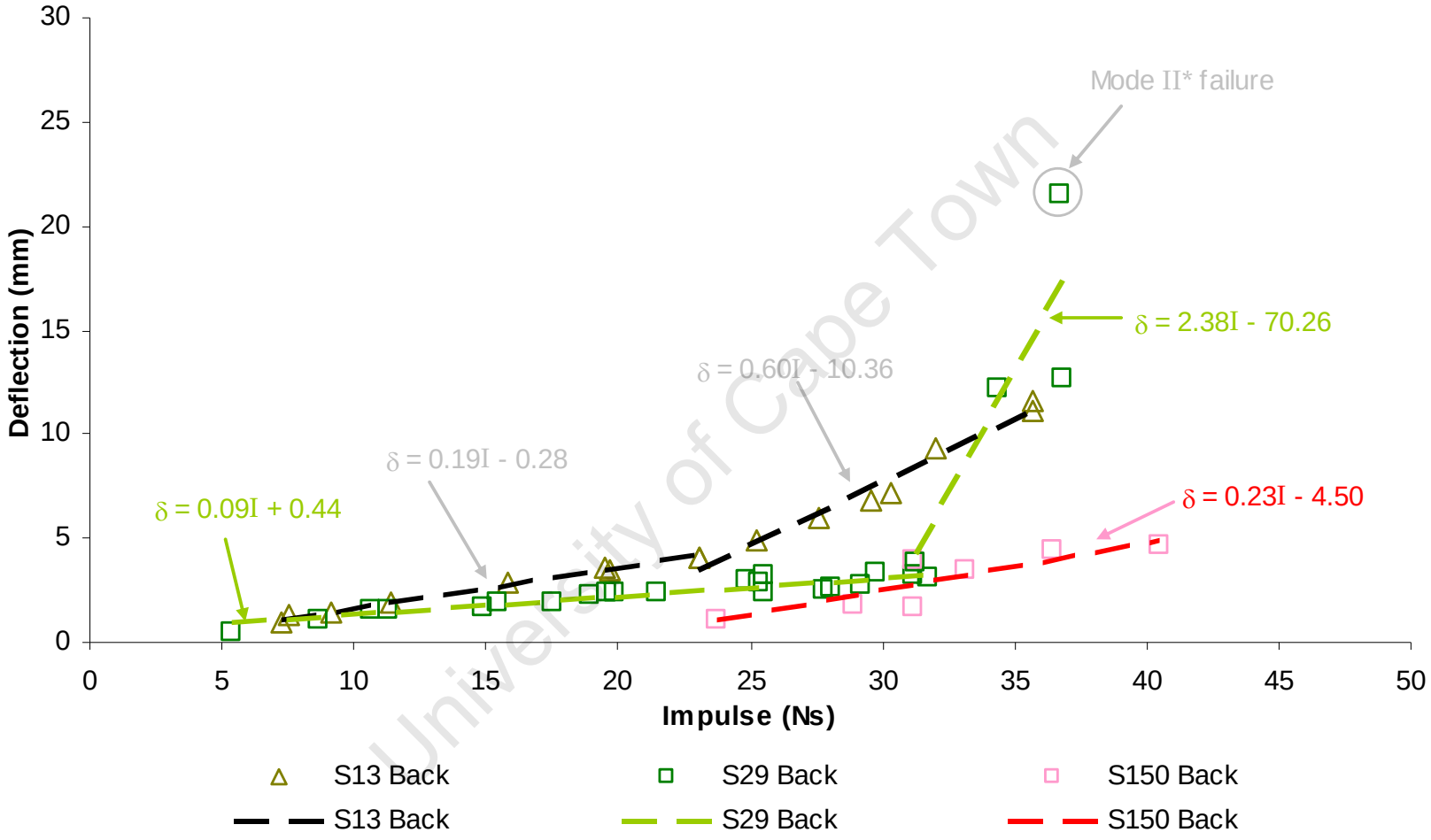

Figure 8-3: Graph of back plate deflection versus impulse of S13, S29 and S150

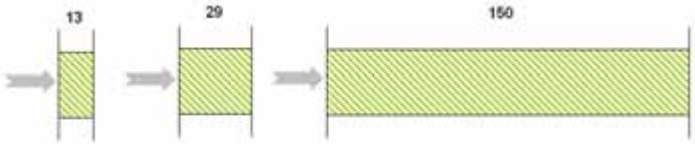

8.2 EFFECT OF FACE PLATE THICKNESS

This section investigates the effect of plate thickness on the blasting response of the sandwich panels. The two test series, namely S29 and S29-1 make use of the same core, but different plate thickness.

8.2.1 Front plate deflections

The photographs of the deflection profile of S29 and S29-1 are shown in Figure 8-4. The sandwich panels were subjected to similar impulse but the S29 plates exhibited much less deflection. In addition, a graph of deflection versus impulse for the front plates of S29-1 and S29 is shown in Figure 8-5. It also shows that at a similar impulse the thicker face plates exhibit much less deflection, as expected due to the higher thickness of the face plates.

Figure 8-4: Plate deflection profile of S29-1 (a) and S29 (b)

A graph of deflection-thickness ratio versus dimensionless impulse for the front plates of S29-1 and S29 is shown in Figure 8-6. The data do not include the torn plates (Modes II* and II failure). The Nurick and Martin empirical relationship (Eq 8.2) and the 90% and 99.9% confidence lines are superimposed on Figure 8-6. The data from S29 panels fall between the empirical relationship and the lower 99.9% confidence line. All data from S29-1 panels are below the prediction. This is because the stiffness of the honeycomb becomes more dominant compared to the stiffness of the front plate and decreased the normalised front plate deflections (see Figure 8-6). As a result, the honeycomb becomes more effective in decreasing the dimensionless front plate deflection of thinner face plates.

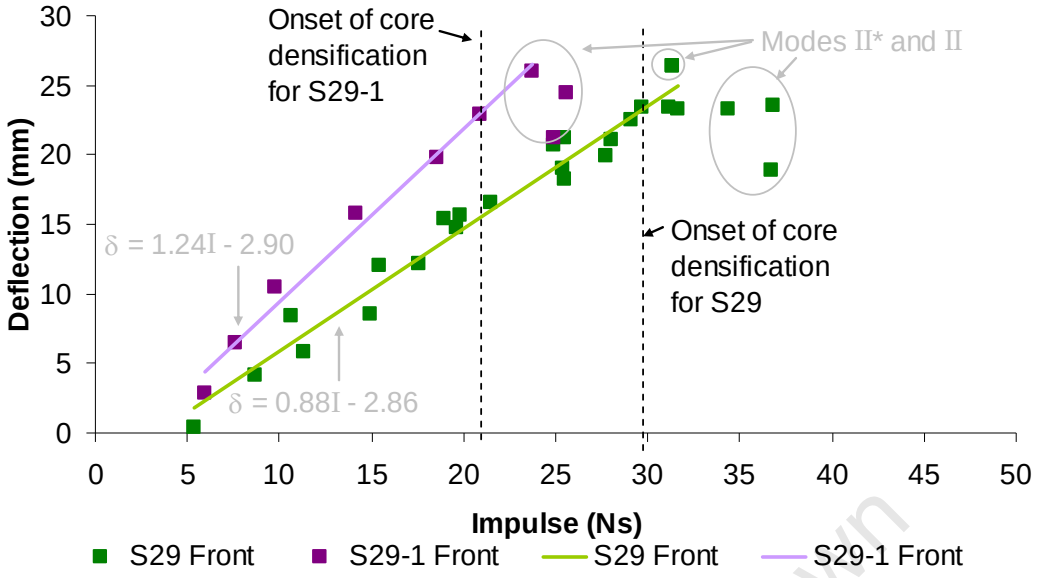

Figure 8-5: Graph of deflection versus impulse of the front plate of S29 and S29-1

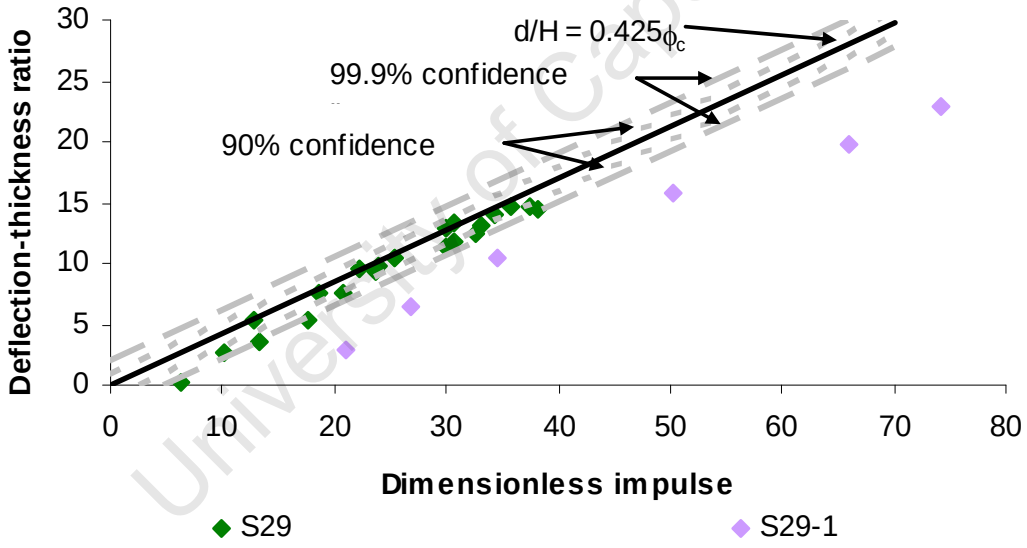

Figure 8-6: Graph of deflection-thickness ratio versus dimensionless impulse of the front plates of S29 and S29-1

8.2.2 Core crushing

A graph of core crushing versus impulse for S29 and S29-1 is shown in Figure 8-7. The two test series used the same honeycomb material and the same core thickness. Therefore the core densification occurs at the same crush distance (approximately 72% strain). However, it is clear that for the same impulse, S29-1 suffers greater core

crushing. This is because the thinner front plate deflects more. This causes greater core crushing, so core densification starts at a smaller impulse for S29-1.

Photographs of two honeycomb cores are shown in Figure 8-8, showing core deformation at a similar impulse for S29 and S29-1 panels. Because the onset of core densification occurs at a lower impulse for S29-1, the specimen shown here is already near completely densification. Conversely, at this impulse, core densification has not yet started for the S29 specimen.

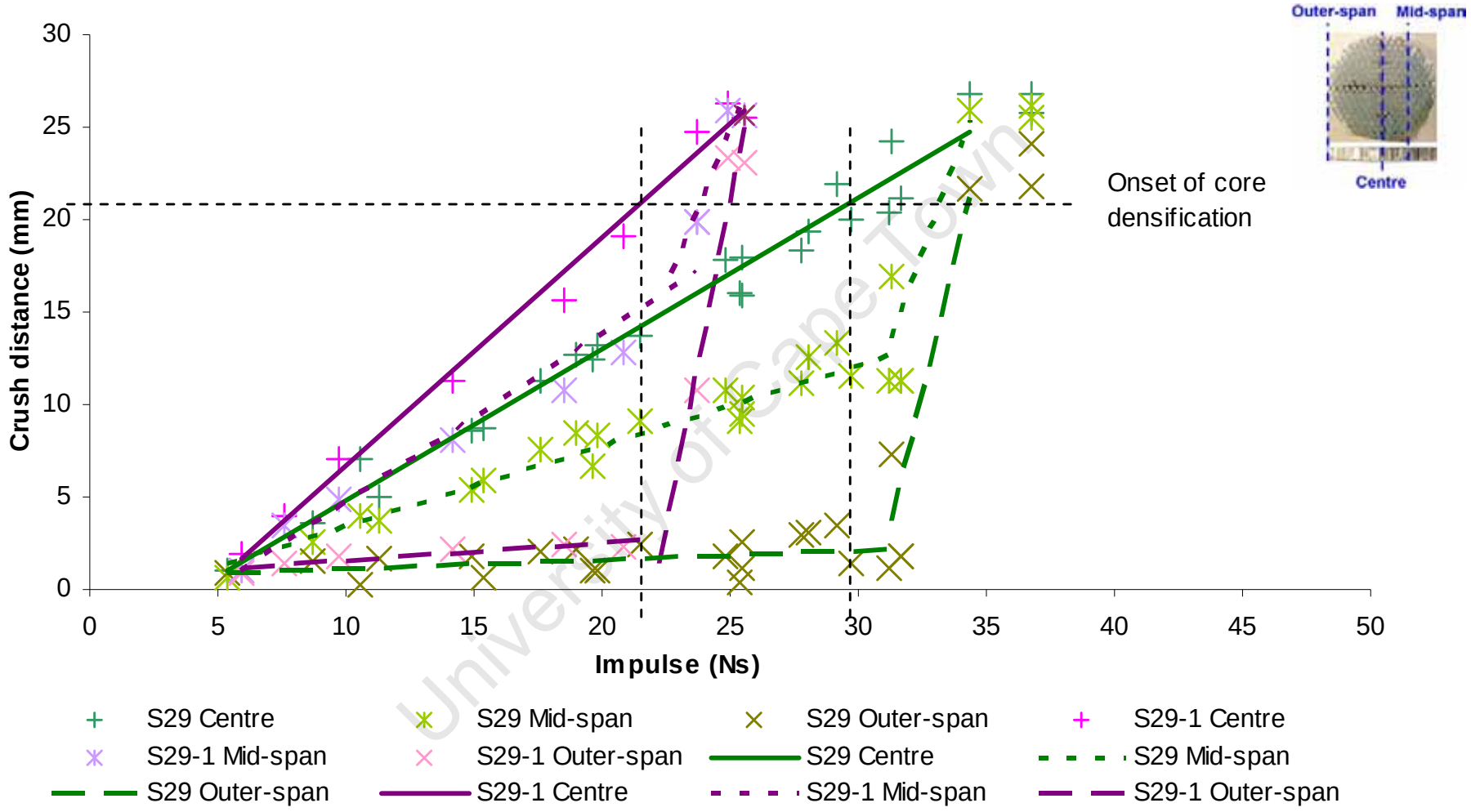

Figure 8-7: Graph of core crushing versus impulse of S29 and S29-1

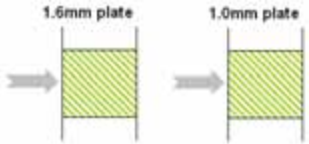

Figure 8-8: Photograph of honeycomb specimens of S29-1 (a) and S29 (b) at a similar impulse range

8.2.3 Back plate deflections

A graph of deflection-thickness ratio versus impulse for the back plates of S29 and S29-1 is shown in Figure 8-9. It can be seen in Figure 8-9 that at the same impulse, S29-1 suffers higher back plate deformation. Even prior to densification and tearing, the back plate deflects higher as the front plate displacements are higher. The onset of core densification and front plate tearing takes place at lower impulse for S29-1 and so the back plate deflection increases at faster rate at lower impulse. Therefore, tearing of the back plate begins at lower impulse for S29-1.

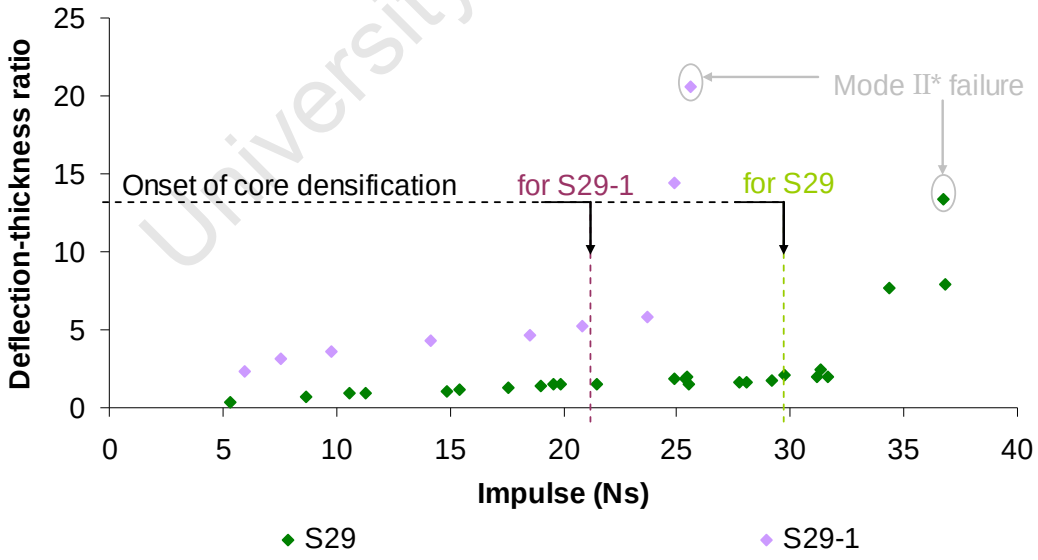

Figure 8-9: Graph of deflection-thickness ratio versus impulse of the back plates of S29 and S29-1

8.3 COMPARISON OF THE S29 AND D29/13 TEST SERIES

This section investigates the effect of inserting an extra 13mm honeycomb core and a steel plate to the response of a sandwich panel. The test series under investigation are S29 and D29/13.

8.3.1 Front plate deflections

The photographs of the deflection profile of D29/13 and S29 are shown in Figure 8-10. The sandwich panels were subjected to a similar impulse range. The front plate of S29 exhibits similar deflection (approximately 0.2 plate thicknesses difference) to the front plate of D29/13. The back plate of S29 suffers a greater deflection than the middle plate (approximately 1 plate thickness) and the back plate (1.25 plate thicknesses) of the D29/13.

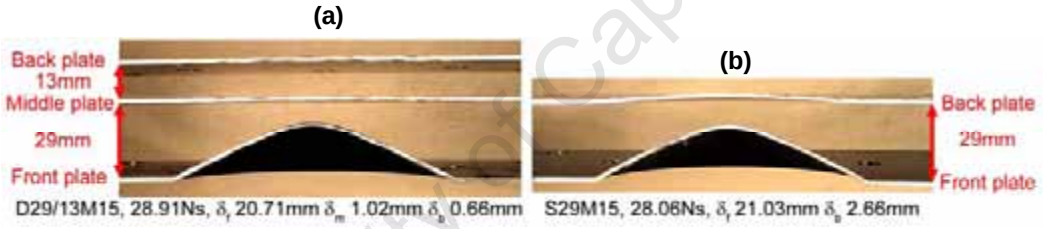

Figure 8-10: Photographs of plate deflection profile of D29/13 (a) and S29 (b) panels, for a charge mass of 15grams

A graph of mid-point deflection versus impulse is shown in Figure 8-11. It can be seen that the front plates from the two test series correlate well with each other. The deflection of the front plate of S29 is slightly higher than that of D29/13. However, this is within the experimental variation.

Graph of deflection-thickness ratio versus dimensionless impulse for the front plates of D29/13 and S29 is shown in Figure 8-12 . The data do not include the torn plates (Modes II* and II failure). The Nurick and Martin empirical relationship (Eq 8.2) and the 90% and 99.9% confidence lines are superimposed on Figure 8-12. All data fall within the 99.9% confidence envelope.

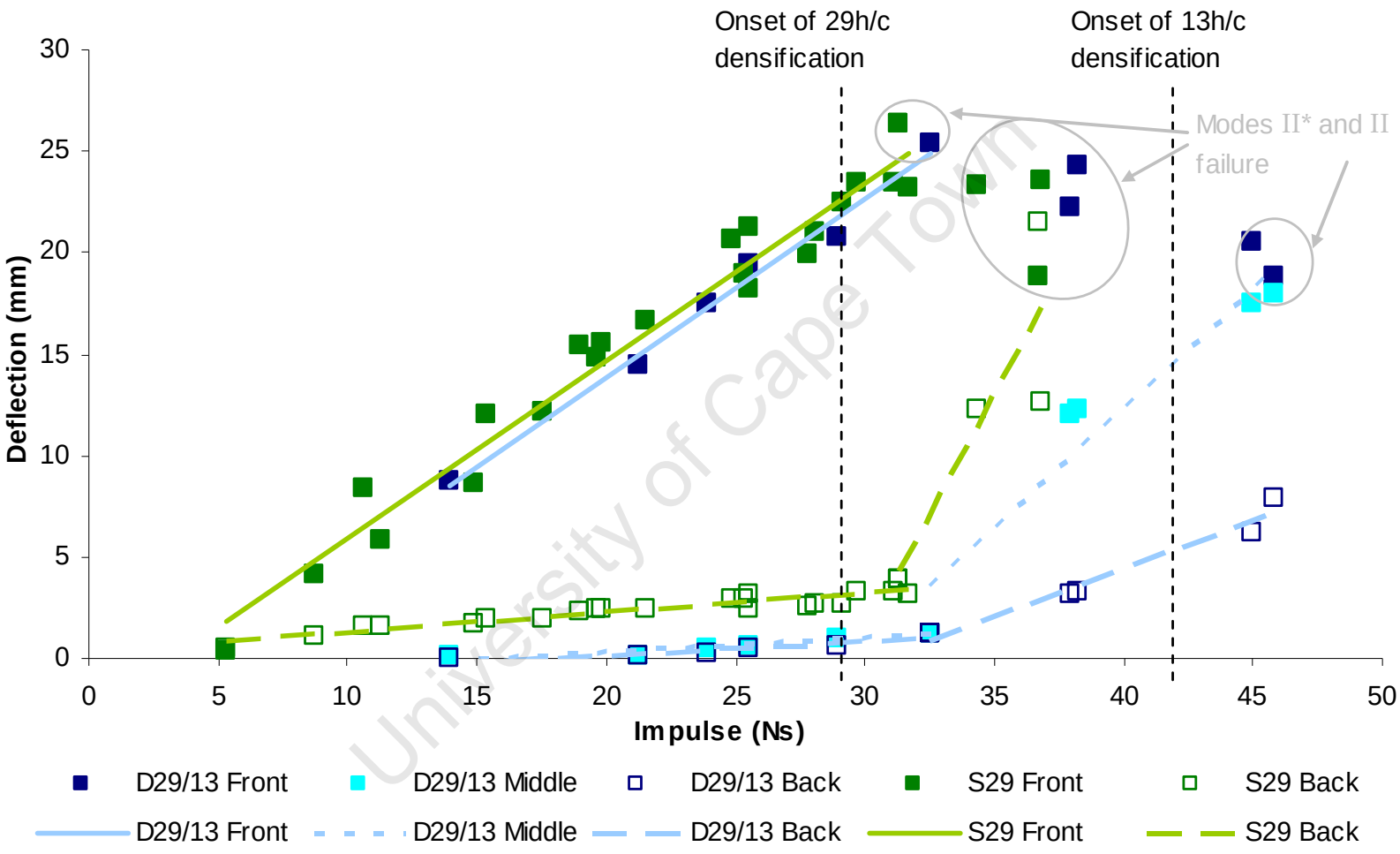

Figure 8-11: Graph of plate deflection versus impulse of D29/13 and S29

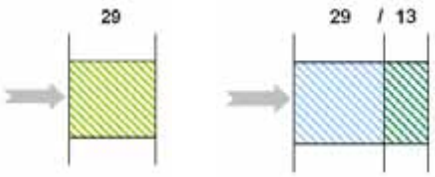

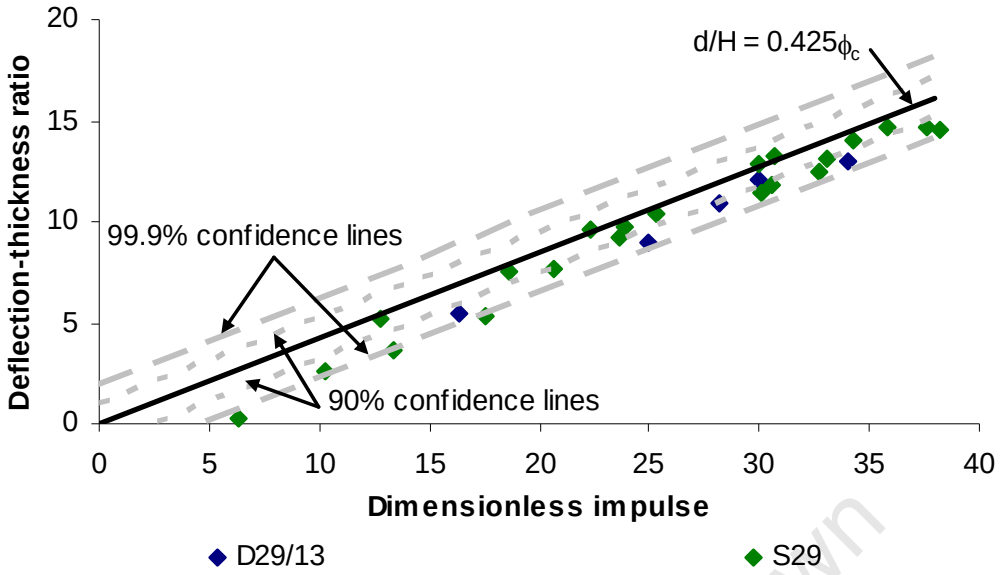

Figure 8-12: Graph of deflection-thickness ratio versus dimensionless impulse of the front plates of D29/13 and S29

8.3.2 Core densification of the 29mm thick honeycomb

Graph of core crushing versus impulse for D29/13 and S29 is shown in Figure 8-13. The 29mm thick honeycomb in test series D29/13 and S29 responded in a similar manner. At impulses higher than 35Ns, the 29mm thick honeycombs in both test series are close to complete densification.

Photographs of the honeycomb cores from two tests are shown in Figure 8-14, which shows core deformation at a similar impulse range for D29/13 and S29. In both cases the centre and mid-span of the 29mm thick honeycombs experience complete densification. However, the outer-span of the 29mm thick honeycomb in D29/13 could still be crushed more. Please note that only the outer-span crushing distance is indicated on Figure 8-14 because the centre and mid-span crush are not clearly visible in the photographs.

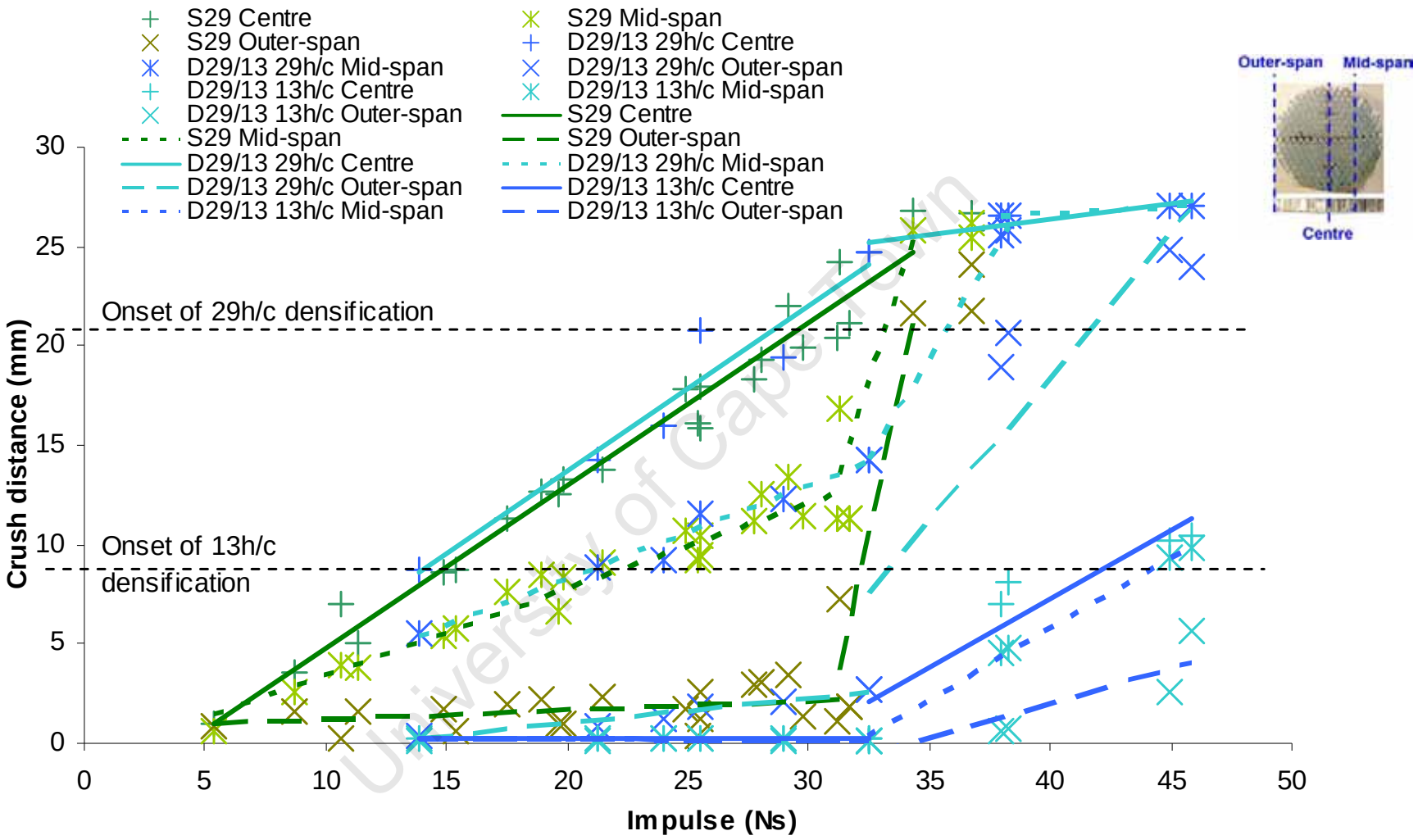

Figure 8-13: Graph of core crushing versus impulse of D29/13 and S29

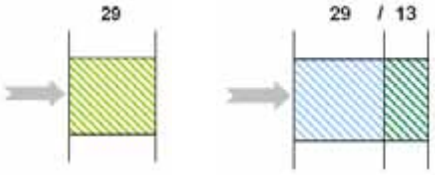

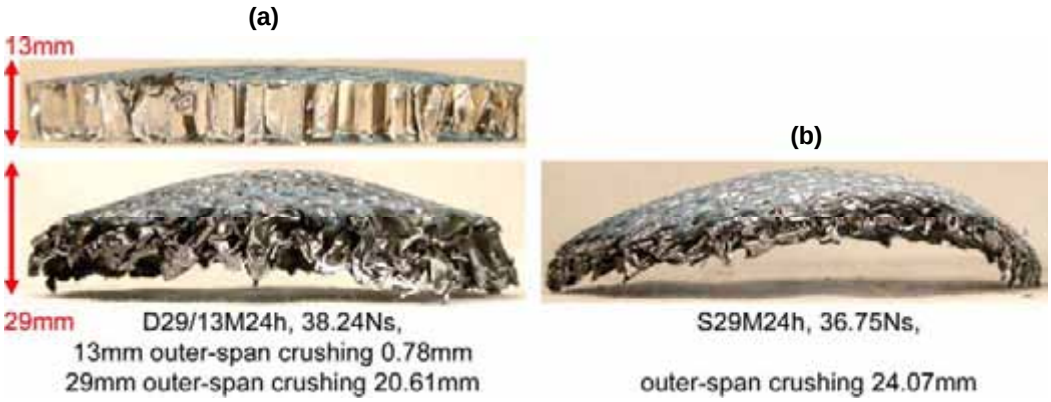

Figure 8-14: Photographs of honeycomb specimens of D29/13 (a) and S29 (b) at a similar impulse range

8.3.3 Middle plate deflections

The middle plate of D29/13 can be compared to the back plate of S29, as shown in Figure 8-11. For the same impulse, the back plate of S29 suffered more deflection than the middle plate of D29/13. The comparison of honeycomb core crushing is shown in Figure 8-13. Before the gradient change at approximately 32Ns, the 29mm thick honeycomb in both test series deformed by similar amount across the radius of the core, as shown in Figure 8-13. Therefore, as shown in Figure 8-11, the middle plate in D29/13 and the back plate in S29 followed similar deflection rate. However, after 32Ns, the middle plate of D29/13 deflected at a much slower rate. This is because the addition of the extra layer behind the middle plate increases the stiffness of the panel; thus providing a higher structural resistance to the panel deformation. This increases the energy absorption of the honeycombs and reduces the deflection of the middle and back plate. Nevertheless, the addition of the extra layer also increases mass by approximately 30%, which can not be overlooked.

9 - CONCLUSIONS

9.1 THE RESPONSE OF THE HONEYCOMB SANDWICH PANELS

From post-test analyses, it was shown that the panels exhibit the following response:

- Front plate deflection and tearing
- Honeycomb core densification
- Honeycomb core crush distance gradient change
- Back plate deflection gradient change and plate tearing

These phenomena do not necessarily occur in a fixed order and not all of them will occur during every test. These depend on the material properties of the sandwich components and the panel configuration, such as core thickness, plate thickness and the various layering. These phenomena are inter-related, as discussed below.

9.1.1 Front plate deflection and tearing

The front plate deflection response are similar to those of a clamped monolithic circular plate subjected to uniformly distributed blast loading [28], with the magnitude of the plate deflection being expected to follow the prediction in [2]. The front plate deflection-impulse curve is usually characterised by a linearly increasing trend-line. The trend ends with the onset of front plate tearing. The deflection at onset of tearing is usually the maximum front plate deflection in Mode I. Thereafter the front plate exhibits Mode II failure (complete tearing) and the deflection starts to decrease with increasing impulse.

9.1.2 Honeycomb core densification

The onset of core densification is characterised via quasi-static compression. It is superimposed on the blast test core compressive data. For aluminium honeycomb, densification takes place at approximately 70-75% strain, regardless of the core thickness (see Section 2.8.3). The onset of core densification occurred at

approximately 21Ns, 30Ns and higher than 40Ns (beyond the tested impulse range) for S13, S29 and S150 panels, respectively. Thicker cores physically delay the onset of densification, as observed in particular during the testing of S150 panels.

9.1.3 Honeycomb core crushing distance gradient change

The honeycomb core experiences changes in the rate of crushing with increasing impulse. An increasing rate is due to front plate tearing. A decreasing crush rate is due to the honeycomb reaching its physical crushing limit (i.e. complete core densification).

9.1.4 Back plate deflection gradient change and plate tearing

The back plate deflection is usually characterised by two trend lines. The first trend line shows relatively little plate deflection because the load transfer is limited by the honeycomb core plateau stress. When the core starts to densify, higher loads are transferred to the back plate and the plate deflects at a faster rate. This ends with the onset of the back plate tearing at sufficiently high impulse.

9.2 EFFECT OF COMBINING AIR-GAP WITH HONEYCOMB CORE

Test series D13a/13 makes use of an air gap and a honeycomb core. The area of contact between the front plate and the honeycomb core was mainly the centre region. This meant the honeycomb material was not fully utilised to regulate load transfer. This is not an optimum use of the honeycomb material.

9.3 EFFECT OF VARYING CORE THICKNESS

The thicker cores sustained higher impulses and increasing the core thickness physically delayed the onset of core densification. Therefore increasing core thickness decreases back plate deflection and delays the back plate tearing. It is also found that for core thicknesses lower than the predicted maximum front plate deflection [2], after

the complete core densification the front plate deforms into the back plate, reducing the front plate deflection.

9.4 EFFECT OF VARYING PLATE THICKNESS

A honeycomb sandwich panel with thinner face plates will have higher front plate deformation. This means the core will densify at a lower impulse and transmit larger forces to the back plate. In addition, the non-dimensional graph showed that the stiffness of the honeycomb material becomes more dominant in the sandwich panels with thinner plates, especially at lower impulses.

9.5 COMPARISON OF THE S29 AND D29/13 TEST SERIES

It is found that the extra layer (i.e. the 13mm thick honeycomb plus the back plate in D29/13) provides better structural resistance to the blast impact; but increased the overall mass of the panel by approximately 30%.

10 - RECOMMENDATIONS

The following recommendations are made considering the experimental results and conclusions:

- Other materials with similar load transfer characteristics as the core (for example cellular solids such as foams) should be investigated to examine the effect of varying core material on panel response. In addition, other honeycomb materials (such as steel) could be considered.

- The effect of sandwich configurations should be investigated further, for example utilising different core materials in a single panel (such as test series D13a/13).

- The effect of core cell configurations (such as square or triangular) on the response of the panel could be investigated.

- The effect of plate material could be investigated. In addition, the effect of different front plate or back plate thickness could also be investigated.

- The transient response of the sandwich panels should also be investigated, such as capturing the details of the deformation of the sandwich panels on a velocity-time or pressure-time history.

11 - REFERENCES

1. MENKES, SB, and OPAT, HJ. “Tearing and shear failures in explosively loaded clamped beams.” Expl. Mech. Volume 13, 1973, pp. 480-486.
2. TEELING-SMITH, RG, and NURICK, GN. “The deformation and tearing of circular plates subjected to impulsive loads.” International Journal of Impact Engineering. Volume 11, No. 1, 1991, pp. 77-92.
3. NURICK, GN, and SHAVE, GC. “The deformation and tearing of thin square plates subjected to impulsive loads - an experimental study.” International Journal of Impact Engineering, Volume 18, No. 1, 1996, pp. 99-116.
4. JONES, N. “Structural Impact” First edition. Cambridge University Press, Cambridge, UK, 1989.
5. NURICK, GN, and MARTIN, JB. “Deformations of thin plates subjected to impulsive loading – a review, Part I – Theoretical consideration”, International Journal of Impact Engineering, Volume 8, No.2, 1989, pp. 159-170.
6. NURICK, GN, and MARTIN, JB. “Deformation of thin plates subjected to impulsive loading – a review, Part II: Experimental studies”, International Journal of Impact Engineering, Volume 8, No. 2, 1989, pp. 171-186.
7. FLECK, NA, and DESHPANDE, VS. “The resistance of clamped sandwich beams to shock loading.” Journal of Applied Mechanics, Volume 71, 2004, pp. 386-401.
8. QUI, X, DESHPANDE, VS, and FLECK, NA. “Dynamic response of clamped circular sandwich plate subject to shock loading.” Journal of Applied Mechanics, ASME, Volume 71, No.5, 2004, pp. 637-645.
9. XUE, Z, and HUTCHINSON, JW. “Preliminary assessment of sandwich plates subject to blast loads.” International Journal of Mechanical Science, Volume 45, No.4, 2003, pp. 687-705.
10. XUE, Z, and HUTCHINSON, JW. “A comparative study of impulse-resistance metal sandwich plates.” International Journal of Impact Engineering, Volume 30, No.10, 2004, pp. 1283-1305.

11. XUE Z, and HUTCHINSON, JW. “Constitutive model for quasi-static deformation of metallic sandwich cores.” International Journal for Numerical Methods in Engineering, Volume 61, No.13, 2004, pp. 2205-2238.

12. VAZIRI, A, and HUTCHINSON, JW. “Metal sandwich plates subject to intense air shocks.” International Journal of Solids and Structures, Volume 44, No.6, 2007, pp. 2021-2035.

13. RABEZUK, T, SAMANIEGO, F, and BELYSCHKO, T. “Simplified model for predicting impulse loads on submerged structures to account for fluid-structure interactions.” International Journal of Impact Engineering, Volume 34, No.2, 2007, pp. 163-177.

14. WADLEY, HNG, DHARMASENA, KP, CHEN, Y, DUDT, P, KNIGHT, D, CHARETTE, R, and KIDDY, K. “Compressive response of multilayered pyramidal lattices during underwater shock loading.” International Journal of Impact Engineering, In press, corrected proof, 2006.

15. WEI, Z, DHARMASENA, KP, WADLEY, HNG, and EVANS, AG. “Analysis and interpretation of a test for characterizing the response of sandwich panels to water blast.” International Journal of Impact Engineering, Volume 34, No.10, 2007, pp. 1602-1618.

16. LIANG, Y, SPUSKANYUK, AV, FLORES, SE, HAYHURST, DR, HUTCHINSON, JW, MCMEEKING, RM, and EVANS, AG. “The response of metallic sandwich panels to water blast.” Journal of Applied Mechanics, Volume 74, No.1, 2007, pp. 81-99.

17. WEI, Z, HE, MY, and EVANS, AG. “Application of a dynamic constitutive law to multilayer metallic sandwich panels subject to impulsive loads.” Journal of Applied Mechanics, Volume 74, No.4, 2007, pp. 636-644.

18. DESHPANDE, VS, and FLECK, NA. “One-dimensional response of sandwich plates to underwater shock loading.” Journal of the Mechanics and Physics of Solids, Volume 53, No.11, 2005, pp. 2347-2383.

19. ZHU, F, and LU, G. “A review of blast and impact of metallic and sandwich structures.” Electronic Journal of Structural Engineering, Volume 7, Special Issue: Loading on Structures, 2007, pp. 92-101.

20. CHUNG KIM YUEN, S, NURICK, GN, THEOBALD, MD, and LANGDON, GS. “Sandwich panels subjected to blast loading” book chapter in “Dynamic Failure of Materials and Structures” Editors: Prof A Shukla, Y Rajapakse, Ravichandran (Springer) submitted.

21. DESHPANDE, VS, HEAVER, A, and FLECK, NA. “An underwater shock simulator.” Proceedings of the Royal Society, A, Volume 462, 2006, pp. 1021-1041.

22. RADFORD, DD, DESHPANDE, VS, and FLECK, NA. “The use of metal foam projectiles to simulate shock loading on a structure.” International Journal of Impact Engineering, Volume 31, No.9, 2005, pp. 1152-1171.

23. RADFORD, DD, MCSHANE, GJ, DESHPANDE, VS, and FLECK NA. “The response of clamped sandwich plates with metallic foam cores to simulated blast loading.” International Journal of Solids and Structures, Volume 43, No.7-8, 2006, pp. 2243-2259.

24. RADFORD, DD, FLECK, NA, and DESHPANDE, VS, “The response of clamped sandwich beams subjected to shock loading.” International Journal of Impact Engineering, Volume 32, No.6, 2006, pp. 968-987.

25. MCSHANE, GJ, RADFORD, DD, DESHPANDE, VS, and FLECK NA. “The response of clamped sandwich plates with lattice cores subjected to shock loading.” European Journal of Mechanics, A/Solids, Volume 25, No.2, 2006, pp. 215-229.

26. GIBSON, LJ, and ASHBY, MF. “Cellular solids, structure and properties.” Second edition. Cambridge University Press, Cambridge, UK, 1997.

27. LU, G, and YU, TX. “Energy absorption of structures and materials.” First edition. Woodhead Publishing Limited, Cambridge England, 2003.

28. BRODERICK, JW. “Investigation into the response of honeycomb sandwich material subjected to impulsive loading”, Undergraduate dissertation, University of Cape Town, 1990.

29. FARROW, GH. “The response of impulsively loaded sandwich plates”, MSc dissertation, University of Cape Town, 1995.

30. NURICK, GN, LANGDON, GS, CHI, Y, and JACOB, N. “Response of blast loaded honeycomb sandwich plates – preliminary experiments.” 6th International Conference on Composite Science and Technology, Durban, South Africa, January 2007 [CD-ROM].

31. KARAGIOZOVA, D, NURICK, GN, and LANGDON, GS. “Behaviour of sandwich panels subject to intense air blasts.” 6th International Conference on Composite Science and Technology, Durban, South Africa, January 2007 [CD-ROM].

32. DHARMASENA, KP, WADLEY, HNG, XUE, Z, and HUTCHINSON, JW. “Mechanical response of metallic honeycomb sandwich panel structures to high-intensity dynamic loading.” International Journal of Impact Engineering, In press, corrected proof, 2007, doi:10.1016/j.ijimpeng.2007.06.008.

33. ZHU, F, ZHAO, L, LU, G, and GAD, E. “Finite element analysis of square metallic sandwich panels under blast loading.” Impast, 2007, pp. 591-598, Bochum.

34. ZHU, F, ZHAO, L, Lu, G, and WANG, Z, “Deformation and failure of blast-loaded metallic sandwich panels – Experimental investigations.” International Journal of Impact Engineering, In press, corrected proof, 2008, doi:10.1016/j.ijimpeng.2007.11.003.

35. KARAGIOZOVA, D, NURICK, GN, LANGDON, GS, CHUNG KIM YUEN, S, CHI, Y and BARTLE, S. “Response of flexible sandwich panels to blast loading.” 16th International Conference on Composite Materials, Japan, July 2007.

36. TILBROOK, MT, RADFORD, DD, DESHPANDE, VS, and FLECK, NA. “Dynamic crushing of sandwich panels with prismatic lattice cores.” International Journal of Solids and Structures, Volume 44, No.18-19, 2007, pp. 6101-6123.

37. “Aeroweb aluminium honeycomb for energy absorption.” Ciba-Geigy Plastics and Additives Company, Duxford, AD-EA/1X, September 1981.

38. “HexWeb honeycomb sandwich design technology.” Hexcel Composites, Duxford, AGU 075b, December 2000.

39. WIERZBICKI, T. “Crushing analysis of metal honeycombs.” International Journal of Impact Engineering, Volume 1, No.2, 1983, pp. 157-74.

40. YAMASHITA, M, and GOTOH, M. “Impact behaviour of honeycomb structures with various cell specifications – numerical simulation and experiment.” International Journal of Impact Engineering, Volume 32, No.1-4, 2005, pp. 618-630.

41. BURTON, WS, and NOOR, AK. “Structural analysis of the adhesive bond in a honeycomb core sandwich panel.” Finite Elements in Analysis and Design, Volume 26, 1997, pp. 213-227.

42. JENSEN, Ø, LANGSETH, M, and HOPPERSTAD, OS. “Experimental investigations on the behaviour of short to long square aluminium tubes subjected to axial loading.” International Journal of Impact Engineering, Volume 30, No.8-9, 2004, pp. 973-1003.

43. YASUI, Y. “Dynamic axial crushing of multi-layer honeycomb panels and impact tensile behaviour of the component members.” International Journal of Impact Engineering, Volume 24, No.6-7, 2000, pp.659-671.

44. JACOB, N. "The Effect of Stand-Off Distance on the Failure of Thin Plates Subjected to Blast Loads", MSc dissertation, University of Cape Town, 2005.

45. NURICK, GN, and RADFORD, AM. “Deformation and tearing of clamped circular plates subjected to localised central blast loads”, Recent developments in computational and applied mechanics (ed. B. D Reddy). A volume in honour of John B Martin, 1997, pp. 276-301.

46. JACOB, N, NURICK, GN, and LANGDON, GS. “The effect of stand-off distance on the failure of fully clamped circular mild steel plates subjected to blast loads.” Engineering Structures, Volume 29, No. 10, 2007, pp. 2723-2736.

47. KINNEY, GF. “Explosive shocks in air.” First edition, Macmillan, New York, 1962.

48. BAKER, WE. “Explosives in air.” University of Texas Press, Austin and London, 1973.

49. NURICK, GN, GELMAN, ME, and MARSHALL, NS. “Tearing of blast loaded plates with clamped boundary conditions”, International Journal of Impact Engineering, Volume 18, Nos. 7-8, 1996, pp. 803-827.

50. XUE, Z, and HUTCHINSON, J. “Crush dynamics of square honeycomb sandwich cores.” International Journal for Numerical Methods in Engineering, Volume 65, 2005 pp. 2221-2245.

51. KARAGIOZOVA, D, Private communication, 2007-10-02.

52. WHARTON, RK, FORMBY, SA, and MERRIFIELD, R. “Airblast TNT equivalence for a range of commercial blasting explosives”, Journal of Hazardous Materials A79, 2000, pp. 31–39.

53. JACOB, N, CHUNG KIM YUEN, S, NURICK, GN, BONORCHIS, D, DESAI, SA, and TAIT, D. “Scaling aspects of quadrangular plates subjected to localised blast loads – experiments and predictions”, International Journal of Impact Engineering, Volume 30, 2004, pp. 1179-1208.

54. KENNEDY, JE. “Behaviour and utilisation of explosives in engineering design.” 12th Annual Symposium, ASME, UNM, Albuquerque, NM, 1972.

55. BALDEN, VH, and NURICK, GN. “Numerical simulation of the post-failure motion of steel plates subjected to blast loading.” International Journal of Impact Engineering, Volume 32, 2005, pp. 14-34.

APPENDIX A – IMPULSE CALCULATIONS

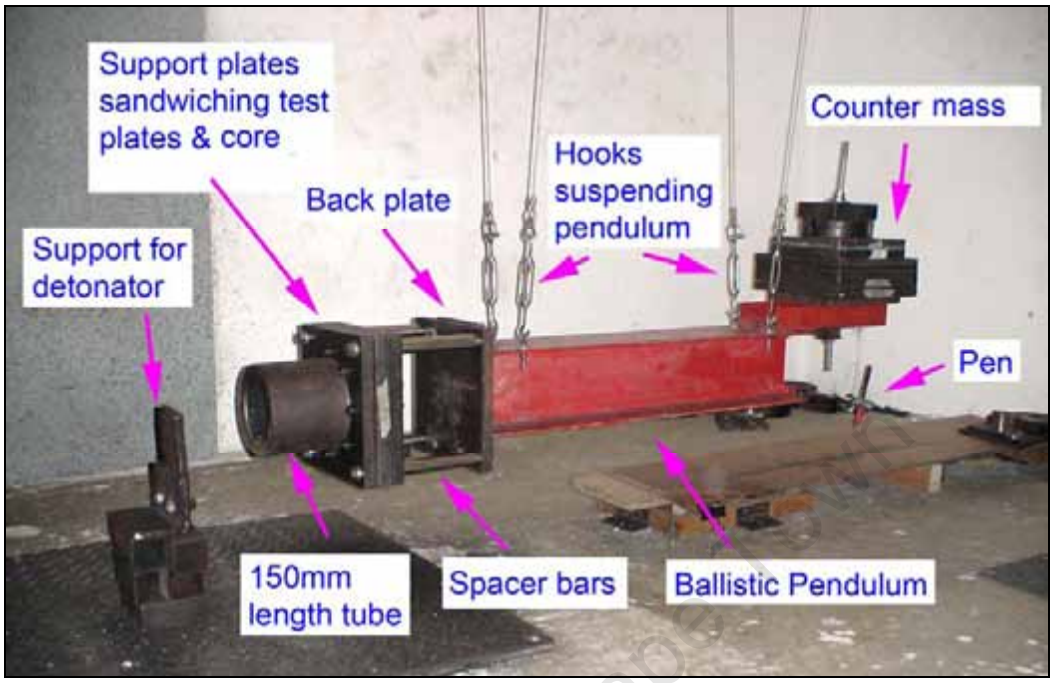

Figure A1: The ballistic pendulum

The ballistic pendulum is shown in Figure A1. The linearised equation of motion of the pendulum is as follows, assuming viscous damping:

$$\ddot{X} + 2\beta\dot{X} + \omega_n{}^2 X = 0 \qquad \textbf{Eq A1}$$

And, $\beta = \dfrac{C}{2M}$, $\omega_n = \dfrac{2\pi}{T}$ and $\omega_d = \left(\omega_n{}^2 - \beta^2\right)^{1/2}$

Where C is the damping coefficient, M is the total mass of the pendulum (experimental rig, balance masses and explosive), and T is the natural period of the pendulum. The solution of Equation A1 is given by

$$X = \frac{e^{-\beta.t}\dot{x}_0 \sin(\omega_d t)}{\omega_d} \qquad \textbf{Eq A2}$$

Where $\dot{x}_0$ is the initial velocity of the pendulum.

Let x_1 be the horizontal displacement at $t = T/4$

And x_2 be the horizontal displacement at $t = 3T/4$

Substituting these values into Equation A2 gives

$$x_1 = \frac{\dot{x}_0 T}{2\pi} e^{(-1/4)\beta.T} \qquad \textbf{Eq A3}$$

And

$$x_2 = \frac{\dot{x}_0 T}{2\pi} e^{(-3/4)\beta.T} \qquad \textbf{Eq A4}$$

Dividing x_1 by x_2

$$\frac{x_1}{x_2} = e^{(1/2)\beta.T} \qquad \textbf{Eq A5}$$

The damping constant is given by

$$\beta = \frac{2}{T} \ln\left(\frac{x_1}{x_2}\right) \qquad \textbf{Eq A6}$$

From Equation A3

$$\dot{x}_0 = \frac{2\pi}{T} x_1 e^{(0.25\beta.T)} \qquad \textbf{Eq A7}$$

Hence the impulse can be calculated by

$$I = M\dot{x}_0 \qquad \textbf{Eq A8}$$

The natural period of the pendulum, T is determined by averaging the time taken for a number of oscillations of the ballistic pendulum. The damping constant is determined for each test using Equation A6. The forward (x_1) and backward (x_2) displacements of the pendulum are calculated from measurements taken from the lines drawn on the tracing paper by the recording pen, as shown in Figure A2.

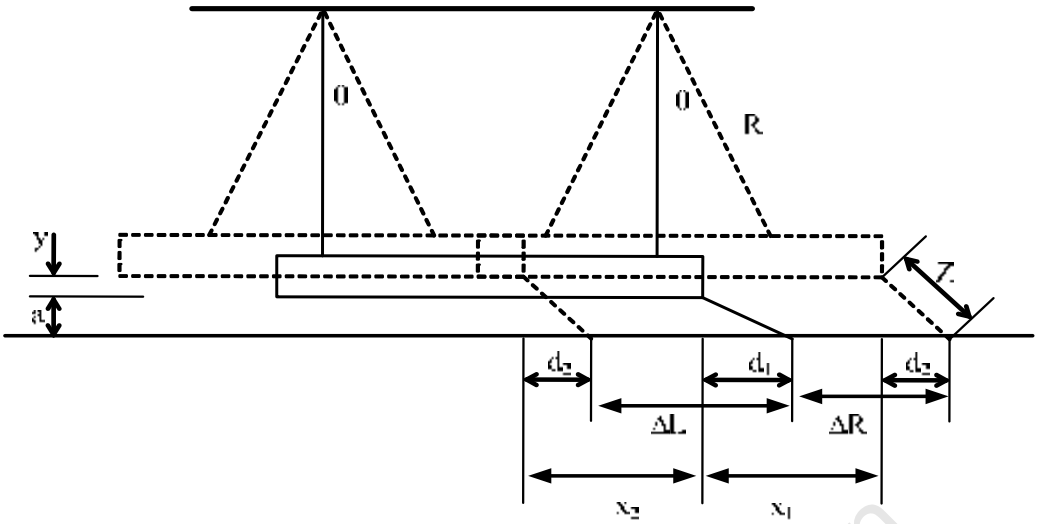

Figure A2: Geometry of the pendulum

It should be noted that the distance moved by the pendulum is not the same as the distance recorded by the pen on the paper. The true displacement of the pendulum is determined using the following method.

The horizontal distance from the end of the I-beam to the tip of the pen when the pendulum is stationary is given by

$$d_1 = \sqrt{\left(Z^2 - a^2\right)} \qquad \textbf{Eq A9}$$

At maximum amplitude of the oscillation the horizontal distance between the end of the I-beam and recording pen decreases, the new distance d_2 is given by

$$d_2 = \sqrt{Z^2 - (a+y)^2} \qquad \textbf{Eq A10}$$

For small angles

$$x_1 = R\theta \text{ and } y = \frac{R\theta^2}{2}$$

Hence

$$y = \frac{x_1^2}{2R} \qquad \textbf{Eq A11}$$

Substituting Equation A11 into Equation A10

$$d_2 = \left[Z^2 - \left(a + \left(\frac{x_1^2}{2R} \right) \right)^2 \right]^{1/2} \qquad \textbf{Eq A12}$$

From Figure A2,

$$x_1 = \Delta R + d_1 - d_2 \qquad \textbf{Eq A13}$$

And

$$x_2 = \Delta L - d_1 + d_2 \qquad \textbf{Eq A14}$$

Substituting Equations A9 and A12 into Equations A13 and A14, the true forward (x_1) and backward (x_2) displacements of the pendulum is given by

$$x_1 = \Delta R + \left(Z^2 - a^2 \right)^{1/2} - \left[Z^2 - \left[a + \frac{x_1^2}{2R} \right]^2 \right]^{1/2} \qquad \textbf{Eq A15}$$

And

$$x_2 = \Delta L - \left(Z^2 - a^2 \right)^{1/2} + \left[Z^2 - \left[a + \frac{x_1^2}{2R} \right]^2 \right]^{1/2} \qquad \textbf{Eq A16}$$

$\triangle L$, $\triangle R$, Z, a, and R are measured and as a result x_1 and x_2 can be calculated. Thereafter, the impulse can be calculated. Table A1 below shows the data of the ballistic pendulum.

Table A1: Data of the ballistic pendulum

Total pendulum mass (Kg)	129.32
R (mm)	2945
Z (mm)	210
a (mm)	160
T (s)	3.41

APPENDIX B – DRAWINGS

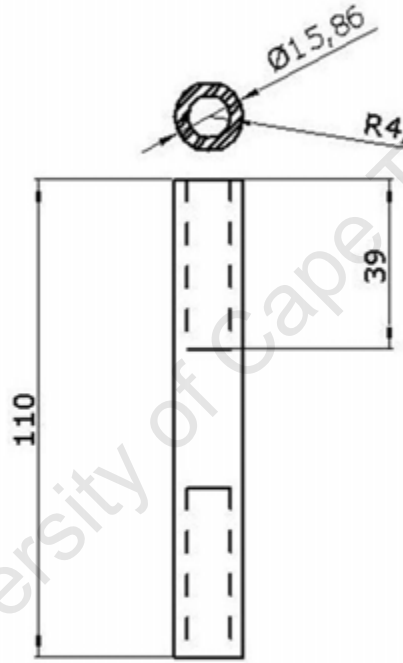

1	SUPPORT BAR	MILD STEEL	8	
PART No.	DESCRIPTION	MATERIAL	No. OFF	REMARKS

HONEY COMB

UNIVERSITY OF CAPE TOWN
DEPARTMENT OF MECHANICAL ENGINEERING

TITLE
SUPPORT BAR

DIMENSIONS IN MILLIMETRES (mm)
TOLERANCE UNLESS OTHERWISE STATED
±0.1mm

SCALE 1 : 1

DATE 24/07/2007

SHEET 1 OF 1

DRAWN BY CHI, Y.

DRAWING NUMBER HONEYCOMB - 006

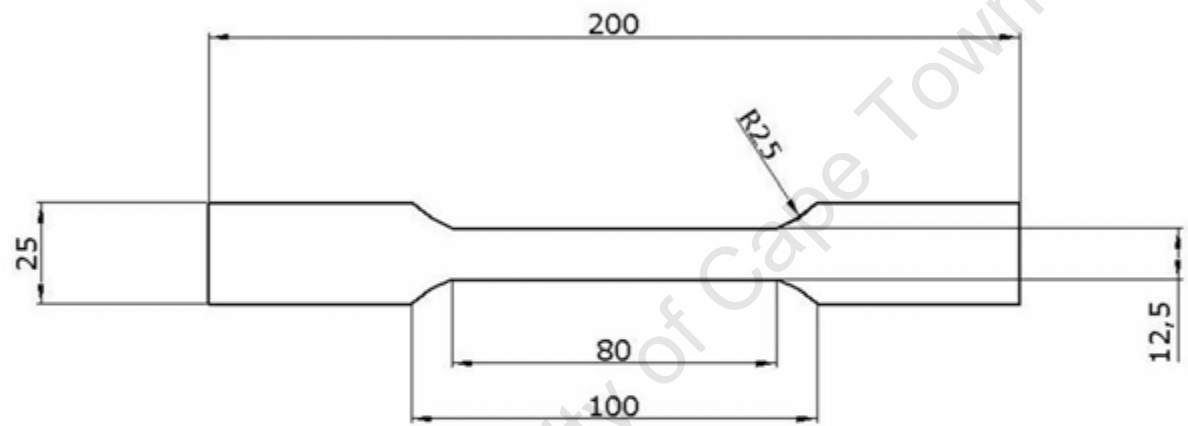

Required thickness: 1.0mm

Name: Yunn-Chih Chi	
Material: Mild Steel	
Quantity: 5 for each sheet	
All measurement in millimeters	
Title: Tensile specimen	
	University Of Cape Town

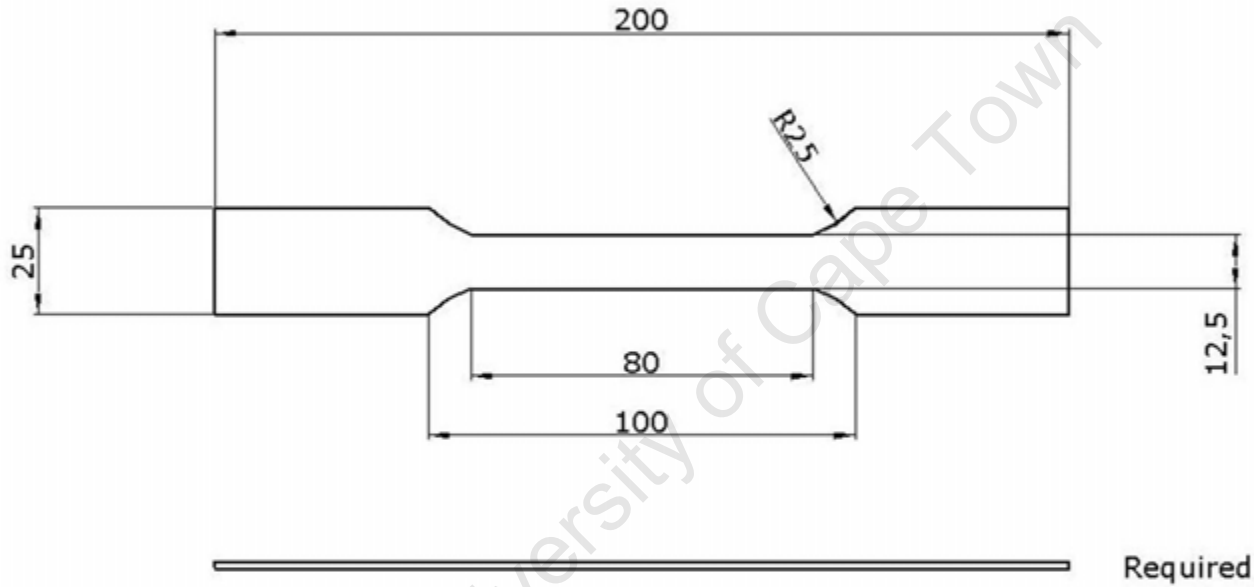

Required thickness: 1.6mm

Name: Yunn-Chih Chi	
Material: Mild Steel	
Quantity: 5 for each sheet	
All measurement in millimeters	
Title: Tensile specimen	
	University Of Cape Town

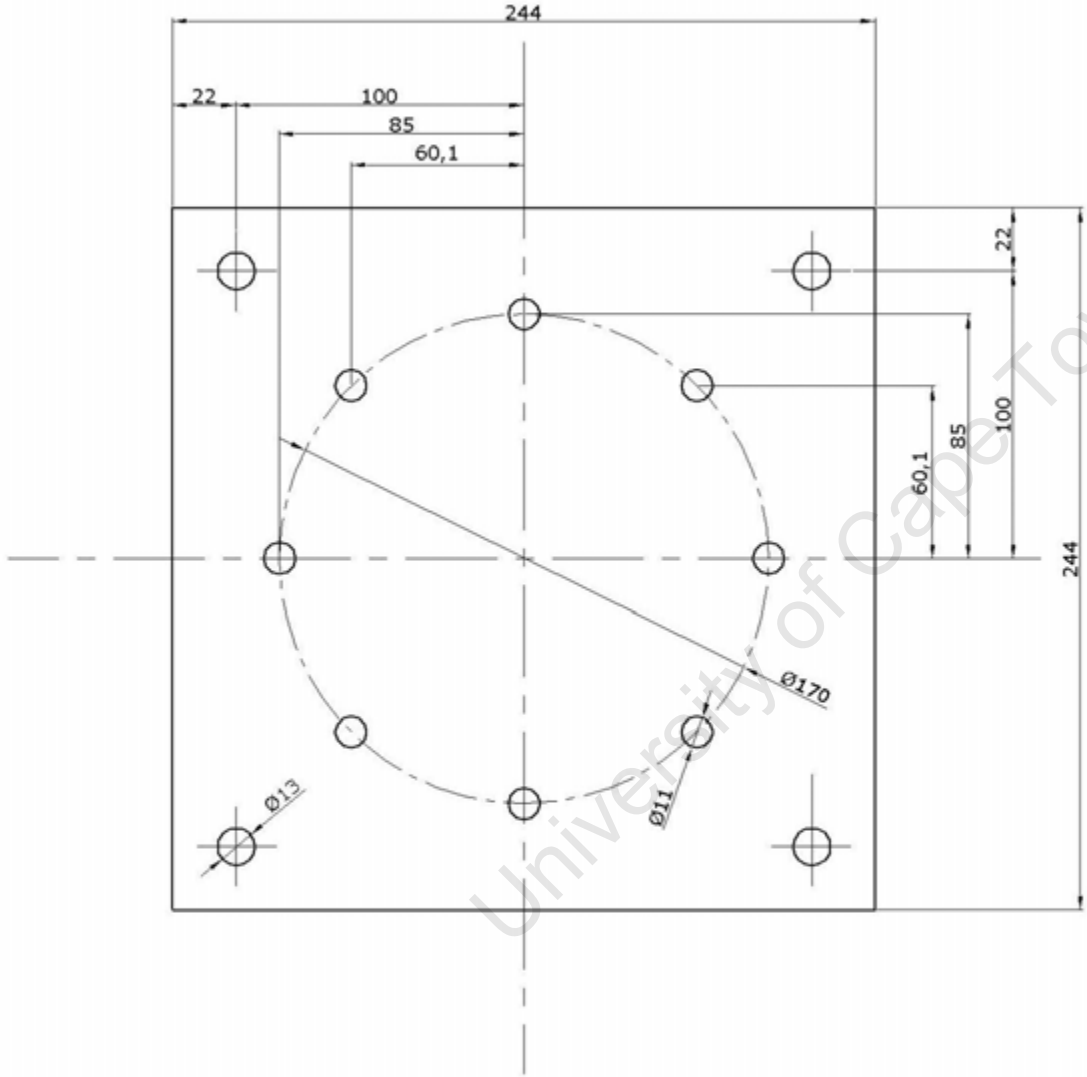

Required thickness: 1.6mm

Name: Yunn-Chih Chi	
Material: Mild Steel	
Quantity: 70	
All measurement in millimeters	
Title: Test Plates	
	University Of Cape Town

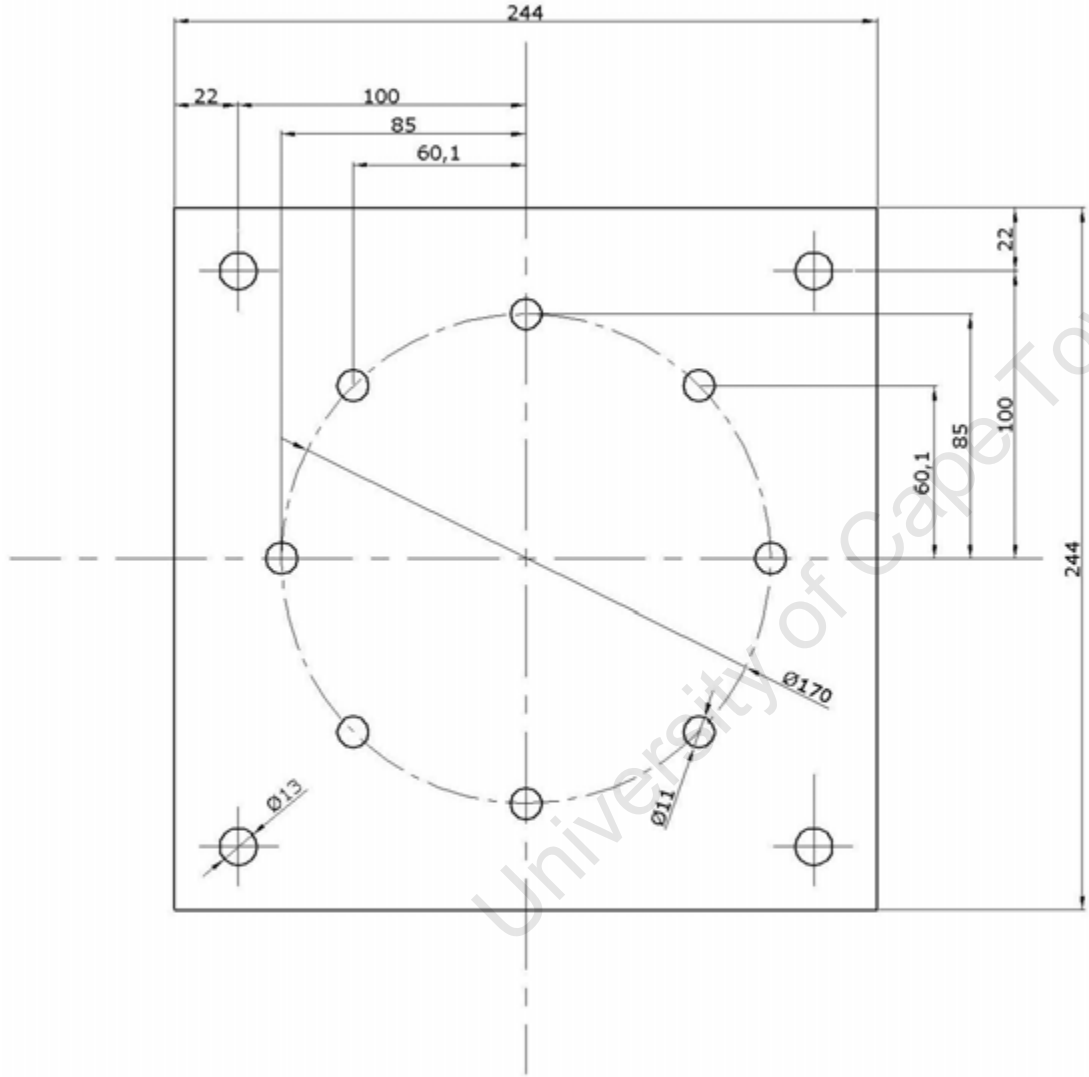

Required thickness: 1.0mm

Name: Yunn-Chih Chi	
Material: Mild Steel	
Quantity: 30	
All measurement in millimeters	
Title: Test Plates	
	University Of Cape Town

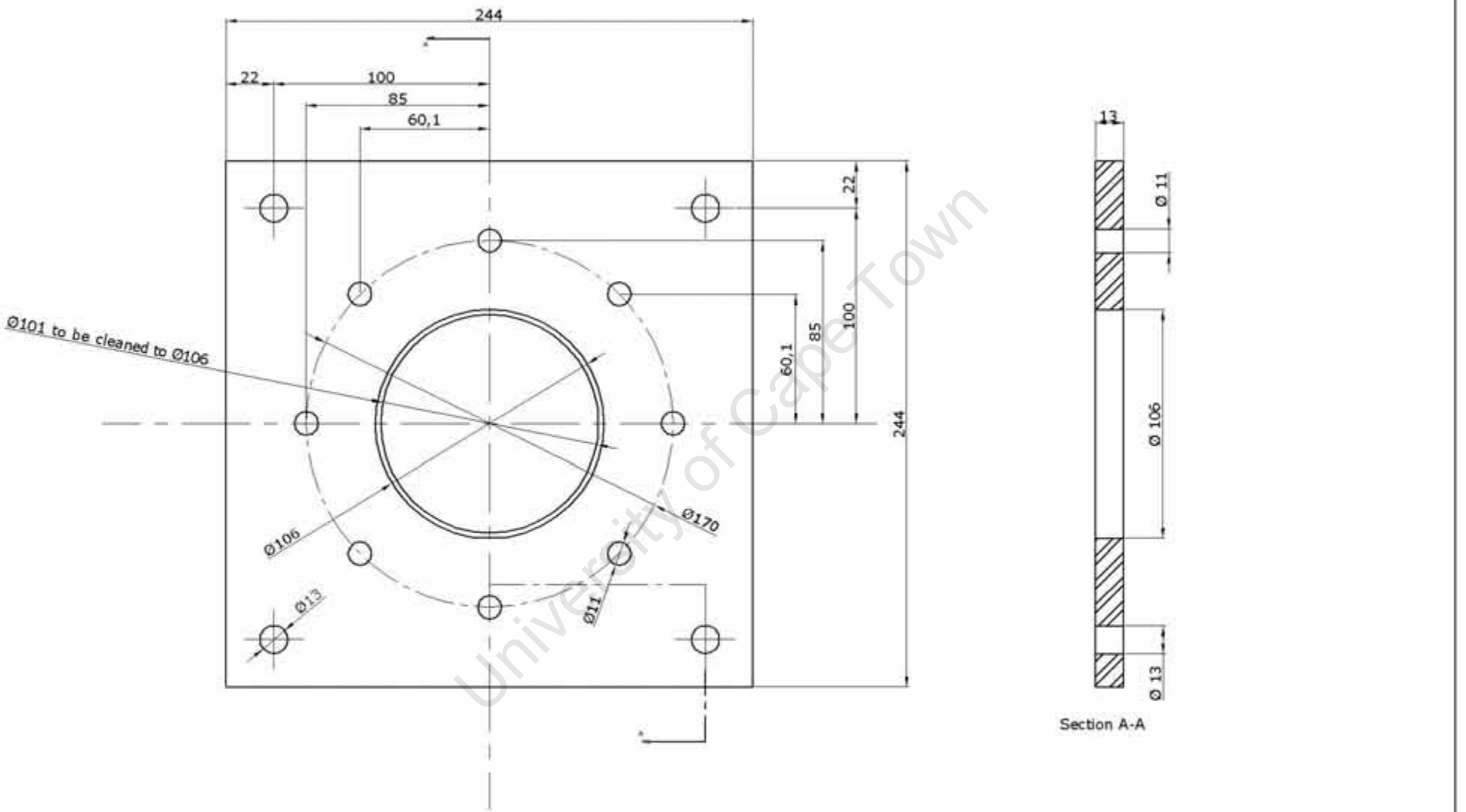

Name: Yunn-Chih Chi	
Material: Mild Steel	
Quantity: 1	
All measurement in millimeters	
Title: 13mm thick Clamp Plate	
	University Of Cape Town

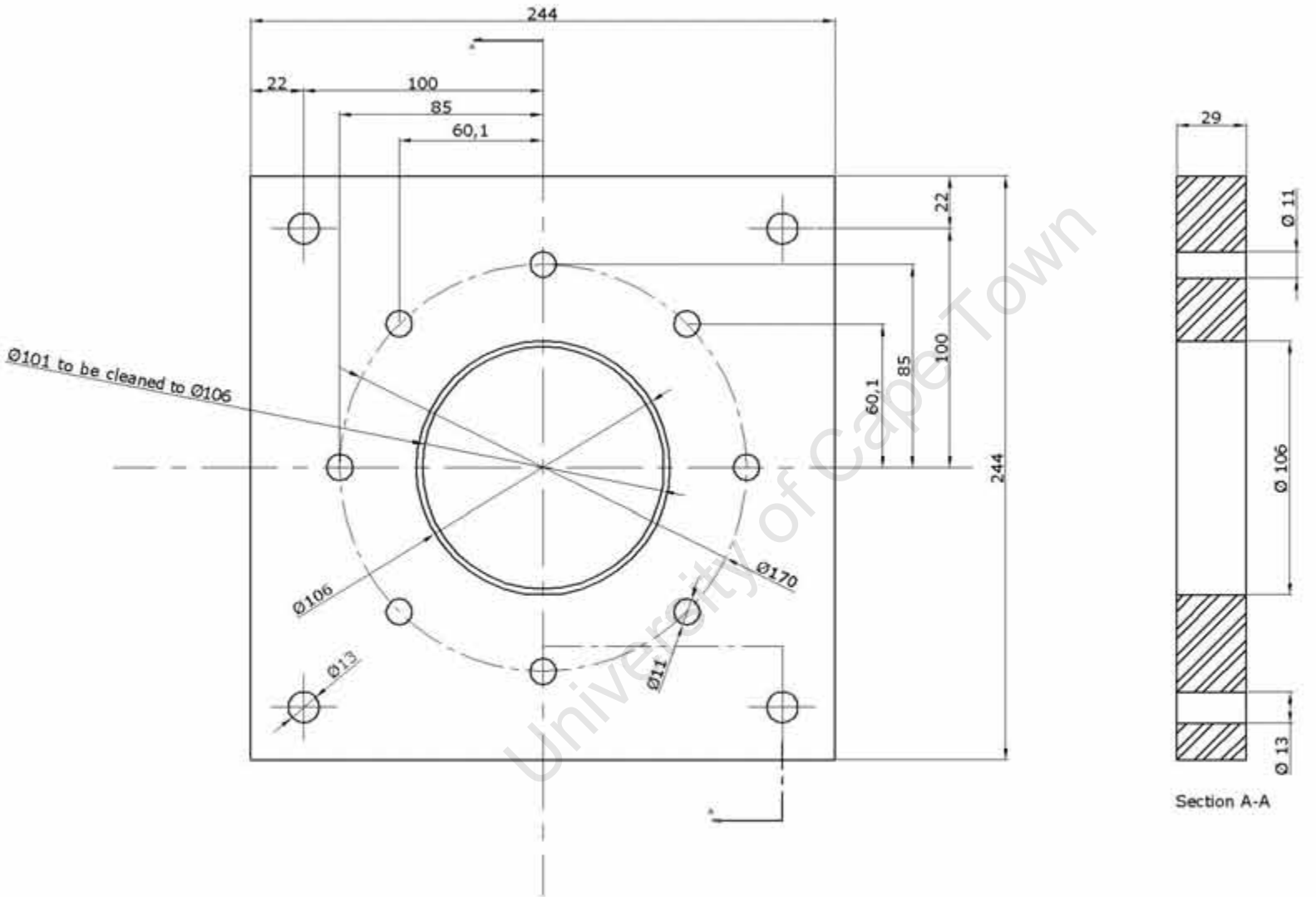

Section A-A

Name: Yunn-Chih Chi	
Material: Mild Steel	
Quantity: 1	
All measurement in millimeters	
Title: 29mm thick Clamp Plate	
	University Of Cape Town

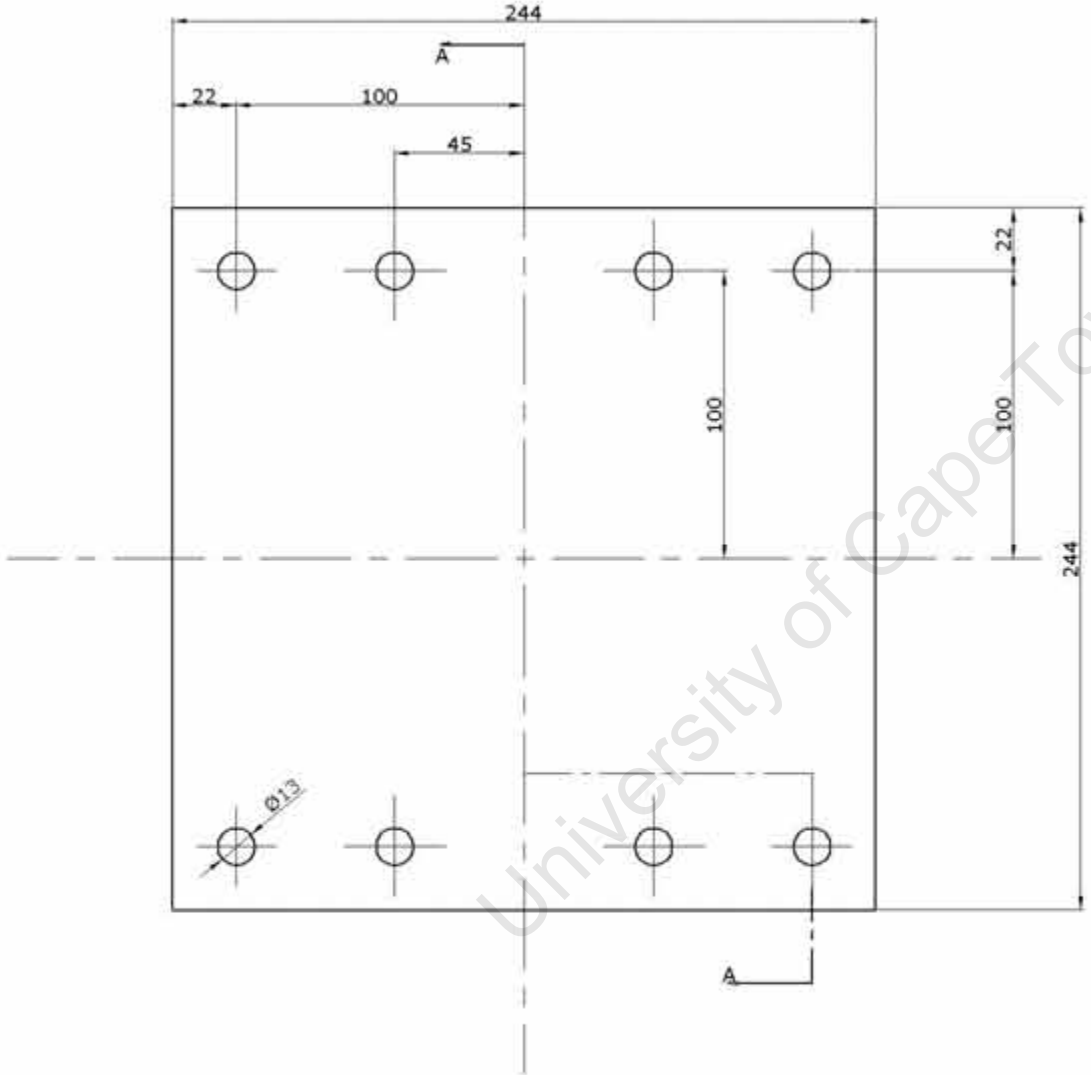

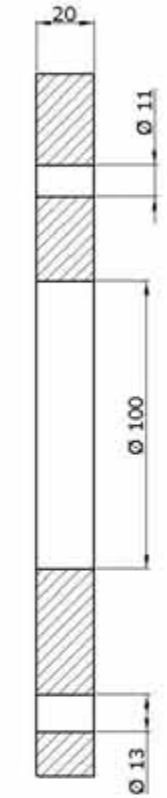

Section A-A

Name: Yunn-Chih Chi	
Material: Mild Steel	
Quantity: 1	
All measurement in millimeters	
Title: Back Plate	
	University Of Cape Town

APPENDIX C – MATERIAL CHARACTERISATION CURVES

This section shows the material characterisation results, which were discussed in Chapter 3. The tensile test engineering stress-strain curves are shown in Figure C1 to Figure C5. The honeycomb compression test results are shown in Figure C6 to Figure C11.

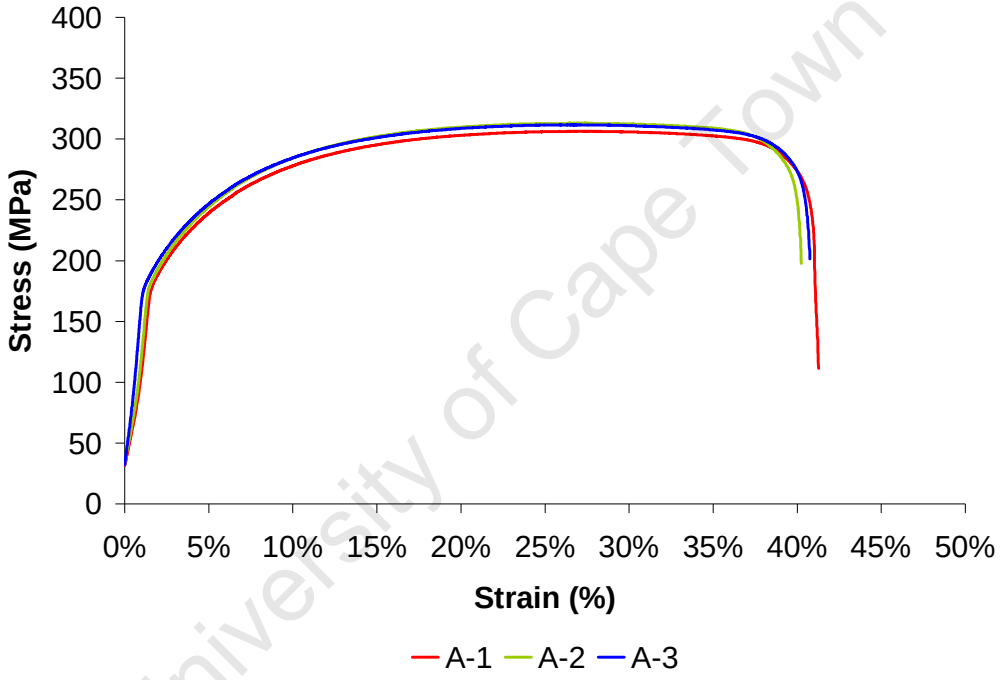

Figure C1: Engineering stress-strain curves of mild steel sheet A

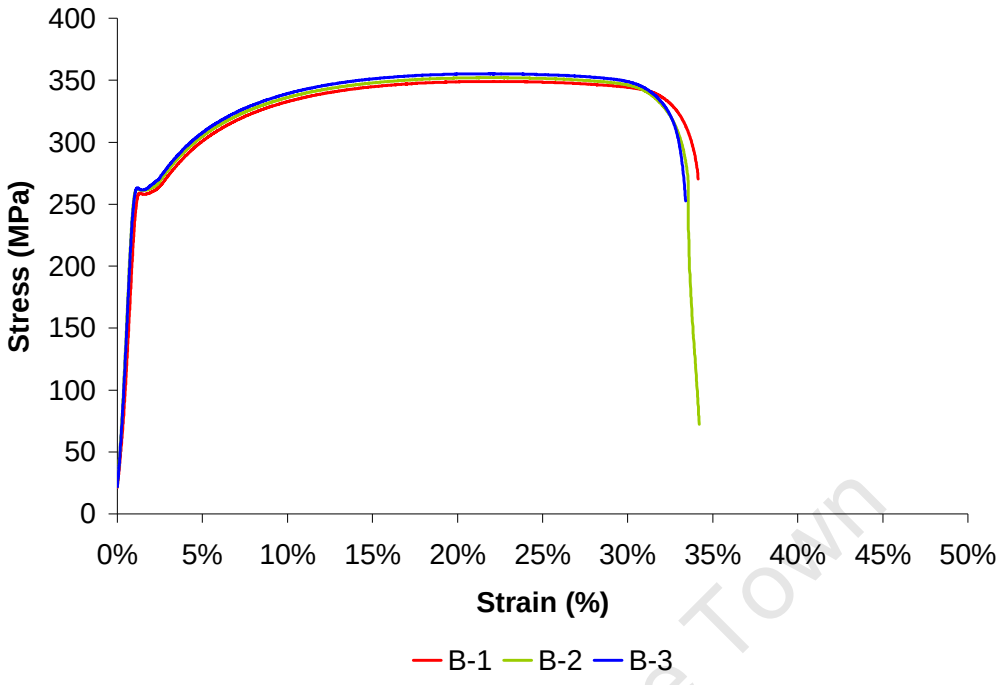

Figure C2: Engineering stress-strain curves of mild steel sheet B

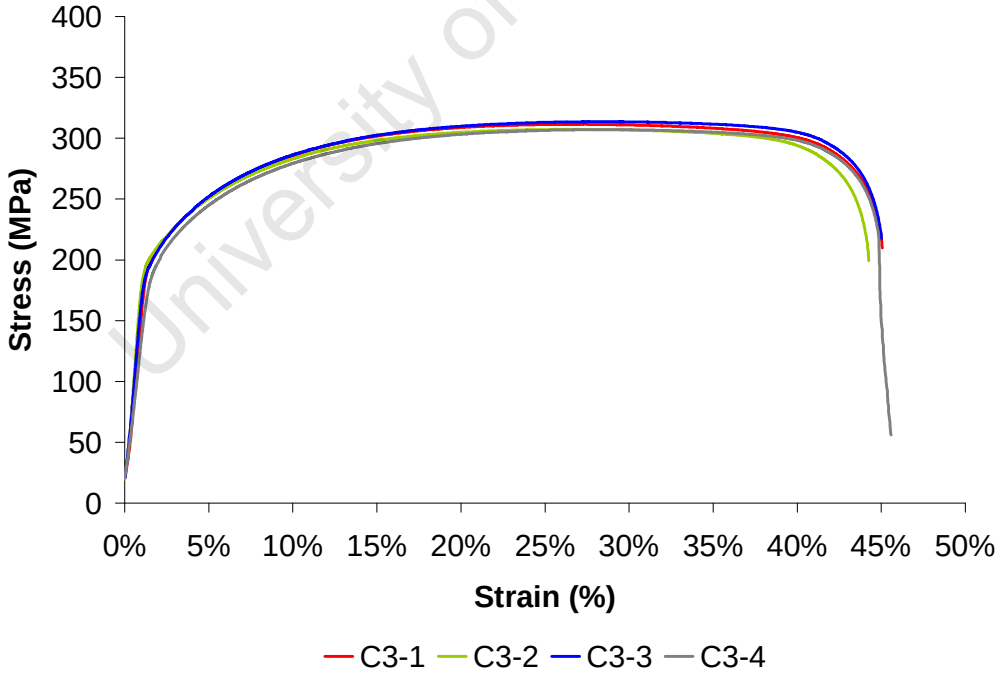

Figure C3: Engineering stress-strain curves of mild steel sheet C_3

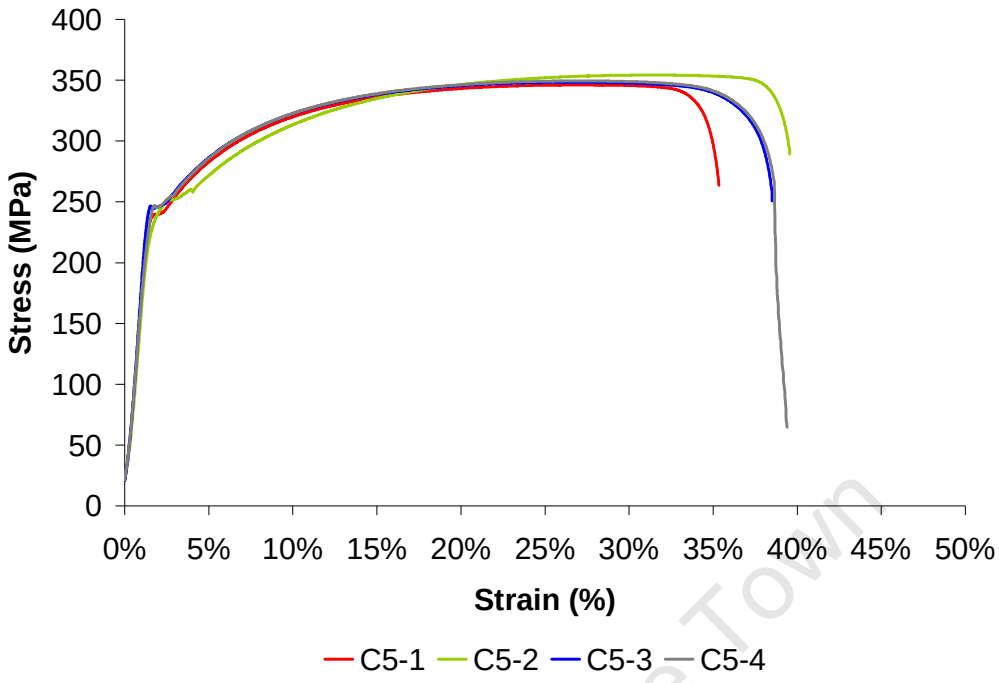

Figure C4: Engineering stress-strain curves of mild steel sheet C_5

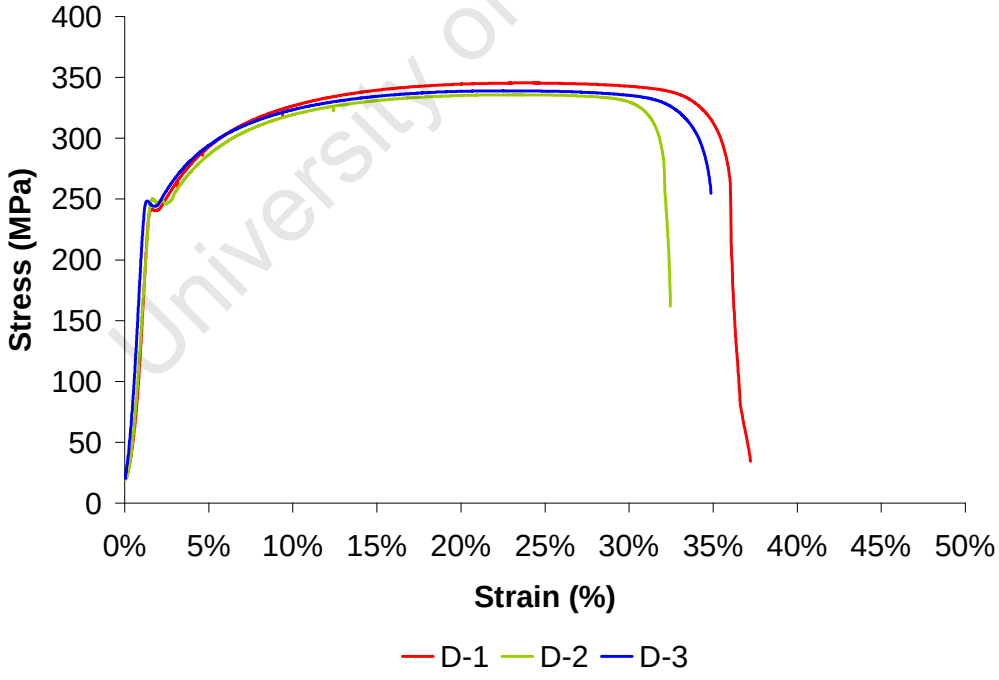

Figure C5: Engineering stress-strain curves of mild steel sheet D

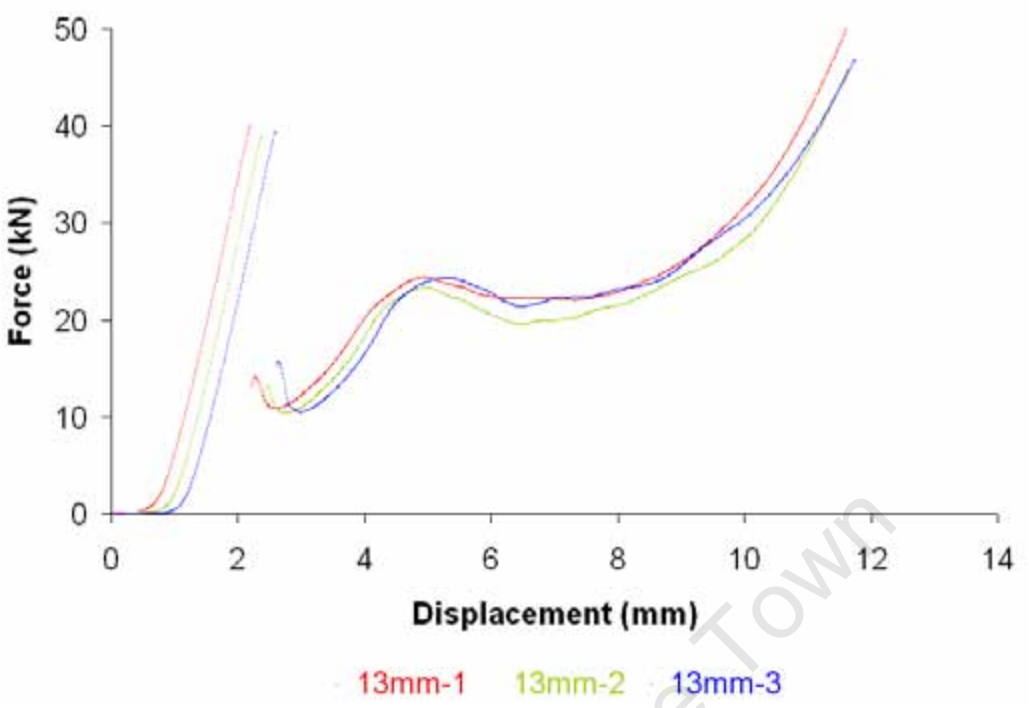

Figure C6: Force versus displacement curves of the 13mm thick honeycomb

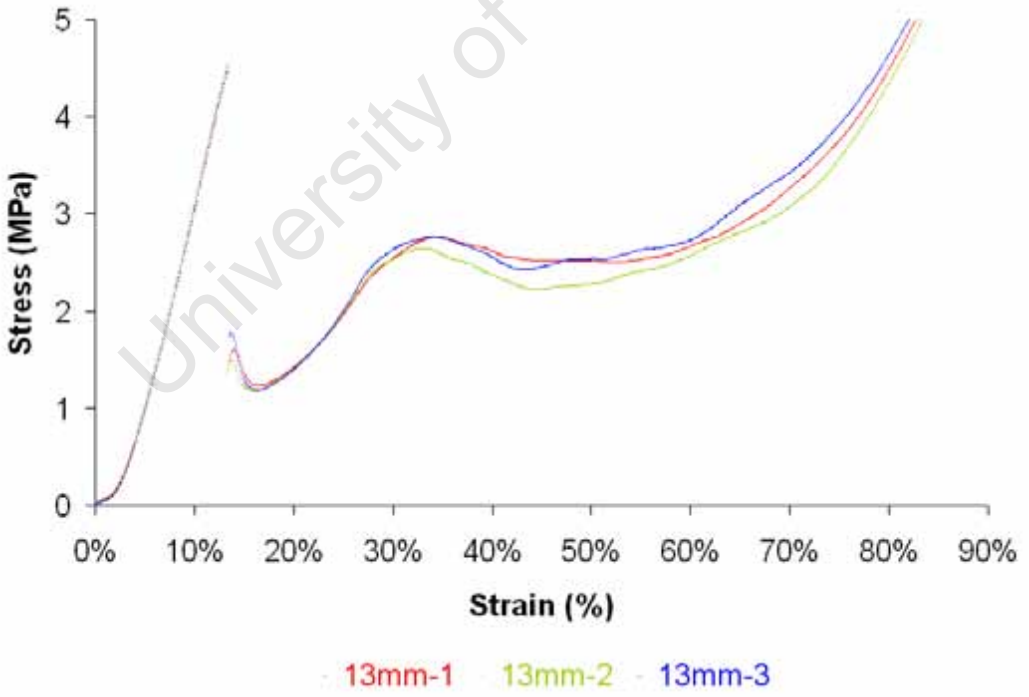

Figure C7: Engineering stress-strain curves of the 13mm thick honeycomb

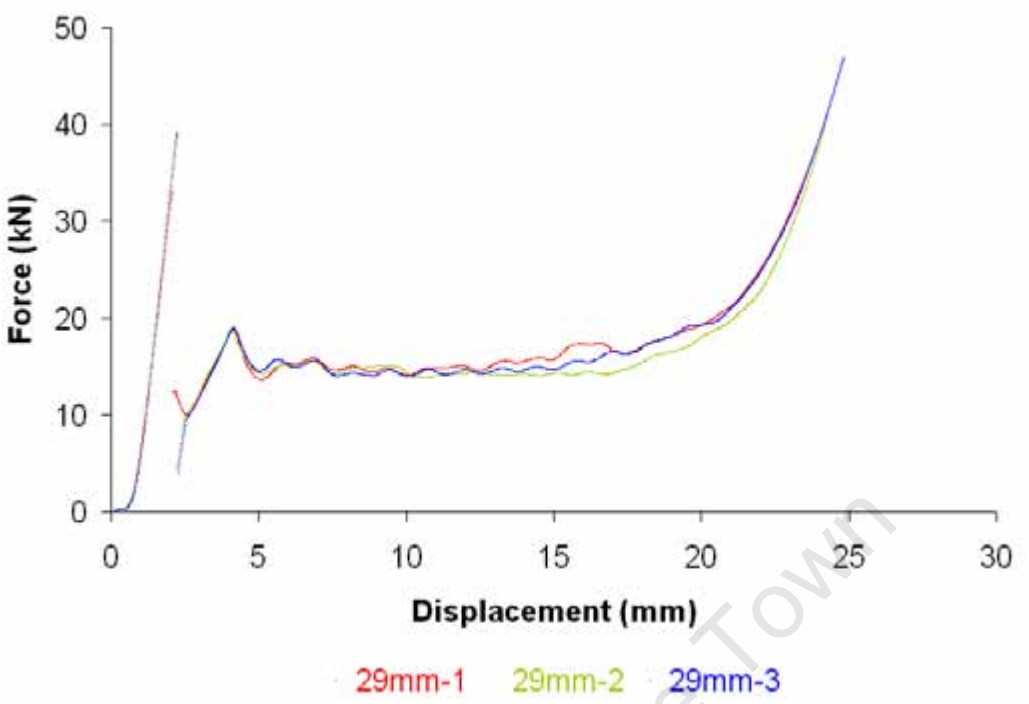

Figure C8: Force versus displacement curves for the 29mm thick honeycomb

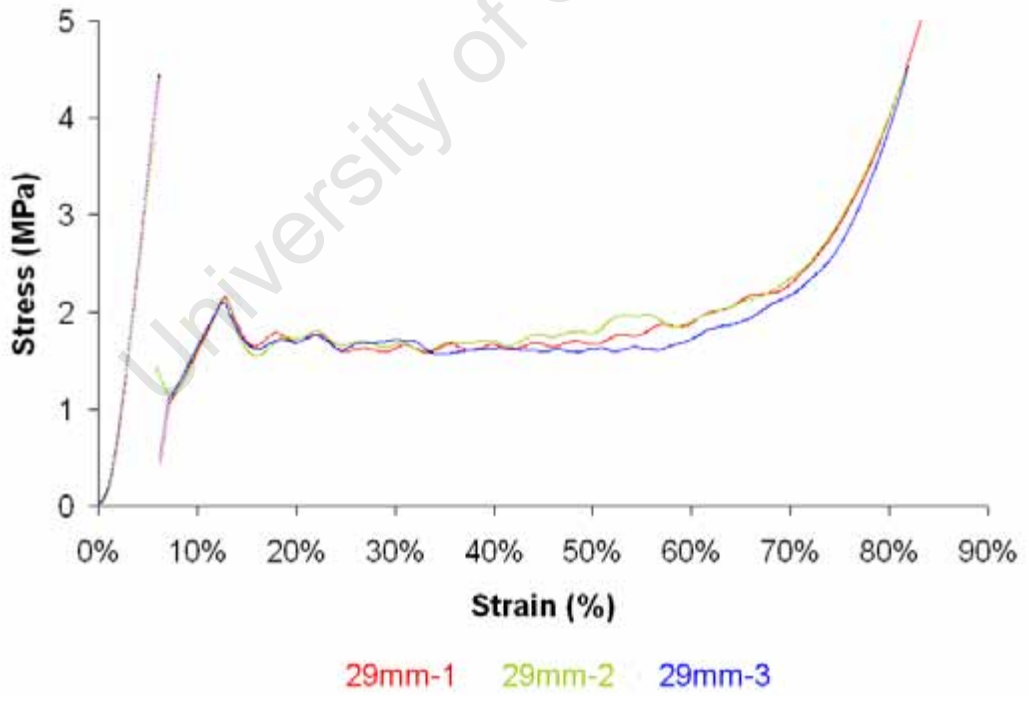

Figure C9: Engineering stress-strain curves of the 29mm thick honeycomb

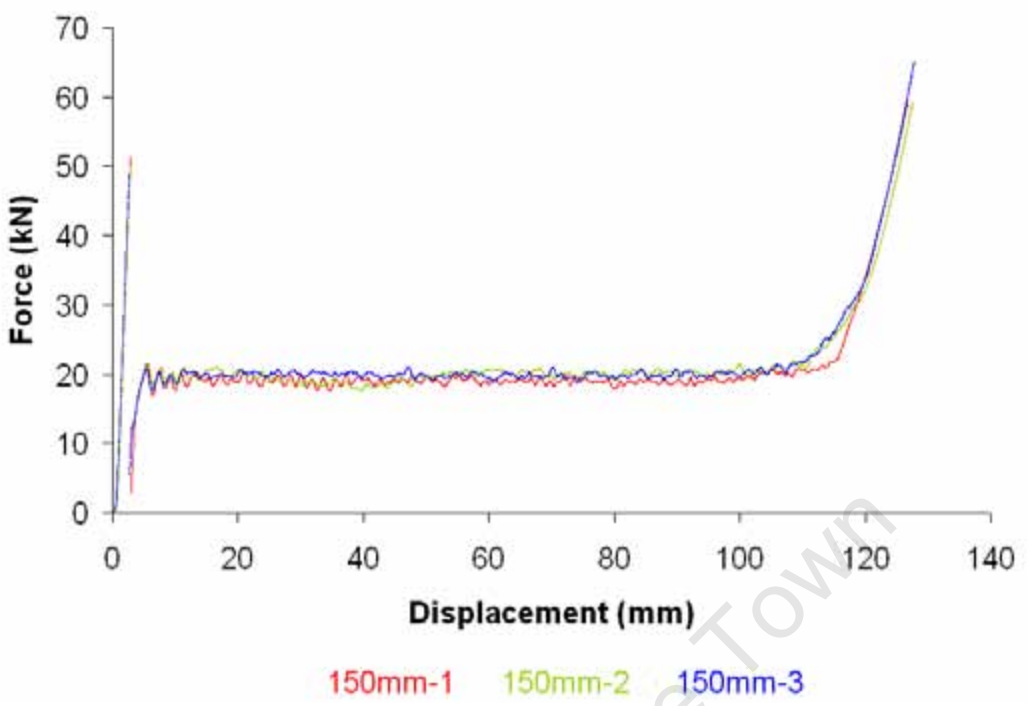

Figure C10: Force versus displacement curves for the 150mm thick honeycomb

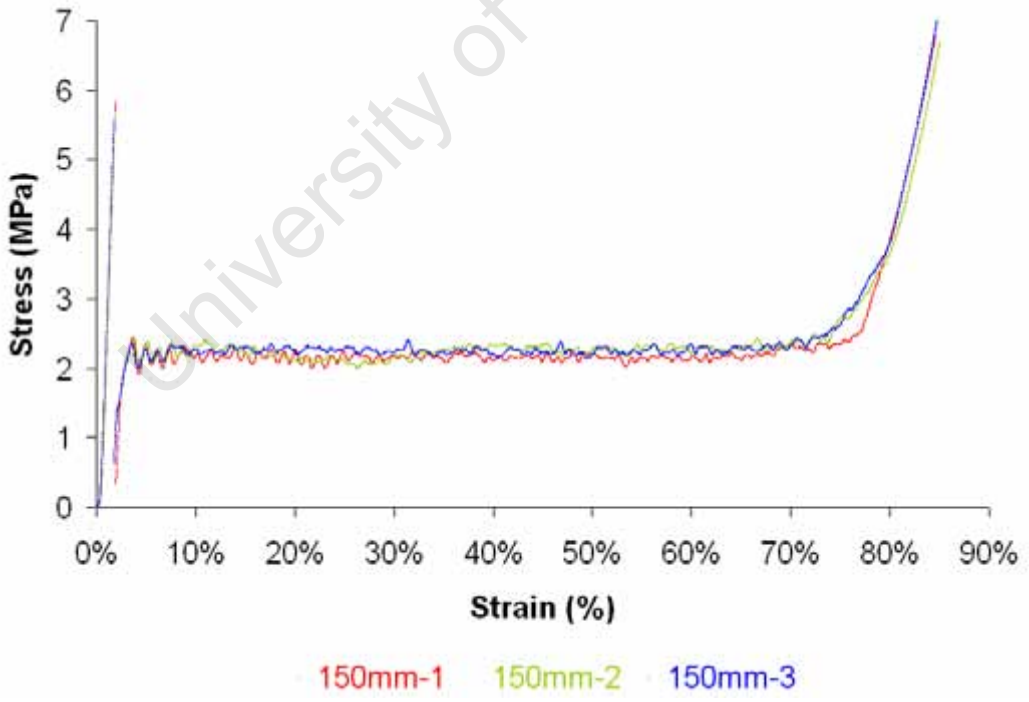

Figure C11: Engineering stress-strain curves of the 150mm thick honeycomb

APPENDIX D – RESULTS OF TEST SERIES S13

This section lists the blasting results of the test series S13. These results are used in the blast performance analysis in Chapter 7 and Chapter 8. More detail on this test series can be found in [30, 31].

Table D1: Sandwich schematics and material properties of test series S13 [30, 31]

<table>
<tr><th colspan="4">S13 sandwich schematics</th></tr>
<tr><td colspan="4"> 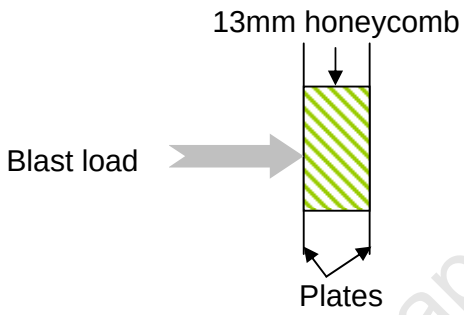
</td></tr>
<tr><th colspan="4">Face plate material properties [30]</th></tr>
<tr><td colspan="2">Face plate 1</td><td colspan="2">Face plate 2</td></tr>
<tr><td>Sheet</td><td>D</td><td>Sheet</td><td>E</td></tr>
<tr><td>Thickness</td><td>1.6mm</td><td>Thickness</td><td>1.6mm</td></tr>
<tr><td>Dynamic stress</td><td>251MPa</td><td>Dynamic stress</td><td>319MPa</td></tr>
<tr><td>Static stress</td><td>209MPa</td><td>Static stress</td><td>265MPa</td></tr>
<tr><th colspan="4">Honeycomb material properties [31]</th></tr>
<tr><td colspan="2">Thickness</td><td colspan="2">13mm</td></tr>
<tr><td colspan="2">Density</td><td colspan="2">71.25Kg/m^3</td></tr>
<tr><td colspan="2">Plateau stress</td><td colspan="2">2.4MPa</td></tr>
<tr><td colspan="2">Onset of densification</td><td colspan="2">72% strain</td></tr>
</table>

Table D2: Blasting results of S13 [30]

Test Number	Plate Thickness (mm)	Charge Mass (g)	Impulse (Ns)	Plate mid-point deflection				Plate failure mode		Dimensionless Impulse (Front plate only)	Honeycomb crush distance		
				Front plate		Back plate		Front plate	Back plate		Outer-span (mm)	Mid-span (mm)	Center (mm)
				(mm)	d/H	(mm)	d/H						
081005b	1.6	24	41.08	17.77	11.11	11.19	6.99	II	II*	45.35	10.44	11.27	11.23
171005b	1.6	22	35.67	20.44	12.78	11.58	7.24	II	I	39.38	7.22	11.23	11.10
081005a	1.6	20	35.69	15.64	9.78	11.06	6.91	II*	I	39.40	6.37	11.06	11.18
200905g	1.6	16	32.05	15.44	9.65	9.38	5.86	II*	I	39.86	5.72	10.45	11.34
171005c	1.6	15	30.29	17.92	11.20	7.22	4.51	I	I	33.44	1.03	9.32	11.10
160905a	1.6	14	29.53	17.68	11.05	6.82	4.26	I	I	36.72	1.46	9.20	10.86
171005a	1.6	13	27.57	16.68	10.43	5.92	3.70	I	I	30.44	1.25	8.64	11.17
021005a	1.6	12	25.23	15.40	9.63	4.95	3.09	I	I	27.86	0.49	8.07	10.50
240905g	1.6	10	23.08	14.01	8.76	4.04	2.53	I	I	25.48	0.69	7.48	10.11
200905f	1.6	8	19.70	11.69	7.31	3.50	2.19	I	I	24.49	0.58	5.40	7.93
240905h	1.6	8	19.49	11.73	7.33	3.56	2.23	I	I	21.51	0.54	5.45	8.61
240905c	1.6	6.5	15.83	9.46	5.91	2.86	1.79	I	I	17.47	0.43	4.78	7.25
200905e	1.6	4	11.39	5.70	3.56	1.96	1.23	I	I	14.17	0.59	2.29	4.97
240905a	1.6	3	9.15	3.38	2.11	1.45	0.91	I	I	10.10	0.09	1.37	3.44
021005f	1.6	2.5	7.54	2.69	1.68	1.28	0.80	I	I	8.32	0.14	0.69	2.70
081005c	1.6	2	7.22	1.62	1.01	0.94	0.59	I	I	7.97	0.05	0.30	0.56